

ORNL  
MASTER COPY



OAK RIDGE NATIONAL LABORATORY

operated by

UNION CARBIDE CORPORATION

for the

U. S. ATOMIC ENERGY COMMISSION



ORNL - TM - 483

76

STRUCTURAL ANALYSIS OF ZIRCALOY FUEL-ELEMENT  
CONTAINERS FOR THE NS SAVANNAH REACTOR

L. R. Shobe

NOTICE

This document contains information of a preliminary nature and was prepared primarily for internal use at the Oak Ridge National Laboratory. It is subject to revision or correction and therefore does not represent a final report. The information is not to be abstracted, reprinted or otherwise given public dissemination without the approval of the ORNL patent branch, Legal and Information Control Department.

LEGAL NOTICE

This report was prepared as an account of Government sponsored work. Neither the United States, nor the Commission, nor any person acting on behalf of the Commission:

- A. Makes any warranty or representation, expressed or implied, with respect to the accuracy, completeness, or usefulness of the information contained in this report, or that the use of any information, apparatus, method, or process disclosed in this report may not infringe privately owned rights; or
- B. Assumes any liabilities with respect to the use of, or for damages resulting from the use of any information, apparatus, method, or process disclosed in this report.

As used in the above, "person acting on behalf of the Commission" includes any employee or contractor of the Commission, or employee of such contractor, to the extent that such employee or contractor of the Commission, or employee of such contractor prepares, disseminates, or provides access to, any information pursuant to his employment or contract with the Commission, or his employment with such contractor.

Contract No. W-7405-eng-26

Reactor Division

STRUCTURAL ANALYSIS OF ZIRCALOY FUEL-ELEMENT  
CONTAINERS FOR THE NS SAVANNAH REACTOR

L. R. Shobe

Date Issued

AUG 1 1967

OAK RIDGE NATIONAL LABORATORY  
Oak Ridge, Tennessee  
operated by  
UNION CARBIDE CORPORATION  
for the  
U.S. ATOMIC ENERGY COMMISSION

•

-

•

•

•

•

•

•

## CONTENTS

|  | <u>Page</u> |
|--|-------------|
| LIST OF FIGURES .....  | vii         |
| LIST OF TABLES .....   | xiii        |
| ABSTRACT .....   | 1           |
| INTRODUCTION .....   | 1           |
| DESIGN INFORMATION .....   | 1           |
| Ship Motions Considered .....  | 3           |
| Deflection Limitations .....   | 3           |
| Fuel-Element Weight and Load Application .....   | 4           |
| Pressure Loadings .....  | 4           |
| Thermal Loading .....  | 6           |
| Allowable Stresses .....   | 6           |
| SUMMARY OF STRUCTURAL ANALYSIS .....   | 6           |
| Ship Motions and Loadings .....  | 6           |
| Normal Ship Motions and Loadings .....   | 6           |
| Unusual Ship Motions .....   | 8           |
| Model Selection .....  | 8           |
| Models for Investigation of Deflections and Stresses<br>from Flexure of the Whole Unit ..... | 9           |
| Local Action Models .....  | 9           |
| Spacer-Bar "Beam" Models .....   | 9           |
| Examination of the Design .....  | 10          |
| Core II Type Fuel Elements - Normal Ship<br>Motions .....                                    | 10          |
| Core II Type Fuel Elements - Unusual Ship<br>Motions .....                                   | 14          |
| Core I Type Fuel Elements .....  | 14          |
| CLOSURE .....  | 14          |
| Appendix A. GRAVITATIONAL AND DYNAMIC LOADS .....  | 17          |
| Magnitudes of the Loads Under Specified Conditions .....                                     | 17          |
| Distribution of the Fuel-Element Loads for Frame<br>Analyses .....                           | 18          |
| Appendix B. MISCELLANEOUS LOADINGS AND DEFLECTIONS .....                                     | 21          |
| Dynamic Loads Resulting from Acceleration Caused by<br>Ship's Roll .....                     | 21          |

|   |    |
|---|----|
| Slender Rod Approximation .....   | 21 |
| Harmonic Motion Approximation .....   | 23 |
| Thermal Deflection and Stresses of the Spacer Bar .....   | 24 |
| The Beam on an Elastic Foundation Loaded with a<br>Temperature Distribution .....   | 25 |
| Deflections Caused by Temperature Distribution .....  | 25 |
| The Beam on an Elastic Foundation .....   | 26 |
| The Deflection of the Spacer Bar .....  | 28 |
| Stresses in the Spacer Bar .....  | 29 |
| Torsional Deformation in Second-Pass Fuel-Element<br>Containers .....   | 30 |
| Appendix C. SELECTION OF MODELS FOR ANALYZING THE<br>FUEL CONTAINERS .....  | 33 |
| Selection of a Model for Determining Stresses and<br>Deflections Caused by Flexure of the Unit as<br>a Whole .....                                    | 33 |
| Stresses and Deflections Obtained by Treating the Core<br>Assembly as a Unit and Considering It To Be<br>Simply Supported .....                       | 33 |
| Stresses and Deflections in a Single Fuel-Element<br>Container Subjected to a Concentrated Load at<br>Mid-Span and a Uniformly Distributed Load ..... | 37 |
| Comparison of the Two Simply-Supported Models .....   | 38 |
| Comments on Stresses and Deflections Caused by<br>Flexure of the Unit as a Whole .....  | 39 |
| Selection of a Model for Considering Stresses and<br>Deflections Caused by Localized Action .....   | 39 |
| Appendix D. RIGID-FRAME ANALYSIS .....  | 43 |
| Method of Analysis .....  | 43 |
| Analyses of the Three Basic Frames .....  | 45 |
| Case I .....  | 46 |
| Case II .....   | 50 |
| Case III .....  | 50 |
| Appendix E. A BEAM ON AN ELASTIC FOUNDATION .....   | 55 |
| A Beam of Infinite Length .....   | 55 |
| The Semi-Infinite Beam with Hinged End .....  | 57 |
| The Semi-Infinite Beam with Fixed End .....   | 59 |

|   |     |
|---|-----|
| Appendix F. ANALYSES OF THE FUEL-ELEMENT CONTAINERS AT<br>MID-HEIGHT OF THE CORE FOR FUEL ELEMENTS OF CORE II TYPE .....                  | 62  |
| Rigid-Frame Calculations for Column 2 when Subjected<br>to Simultaneous 30° Roll, 0.7-g Lateral Heave, and<br>0.3-g Vertical Heave .....  | 62  |
| Rigid-Frame Calculations for Column 1 when Subjected<br>to Simultaneous 30° Roll, 0.7-g Lateral Heave, and<br>0.3-g Vertical Heave .....  | 69  |
| Determination of Fuel-Element Container Wall Thicknesses<br>Based on Bending Moments in the Intermediate Fuel-<br>Element Container ..... | 75  |
| Point A of Member AD in the Intermediate Fuel-Element<br>Container of the Column 1 Model .....  | 76  |
| Point J <sub>L</sub> of Member AF in the Intermediate Fuel-Element<br>Container of the Column 2 Model .....                               | 78  |
| Transverse Sections of the Peripheral Fuel-Element<br>Container Walls .....   | 79  |
| Member AD, Bottom Frame, Column 1 Model .....   | 80  |
| Member AF, Bottom Frame, Column 2 Model .....   | 83  |
| Unusual Ship Motions .....  | 86  |
| The Connecting Members .....  | 86  |
| Connecting Member for AD, Bottom Frame,<br>Column 1 Model .....   | 87  |
| Connecting Member for AF, Bottom Frame,<br>Column 2 Model .....   | 92  |
| Appendix G. ANALYSES OF THE FUEL-ELEMENT CONTAINER ASSEMBLY<br>AT OR NEAR THE TOP OF THE CORE FOR FUEL ELEMENTS OF<br>CORE I TYPE .....   | 105 |
| Geometrical and Physical Constants of the Spacer<br>Bar "Beam" .....  | 105 |
| Moments and Deflections in the Spacer Bar "Beams" .....   | 110 |
| Transverse Sections of the Intermediate Fuel-<br>Element Container Walls .....  | 110 |
| Transverse Section at the Point of Maximum<br>Deflection .....  | 111 |
| Transverse Sections Near the Top Point of Applica-<br>tion of the Fuel-Element Loads .....  | 113 |
| Spacer Bar "Beam" at Top of Core .....  | 116 |
| Transverse Sections of Peripheral Container Walls .....   | 119 |
| Appendix H. STRESS AND FATIGUE STRENGTH DATA .....  | 134 |



## LIST OF FIGURES

|  | <u>Page</u> |
|--|-------------|
| Fig. 1. NS SAVANNAH Fuel-Element Container Assembly .....  | 2           |
| Fig. 2. Maximum Pressure Differential Across Container Walls with No Core Bypass Flow .....  | 5           |
| Fig. 3. Bending-Moment Diagrams and Deflections of Column 1 Fuel-Element Container Walls at Mid-Height of the Core for Core II Type Fuel Elements .....    | 11          |
| Fig. 4. Bending-Moment Diagrams and Deflections of Column 2 Fuel-Element Container Walls at Mid-Height of the Core for Core II Type Fuel Elements .....    | 12          |
| Fig. 5. Cross Section of a Portion of the Fuel-Element Container Assembly .....  | 15          |
| Fig. A1. Free-Body Diagram of a Core II Type Fuel Element .....  | 20          |
| Fig. A2. Free-Body Diagram of a Fuel-Element Container as a Simple Beam .....  | 20          |
| Fig. A3. A Plate Simply Supported on Four Sides Carrying a Concentrated Load at Mid-Point and a Simple Beam Carrying a Concentrated Load at Mid-Span ..... | 20          |
| Fig. B1. A Rod Swinging in a Vertical Plane About an Axis at O .....   | 32          |
| Fig. B2. A Beam of Finite Length on an Elastic Foundation .....  | 32          |
| Fig. B3. Cross Section of Spacer Bar Used in Stainless Steel Fuel-Element Assembly .....   | 32          |
| Fig. B4. Fuel-Element Container Loaded in Torsion .....  | 32          |
| Fig. C1. Beam Sections .....   | 41          |
| Fig. C2. Fuel-Element Container as a Beam Fixed at One End and Simply Supported at the Other .....   | 41          |
| Fig. C3. Fuel-Element Container as a Simply Supported Beam .....   | 41          |
| Fig. C4. Orientation of NS SAVANNAH Fuel-Element Containers Used in Analyzing Stresses Arising from Plate Action .....                                     | 42          |
| Fig. C5. Container Assembly Models Used in Analyzing Stresses from Plate Action of NS SAVANNAH Fuel-Element Containers .....                               | 42          |
| Fig. D1. Basic Rigid-Frame Models Used in Stress Analysis of NS SAVANNAH Fuel-Element Containers .....   | 52          |

|          |   |    |
|----------|---|----|
| Fig. D2. | Steps in Developing the Slope-Deflection Method. ....   | 52 |
| Fig. D3. | Basic Frame of Case I. ....   | 52 |
| Fig. D4. | Bending Moment Diagram by Parts for Half of Beam AF for Basic Frame of Case I. ....   | 53 |
| Fig. D5. | Bending Moment Diagram by Parts for Half of Beam CD for Basic Frame of Case I. ....   | 53 |
| Fig. D6. | Basic Frame of Case II. ....  | 54 |
| Fig. D7. | Basic Frame of Case III. ....   | 54 |
| Fig. E1. | A Beam of Infinite Length on an Elastic Foundation. ....  | 61 |
| Fig. E2. | A Beam of Semi-infinite Length, Hinged at One End, and on an Elastic Foundation. ....   | 61 |
| Fig. E3. | A Beam of Semi-infinite Length, Fixed at One End, and on an Elastic Foundation. ....  | 61 |
| Fig. F1. | Column 2 Fuel-Element Container Assembly Model. ....  | 93 |
| Fig. F2. | Model Beam and Bending-Moment Diagram for the Bottom of the Upper Second Pass Fuel-Element Container in Column 2, at Mid-Height of Core, for Core II Type Fuel Elements. ....     | 93 |
| Fig. F3. | Model Beam and Bending-Moment Diagram for the Top of the Third Pass Fuel-Element Container in Column 2, at Mid-Height of the Core, for Core II Type Fuel Elements. ....           | 93 |
| Fig. F4. | Model Beam and Bending-Moment Diagram for the Top of the Upper Second Pass Fuel-Element Container in Column 2, at Mid-Height of the Core, for Core II Type Fuel Elements. ....    | 94 |
| Fig. F5. | Model Beam and Bending-Moment Diagram for the Bottom of the Third Pass Fuel-Element Container in Column 2, at Mid-Height of the Core, for Core II Type Fuel Elements. ....        | 94 |
| Fig. F6. | Model Beam and Bending-Moment Diagram for the Top of the Lower Second Pass Fuel-Element Container in Column 2, at Mid-Height of the Core, for Core II Type Fuel Elements. ....    | 95 |
| Fig. F7. | Model Beam and Bending-Moment Diagram for the Bottom of the Lower Second Pass Fuel-Element Container in Column 2, at Mid-Height of the Core, for Core II Type Fuel Elements. .... | 95 |
| Fig. F8. | Column 1 Fuel-Element Container Assembly Model. ....  | 96 |

|           |   |     |
|-----------|---|-----|
| Fig. F9.  | Model Beam and Bending-Moment Diagram for the Bottom of the Top Fuel-Element Container in Column 1, at Mid-Height of the Core, for Core II Type Fuel Elements. ....   | 96  |
| Fig. Fl0. | Model Beam and Bending-Moment Diagram for the Top of the Intermediate Fuel-Element Container in Column 1, at Mid-Height of the Core, for Core II Type Fuel Elements. ....   | 96  |
| Fig. Fl1. | Model Beam and Bending-Moment Diagram for the Top of the Top Fuel-Element Container in Column 1, at Mid-Height of the Core, for Core II Type Fuel Elements. ....  | 97  |
| Fig. Fl2. | Model Beam and Bending-Moment Diagram for the Bottom of the Intermediate Fuel-Element Container in Column 1, at Mid-Height of the Core, for Core II Type Fuel Elements. ....  | 97  |
| Fig. Fl3. | Model Beam and Bending-Moment Diagram for the Top of the Bottom Fuel-Element Container in Column 1, at Mid-Height of the Core, for Core II Type Fuel Elements. ....   | 98  |
| Fig. Fl4. | Model Beam and Bending-Moment Diagram for the Bottom of the Bottom Fuel-Element Container in Column 1, at Mid-Height of the Core, for Core II Type Fuel Elements. ....  | 98  |
| Fig. Fl5. | Significant Maximum Bending Moments and Deflections in Column 1, at Core Mid-Height, for Core II Type Fuel Elements and Normal Ship Motions. ....   | 99  |
| Fig. Fl6. | Significant Maximum Bending Moments and Deflections in Column 2, at Core Mid-Height, for Core II Type Fuel Elements and Normal Ship Motions. ....   | 100 |
| Fig. Fl7. | Repeating Section of Fuel-Element Container Wall at Mid-Span with $t = 0.14$ in. ....   | 101 |
| Fig. Fl8. | Model Beam and Bending-Moment Diagram for the Member AD of the Bottom Fuel-Element Container in Column 1, at Mid-Height of the Core, for Core II Type Fuel Elements with the Mid-Span Deflection Limited to 0.05 in. .... | 102 |
| Fig. Fl9. | Model Beam and Bending-Moment Diagram for the Member AF of the Bottom Fuel-Element Container in Column 2, at Mid-Height of the Core, for Core II Type Fuel Elements with the Mid-Span Deflection Limited to 0.06 in. .... | 102 |
| Fig. F20. | Significant Maximum Bending Moments and Deflections at Mid-Height of the Core for Core II Type Fuel Elements and Unusual Ship Motions. ....   | 103 |

|           |   |     |
|-----------|---|-----|
| Fig. F21. | Connecting Member for Peripheral Walls of Fuel Containers. ....   | 104 |
| Fig. F22. | Connecting Member Equivalent Steel Section. ....  | 104 |
| Fig. F23. | The Connecting Member as a Simple Beam for Core II Type Fuel Elements. ....   | 104 |
| Fig. G1.  | Cross Section of Spacer Bar "Beam" First Assumed. ....  | 120 |
| Fig. G2.  | Simple Beam Model of Fuel-Element Container Wall. ....  | 120 |
| Fig. G3.  | Model Beams and Bending-Moment Diagrams for the Bottom of the Upper Second Pass Fuel-Element Container in Column 2, 16 in. from the Assumed Simple Support at the Top of the Core, for Core I Type Fuel Elements. ....                  | 121 |
| Fig. G4.  | Model Beams and Bending-Moment Diagrams for the Top of the Third Pass Fuel-Element Container in Column 2, 16 in. from the Assumed Simple Support at the Top of the Core, for Core I Type Fuel Elements. ....                            | 122 |
| Fig. G5.  | Model Beams and Bending-Moment Diagrams for the Bottom of the Upper Second Pass Fuel-Element Container in Column 2, at the Top of the Core, for Core I Type Fuel Elements, with $e = 3$ in. ....  | 123 |
| Fig. G6.  | Model Beams and Bending-Moment Diagrams for the Top of the Third Pass Fuel-Element Container in Column 2, at the Top of the Core, for Core I Type Fuel Elements, with $e = 3$ in. ....  | 124 |
| Fig. G7.  | Model Beams and Bending-Moment Diagrams for the Bottom of the Upper Second Pass Fuel-Element Container in Column 2, 10 in. from the Assumed Simple Support at the Top of the Core, for Core I Type Fuel Elements, with $e = 5$ in. .... | 125 |
| Fig. G8.  | Model Beams and Bending-Moment Diagrams for the Top of the Third Pass Fuel-Element Container in Column 2, 10 in. from the Assumed Simple Support at the Top of the Core, for Core I Type Fuel Elements, with $e = 5$ in. ....           | 126 |
| Fig. G9.  | Model Beams and Bending-Moment Diagrams for the Bottom of the Upper Second Pass Fuel-Element Container in Column 2, 10 in. from the Assumed Fixed End at the Top of the Core, for Core I Type Fuel Elements, with $e = 5$ in. ....      | 127 |

|           |  |     |
|-----------|--|-----|
| Fig. G10. | Model Beams and Bending-Moment Diagrams for the Top of the Third Pass Fuel-Element Container in Column 2, 10 in. from the Assumed Fixed End at the Top of the Core, for Core I Type Fuel Elements, with $e = 5$ in. ....               | 128 |
| Fig. G11. | Model Beams and Bending-Moment Diagrams for the Bottom of the Upper Second Pass Fuel-Element Container in Column 2, 6 in. from the Assumed Simple Support at the Top of the Core, for Core I Type Fuel Elements, with $e = 3$ in. .... | 129 |
| Fig. G12. | Model Beams and Bending-Moment Diagrams for the Top of the Third Pass Fuel-Element Container in Column 2, 6 in. from the Assumed Simple Support at the Top of the Core, for Core I Type Fuel Elements, with $e = 3$ in. ....           | 130 |
| Fig. G13. | Model Beams and Bending-Moment Diagrams for the Bottom of the Upper Second Pass Fuel-Element Container in Column 2, 6 in. from the Assumed Fixed End at the Top of the Core, for Core I Type Fuel Elements, with $e = 3$ in. ....      | 131 |
| Fig. G14. | Model Beams and Bending-Moment Diagrams for the Top of the Third Pass Fuel-Element Container in Column 2, 6 in. from the Assumed Fixed End at the Top of the Core, for Core I Type Fuel Elements, with $e = 3$ in. ....                | 132 |
| Fig. G15. | Fixed End of Spacer Bar Beam First Assumed. ....   | 133 |
| Fig. G16. | The Connecting Member as a Simple Beam for Core I Type Fuel Elements. ....   | 133 |
| Fig. H1.  | Design Fatigue Strength Curve for Annealed Zircaloy-2 at 600°F Based on Navy Code Requirements. ....   | 138 |
| Fig. H2.  | Design Fatigue Strength Curves. ....   | 138 |
| Fig. H3.  | Modified Goodman Fatigue Diagrams. ....  | 139 |



LIST OF TABLES

|  | <u>Page</u> |
|--|-------------|
| Table A1. Ship Motions and Fuel Container Loads.....                     | 18          |
| Table G1. Moments and Deflections in the Assumed<br>Spacer Bar Beam..... | 111         |



STRUCTURAL ANALYSIS OF ZIRCALOY FUEL-ELEMENT CONTAINERS  
FOR THE NS SAVANNAH REACTOR

L. R. Shobe\*

Abstract

Structural evaluations were made of the 15% cold-worked Zircaloy fuel-element containers proposed for the NS SAVANNAH reactor. These evaluations, which are consistent with the Navy Code,<sup>1</sup> permitted the sizing of components so that under conservative loading conditions both stress and deflection limitations would be met. The necessary design modifications were specified for the fuel-element container assembly.

INTRODUCTION

The fuel-element container assembly of the existing NS SAVANNAH reactor consists of 32 essentially square fuel-element containers separated by spacer bars and surrounded by an inner thermal shield, as shown in Fig. 1. Since consideration is being given to replacing the stainless steel fuel-element containers with similar containers of Zircaloy, a study was undertaken to determine the wall thickness required to maintain structural integrity and to limit deflections to tolerable values during operation.

DESIGN INFORMATION

It was stipulated that the fuel-element container assembly design should be adequate for future NS SAVANNAH reactor cores. It was also recognized that the design must be conservative because of the many unknowns involved. Since it was impossible to predict the exact form which future fuel-element assemblies might take, it was assumed that a

---

\*Consultant, University of Tennessee.

<sup>1</sup>"Tentative Structural Design Basis for Reactor Pressure Vessels and Directly Associated Components," PB151987, 1 December 1958 Revision, Department of Commerce, Office of Technical Services.

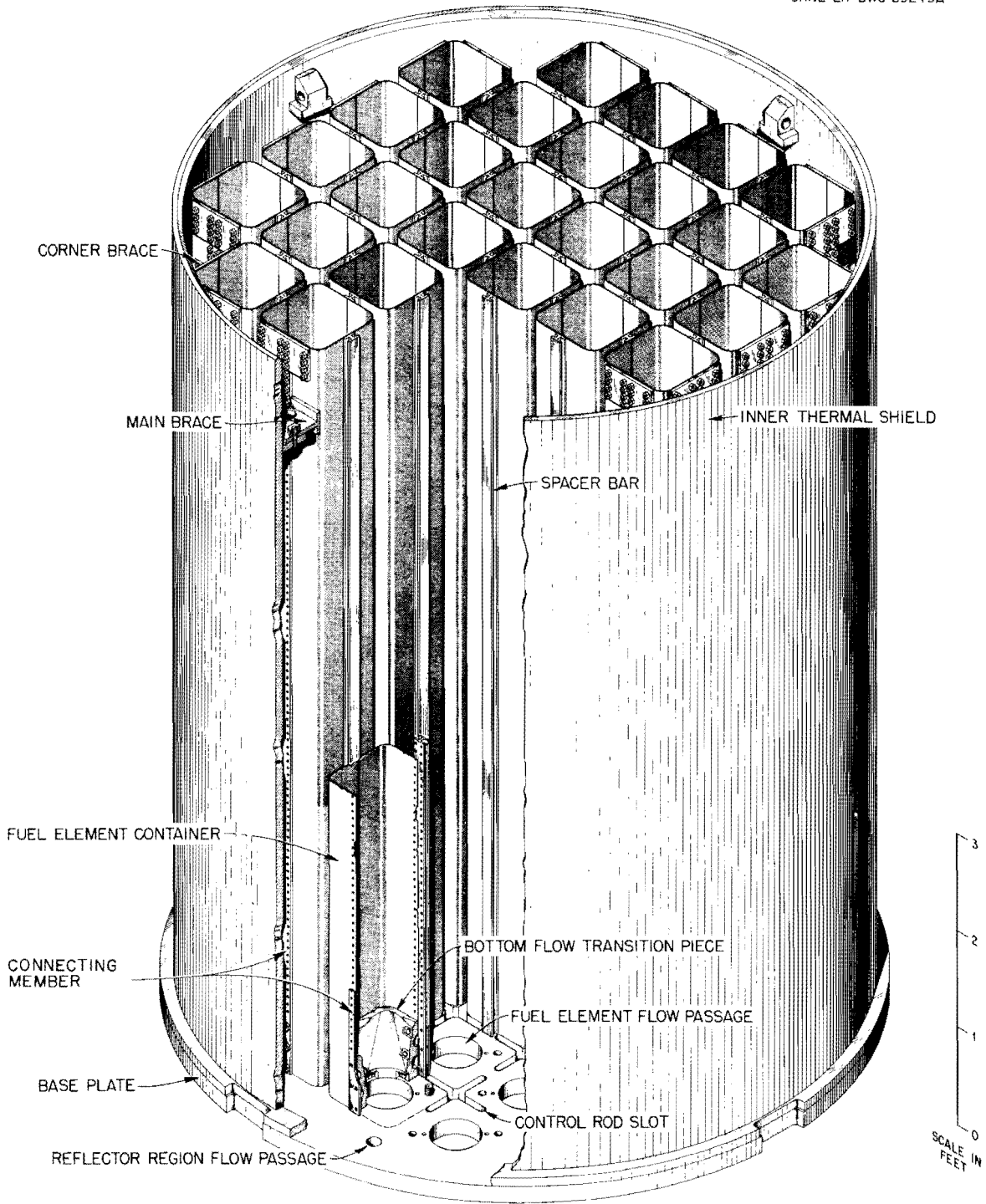


Fig. 1. NS SAVANNAH Fuel-Element Container Assembly.

design which would be adequate for fuel elements of either the core I or core II types would be satisfactory. The specific conditions and limitations are discussed in the following sections.

#### Ship Motions Considered

The various ship motions that are considered as normal in ship operations were outlined in USAEC Contract AT(04-3)-189, Project Agreement No. 2. These motions are:

1. 30° roll with a 14-sec period,
2. 7° pitch with a 7-sec period,
3. 0.25-g fore and aft acceleration,
4. 0.7-g lateral heave,
5. 0.3-g vertical heave.

The simultaneous occurrence of any combination or of all these motions is considered a possibility. In addition, the unusual circumstance of the ship lying on its side and having a vertical heave of 2 g was considered. The only concern under this extreme condition was that of limiting the deflection so as to permit control rod insertion.

#### Deflection Limitations

Deflection of the fuel-element container walls must be limited so that the walls neither interfere with control rod movement nor restrict the coolant flow around the fuel elements. Specific deflection and dimension limitations are:

1. The outside dimensions of the fuel-element containers shall remain the same as those in the existing design (see Babcock and Wilcox Drawing No. 10423F-4). Any increase in thickness of the fuel-element container wall necessitated by the material change must be made by decreasing the inside dimension of the fuel-element container.

2. The sum of the outward movements of two fuel-element container walls which partially define a control rod channel must not exceed 0.237 in. for the unusual case of the ship lying on its side and having a vertical heave of 2 g. Outward movement is defined as a movement toward

the control rod; no credit is to be taken for inward movement in obtaining the sum.

3. The sum of the inward deflections of two opposing fuel-element container walls must be such that the minimum inside dimension of the fuel-element container is not less than the maximum width of a fuel element. Use of the outside dimension of 8.982 in. and of the reference envelope dimension of 8.557 in. from Babcock and Wilcox Drawings No. 10423F-4 and 10424F-10, respectively, permit inward deflections whose sum is 0.145 in. for a container wall thickness of 0.14 in.

#### Fuel-Element Weight and Load Application

A weight of 760 lb was specified for a bundle of fuel elements. It was further specified that the load imposed by the fuel elements on the fuel-element containers should be applied in one of the following ways:

1. one-half the load at the top and one-half at the bottom (corresponding to core I type fuel elements shown on Babcock and Wilcox Drawing No. 10424F-10),
2. one-half the load at the mid-height of the fuel-element container and one-fourth the load at each end (corresponding to core II type fuel elements shown on General Electric Drawing No. 196E923).

#### Pressure Loadings

The design pressure drop across a fuel-element container wall (coolant channel pressure minus control rod channel pressure) was assumed to vary linearly from bottom to top of the fuel-element containers, as shown in Fig. 2. For four-pump operation the variations from bottom to top are +4.5 psi to +9.2 psi for the second pass and -2.0 psi to -5.6 psi for the third pass. It is to be noted that these design pressure differentials are approximately 30% greater than those of the present reactor.

UNCLASSIFIED  
ORNL-LR-DWG 60550

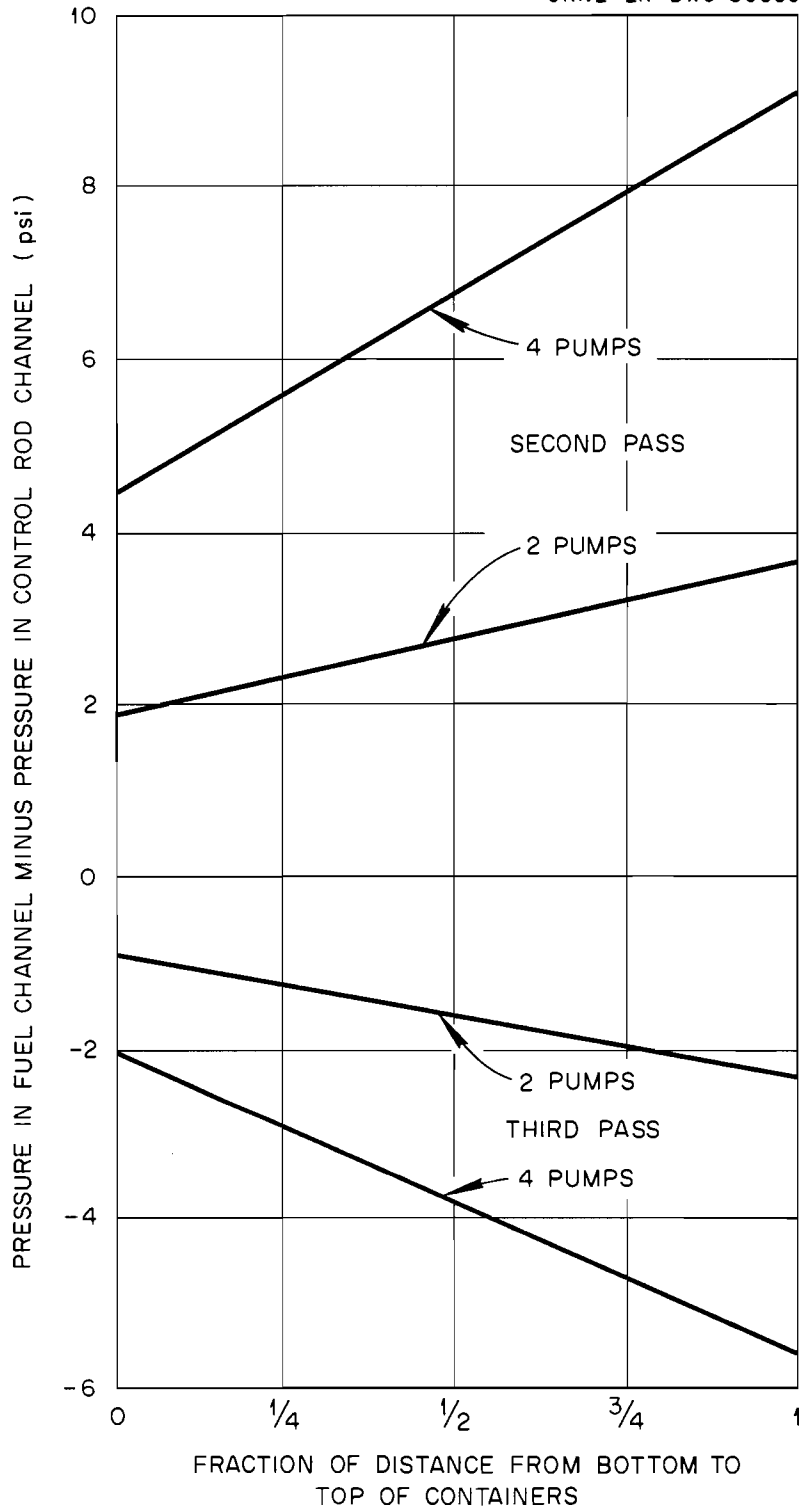


Fig. 2. Maximum Pressure Differential Across Container Walls with no Core Bypass Flow.

### Thermal Loading

Temperature differentials between the second and third passes cause both stresses and deflections in the separator bars and walls of the fuel-element containers. A maximum temperature differential of 6.04°F between the two flanges of the separator bar was used.<sup>2</sup>

### Allowable Stresses

The allowable stress intensities consistent with the Navy Code<sup>1</sup> for 15% cold-worked Zircaloy were determined as explained in Appendix H.

They are as follow:

- $S_m$ , the allowable membrane stress intensity = 17,600 psi,
- $S_p$ , the allowable primary plus secondary stress intensity = 31,700 psi.

The design fatigue strength curve and fatigue diagrams are also included in Appendix H.

## SUMMARY OF STRUCTURAL ANALYSIS

### Ship Motions and Loadings

#### Normal Ship Motions and Loadings

Of the ship motions considered and listed above under Design Information, the 30° roll in 14 sec combined with simultaneous 0.3-g vertical and 0.7-g lateral heaves (assumed to be normal to the ship's longitudinal vertical plane of symmetry) would constitute the most severe normal operating condition. Consequently, this was the only normal operating condition examined.

Mechanical Loads and Their Distribution. The magnitudes of the mechanical loads to be applied to the fuel-element containers by the fuel elements and the length of wall at mid-height of the core over which to distribute them are determined in Appendix A. Under normal operating

---

<sup>2</sup>T. D. Anderson, "A Thermal Analysis of Zircaloy Fuel Element Containers for the NS SAVANNAH Reactor," USAEC Report ORNL-TM-197, Oak Ridge National Laboratory, November 16, 1962.

conditions the maximum total load is 1026 lb. As was stated above in the Design Information section, the design must be adequate for the application of these loads in either of two ways: 50% at each end or 50% at the center and 25% at each end of the fuel-element container.

The length of the fuel-element container wall over which to distribute 50% of the load for subsequent frame analysis was established as 12 in. for a point of application at mid-height of the core. At the top end, for frame analysis, the load was distributed over a length equal to twice the distance from the point of load application to the point of support of the fuel-element container. Low pressure differentials made consideration of the bottom end of the fuel-element container unnecessary.

Pressure Loadings. The pressure loadings at various points along the length of a container wall were taken directly from Fig. 2.

Dynamic Loading from Acceleration Caused by Ship's Roll. Dynamic loads may result as a consequence of the angular acceleration caused by the ship's roll. The angular acceleration of the ship about a longitudinal axis is a function of the angular velocity, as well as of the angular displacement. It is also a function of the moment of inertia of the ship with respect to the longitudinal axis through the center of gravity of the ship in its particular condition (loaded, unloaded, or partially loaded) at the time of roll and of the distance of the metacenter above the center of gravity for the same condition. Since data were not available to permit utilization of these functions, two approximations were made.

First, it was assumed that the roll of the ship approximated the motion of a long rod swinging as a pendulum. This approximation gave a maximum angular acceleration of  $0.104 \text{ radians/sec}^2$  (see p. 23). The second approximation assumed simple harmonic motion for the ship's roll and gave a maximum angular acceleration of  $105 \text{ radians/sec}^2$  (see p. 24).

With the center of roll 4 ft below the top of the core, either of these values for angular acceleration gives the top of the fuel elements a linear acceleration of approximately  $0.4 \text{ ft/sec}^2$ , which may be ignored when compared with  $0.7 \text{ g}$ , or  $22.54 \text{ ft/sec}^2$ . Since, the dynamic loads from the angular acceleration of the ship's roll were negligible, they were not considered further.

Deflections and Stresses from Temperature Differentials. It was believed that the temperature differentials between the second- and third-pass containers would induce bowing and stresses of significant magnitude in the spacer bars. A theoretical analysis by Moore (see pp. 24 to 30) in which the spacer bars were treated as beams on elastic foundations showed that the bowing and attendant stresses were quite small. The effect of bowing of the spacer bars was therefore neglected in loading the models.

Deflections and Stresses from Torsion Caused by Nonsymmetrical Loading. Inspection of Fig. 1 (see also Fig. C4, Appendix C) indicates that the second-pass fuel-element containers are not symmetrically supported. As a consequence, the fuel-element containers are subjected to torque upon application of the fuel-element loads. An analysis of the deflections and stresses from such torque under conservative conditions (see pp. 30 to 31) indicated that they were of negligible magnitude.

#### Unusual Ship Motions

The loading conditions for the unusual condition of the ship on its side and having a vertical acceleration of 2 g are the same as those of the normal operating conditions, with one exception. The exception is that the total load of the fuel element is 2280 lb, rather than 1026 lb. This load is determined in Appendix A.

#### Model Selection

The selection of a model was accomplished by a process of elimination. It is doubtful that there is a single fuel-element container that is exactly symmetrically supported, even when subjected only to pressure loads. The least symmetry exists in a corner second-pass container. As was pointed out earlier, one second-pass container was loaded as a torsion member under conservative conditions, and the deflection and stresses from torsion were shown to be of minor magnitude (see pp. 30 to 31). Hence, in the rigid frame analyses of the containers, symmetrical supports were assumed.

### Models for Investigation of Deflections and Stresses from Flexure of the Whole Unit

Three different models were considered for determining the stresses and deflections from beam action of the fuel-element containers, that is, action of the unit as a whole, which neglects localized stresses and deflections. First, the entire assembly of 32 fuel-element containers (with the weight but not the strengthening effect of the spacer bars considered) was treated as a simply supported builtup beam. Second, a single fuel-element container was considered as a beam fixed at one end and simply supported at the other. The third and most conservative consideration was that of a single fuel-element container acting as a simply supported beam; this model was chosen for the beam analysis (see p. 38).

### Local Action Models

For determining the stresses and deflections from plate action, that is, localized stresses and deflections from pressure and concentrated loads in the walls of the fuel-element containers, two models were used: one for a column of three second-pass containers and one for a column consisting of a second-pass container at top and bottom with a third-pass container in the center. These models are shown on Fig. C.5 (Appendix C) and the reasons for their selection are presented on pages 39 and 40. The analyses of these models utilized the three basic frame loadings described in Appendix D and designated Cases I, II, and III.

### Spacer-Bar "Beam" Models

For either core I or core II type fuel elements in the fuel-element containers, the spacer bars will behave as beams on elastic foundations. The true end condition is unknown, but it is intermediate between the fixed and the simply supported conditions. For this reason, two models were chosen: one simply supported and one with a fixed end, but both semi-infinite in length because of physical and geometrical properties. Both models utilized portions of the attached container walls as "cover plates" and were therefore dubbed "beams." The theoretical development for these beams is in Appendix E.

### Examination of the Design

With the loads established, the models determined, and the general equations developed, the actual examination of the existing design was begun for the purpose of determining the design changes necessary to permit the use of Zircaloy as the fuel-element container metal. Throughout the examination the fatigue analyses were based on only one class of cycles; namely, that class in which the 30° clockwise roll combined with simultaneous 0.3-g vertical and 0.7-g lateral heaves (assumed to be normal to the ship's longitudinal vertical plane of symmetry) constituted one of the symmetrical extremes. Use of this cycle leads to conservative results because the cycle is the most severe of the normal operating cycles.

#### Core II Type Fuel Elements - Normal Ship Motions

The critical elevation in the core for core II type fuel elements is either at the mid-height of the core or near the top. The section near the top is more critical for core I type fuel elements than for core II elements and therefore was not examined for core II type fuel elements. The analyses of the mid-height section are presented in Appendix F.

The stresses and deflections from general flexure of the fuel-element container as a unit are listed on page 38. Localized stresses and deflections were obtained by analyzing the container assembly models shown in Figs. F1 and F8 (Appendix F). The general shapes of the bending-moment diagrams and the deflections of the mid-points, which were shown for all practical purposes to be the maximum deflections of the upper and lower walls (as seen in Figs. F1 and F8), are summarized in Figs. 3 and 4.

For a wall thickness of 0.14 in., the maximum primary stress intensity occurs at a corner of the bottom frame of the column 1 model and is 18,100 psi, provided the deflection of the mid-point of the bottom of the frame is limited to 0.05 in. This primary stress intensity exceeds the allowable value of 17,600 psi (see p. 135). Because of its load-carrying capacity, the connecting member (see Figs. 1 and F21), as now designed, will limit the maximum deflection of the fuel-element container wall at mid-span. Under this condition, as a result of the limit

MOMENTS ARE IN lb-in.  
POSITIVE SIGN INDICATES TENSION ON INSIDE OF FRAME  
DEFLECTIONS ARE AT MID-SPAN AND ARE IN INCHES FOR  
 $f = 0.14$  in.

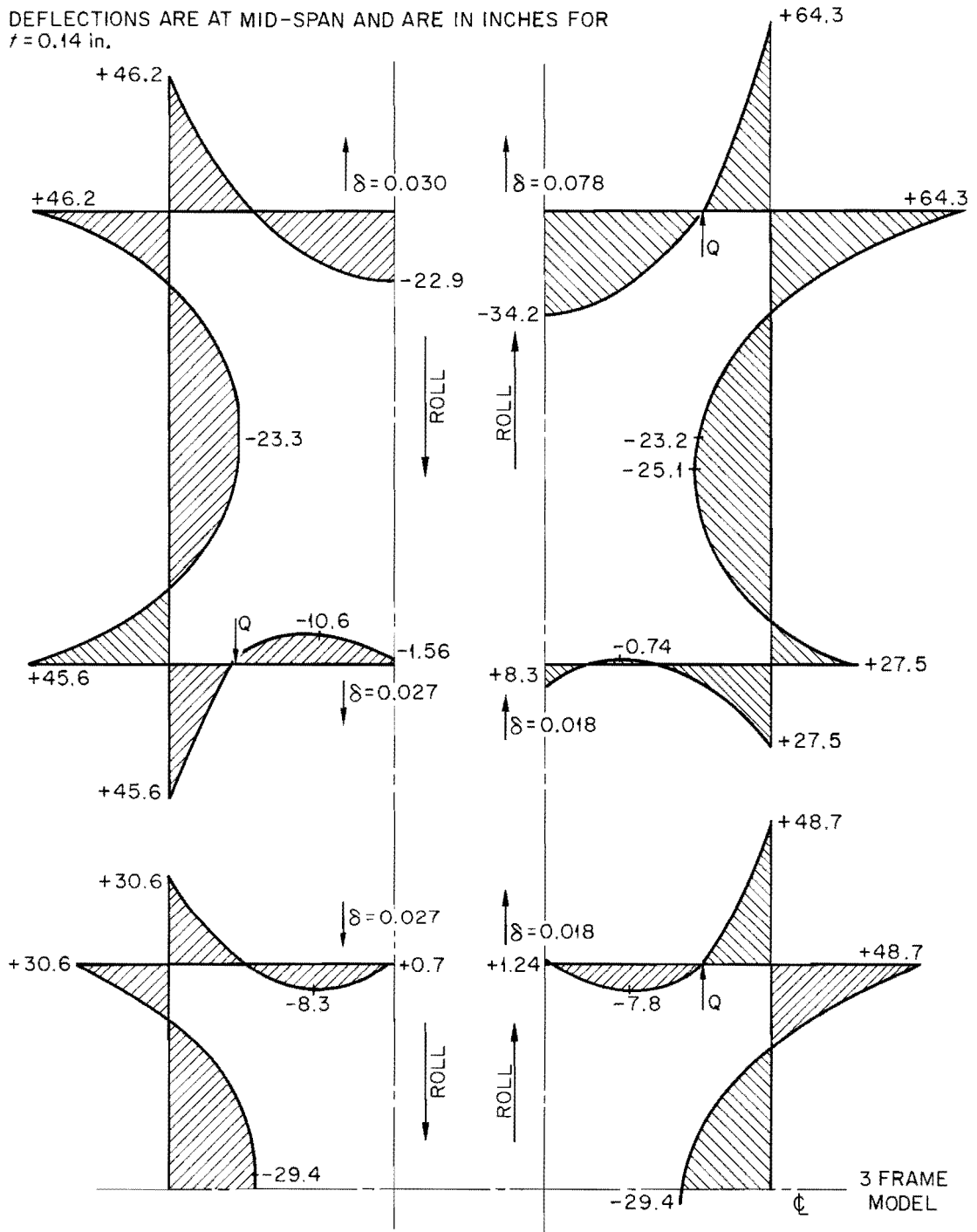


Fig. 3. Bending-Moment Diagrams and Deflections of Column 1 Fuel-Element Container Walls at Mid-Height of the Core for Core II Type Fuel Elements.

MOMENTS ARE IN lb-in.  
POSITIVE SIGN INDICATES TENSION ON INSIDE OF FRAME  
DEFLECTIONS ARE AT MID-SPAN AND ARE IN INCHES FOR  
 $f = 0.14$  in.

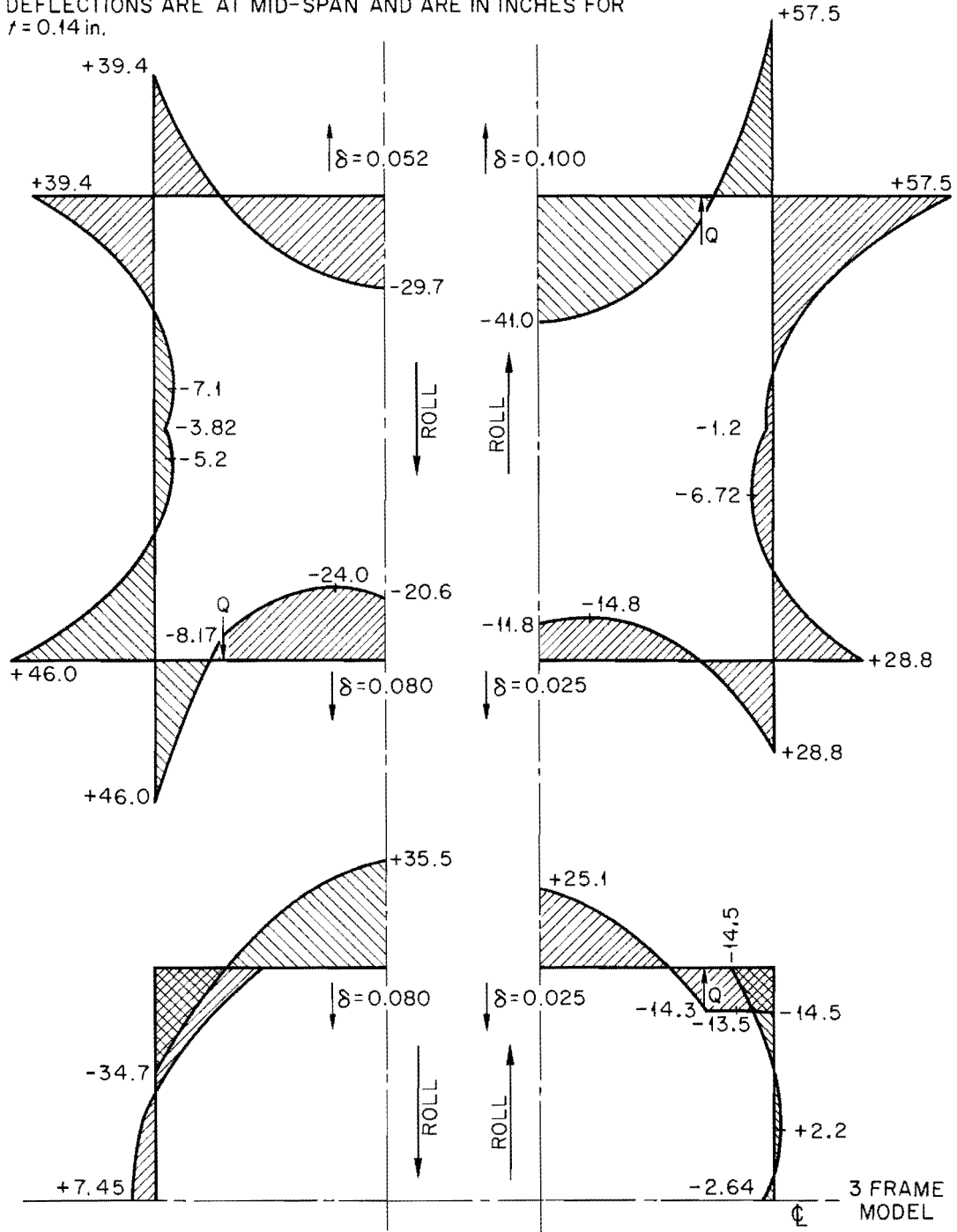


Fig. 4. Bending-Moment Diagrams and Deflections of Column 2 Fuel-Element Container Walls at Mid-Height of the Core for Core II Type Fuel Elements.

on deformation, the stresses at the corner may be considered secondary in nature, and the allowable stress intensity is 31,700 psi (see p. 135). Since with no support at mid-span the stress intensity at the corner of the frame is approximately 20,000 psi, the primary plus secondary stress intensity limitation is met. Fatigue analyses showed the corners to be good for an infinite number of cycles. The 0.14-in. wall thickness is therefore adequate at the corners of the frames.

The wall thickness of 0.14 in. was found to be inadequate at the mid-span point  $K_B$  (see Fig. F1 and p. 84) at the core mid-height. A fatigue analysis (see pp. 85 and 86) indicated that a fuel-element container wall thickness of 0.22 in. would be adequate at the point of attachment to the connecting member. Of course this means that the spacer-bar flanges and the connecting members must also be heavier, with less space between the flanges of the spacer bars. It was decided to make the spacer bar solid, since little space would be left between the flanges.

It should be noted that the fatigue analyses of the container walls at the points of attachment to the spacer bars and connecting members are based on the best available information on stress concentration factors and fatigue strength. If it is felt to be undesirable to increase the thickness of the fuel-element container walls at the edges, it is suggested that fatigue tests on models of the joints be conducted as a final check to determine whether the thicker edges on the walls and the solid spacer bars are necessary.

The connecting members must also serve as structural members. They must be either sufficiently rigid to restrict mid-span deflections, that is, rigid enough that the primary stress intensities in the peripheral frames do not exceed 17,600 psi, or they must be strong enough to carry additional loads if the primary stress intensity is exceeded. Steel was chosen as the material for the connecting member because of its greater rigidity than that of Zircaloy, and an I-section was used for economic reasons. Specifically, AISI type 347 stainless steel was chosen because of its allowable primary membrane stress intensity of 14,000 psi at 600°F. The analyses of these connecting members are discussed on pages 86-92.

### Core II Type Fuel Elements - Unusual Ship Motions

It was stated that the insertion of the control rods would be the only concern for the unusual condition of the ship on its side and subjected to a vertical heave of 2 g. Since the connecting members tend to convert the column 1 model into a column 2 model and since inspection of Figs. F15 and F16 indicates that the column 2 model deflects more than the column 1 model, only the column 2 model was analyzed. The results are summarized in Fig. F21, where it is seen that the maximum deflection of 0.10 in. is within the limits set for the design (see p. 3).

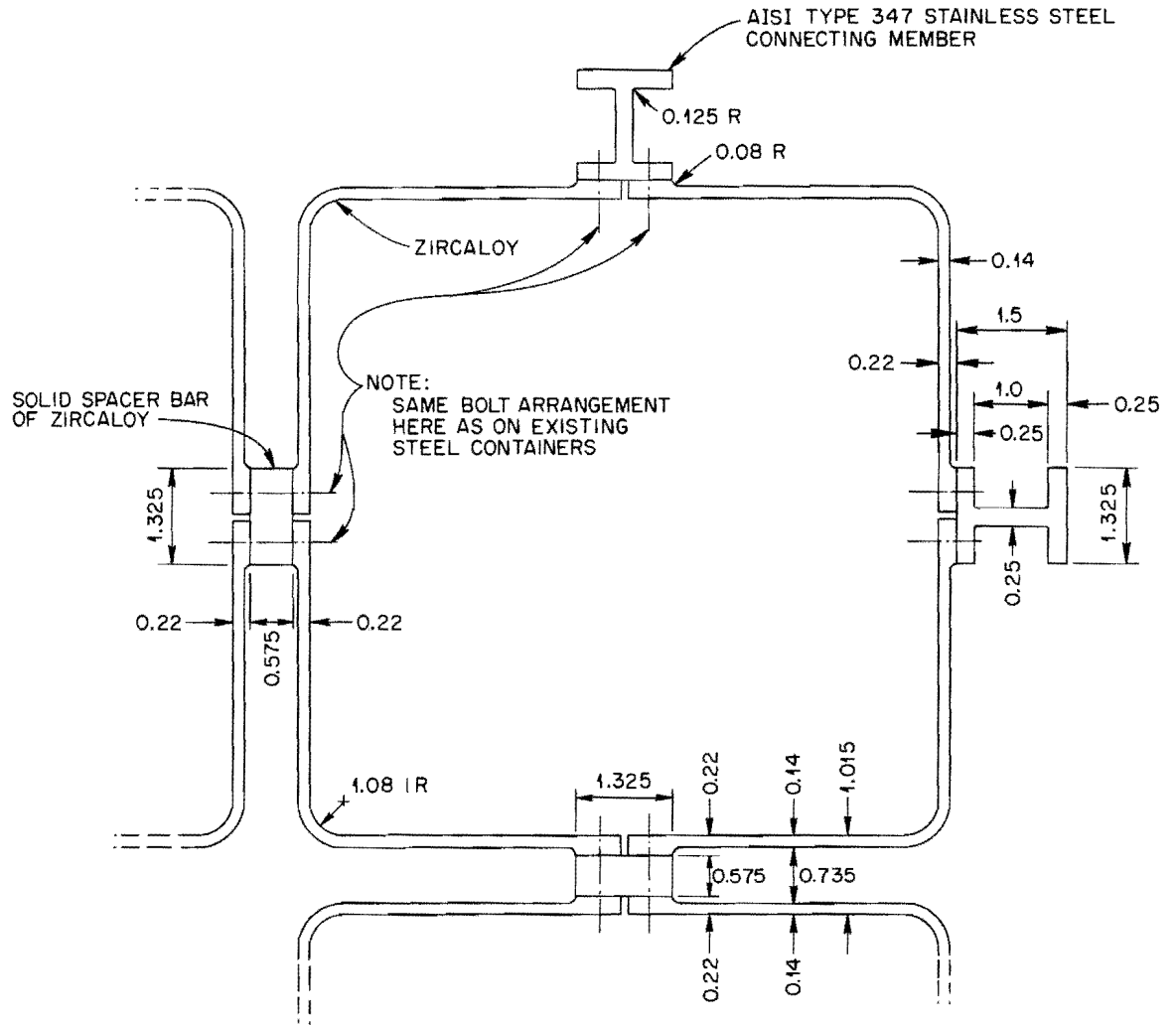
### Core I Type Fuel Elements

As stated on page 111, the analysis of core I type fuel elements was limited to the region between the top second-pass and the adjacent third-pass containers in the column 2 model. The spacer bar between the two containers was treated as a "beam" on an elastic foundation. An IBM-7090 program was written and used for calculating the bending moments and deflections at 1-in. increments along the beam. Deflections from the IBM-7090 output and the rigid frame analyses of Appendix D were used to construct bending-moment diagrams for six different load and location conditions, all of which were considered to be critical. The wall thickness of 0.14 in. was again found to be adequate, except at point  $K_T$  (see Fig. F1 and pp. 116 and 117) at the top of the core for core I type fuel elements. The fatigue analysis on pages 117 and 118 indicates that a fuel-element container wall thickness of 0.22 in. at the points of attachment to the spacer bars is adequate.

### CLOSURE

The dimensions and shapes of the components of the core structure are shown in Fig. 5. It is intended that the bolt spacing, edge distance, and size shall conform to those in the existing stainless steel core structure. The main brace at the top of the core is to be moved upward to ensure positive support of the nozzles in the fuel-element containers at the top of the core. Extreme care must be used in welding

UNCLASSIFIED  
ORNL-LR-DWG 77566



NOTE:  
ALL DIMENSIONS ARE IN INCHES

Fig. 5. Cross Section of a Portion of the Fuel-Element Container Assembly.

the bolts in the fuel-element container wall connections. Otherwise the effect of cold working may be lost.

Appendix A

## GRAVITATIONAL AND DYNAMIC LOADS

As mentioned in the Design Information on page 4, the design must be adequate to carry the fuel-element loads if applied 50% at each end of a fuel-element container for core I type fuel elements or 50% at the center and 25% at each end of a container for core II type fuel elements. It was therefore necessary to determine the magnitudes of the fuel-element loads under the different operating conditions specified in the Design Information on page 3.

Magnitudes of the Loads Under Specified Conditions

The fuel-element weight specified was 760 lb, and for core II type fuel elements the free-body diagram indicated in Fig. A1 was assumed. The values of  $R_2$ , that is, the forces exerted by the fuel element on the container wall at mid-height of the core, are the following for different combinations of ship motions:

|  | <u><math>R_2</math> (lb)</u> |
|--|------------------------------|
| 30° roll, $2[380 \sin 30^\circ (1/2)]$   | 190                          |
| 30° roll and 0.7-g lateral heave (heave assumed perpendicular to fuel bundle),<br>$190 + \frac{1}{2} \frac{760}{g} (0.7g)$                           | 456                          |
| 30° roll and 0.3-g vertical heave,<br>$190 + \frac{1}{2} \frac{760}{g} (0.3g) \sin 30^\circ$   | 247                          |
| 7° pitch and 0.3-g vertical heave,<br>$2 \left[ 380 \sin 7^\circ \left( \frac{1}{2} \right) \right] + \frac{1}{2} \frac{760}{g} (0.3g) \sin 7^\circ$ | 60.2                         |
| Fore and aft acceleration of 0.25 g,<br>$\frac{1}{2} \frac{760}{g} (0.25g)$  | 95                           |
| Ship on its side and with 2-g vertical heave,<br>$\frac{1}{2} 760 + \frac{1}{2} \frac{760}{g} (2g)$  | 1140                         |

A free-body diagram of the fuel-element container considered as a simply supported beam is shown in Fig. A2. This is the model selected in Appendix C for considering the elastic action of the fuel-element container as a unit. The load  $R_2$  is applied by the fuel element, and  $W_e$  is the effective distributed load of the fuel-element container, including both gravitational and dynamic effects. The values of  $W_e$  were obtained in the same way as were the values of  $R_2$ , and both are tabulated in Table A1.

Table A1. Ship Motions and Fuel-Element Container Loads

| Ship Motion  | $R_2$ (lb) | $W_e$ (lb) |
|--|------------|------------|
| 30° roll   | 190        | 50         |
| 30° roll and 0.7-g lateral heave (heave assumed perpendicular to fuel container) | 456        | 120        |
| 30° roll and 0.3-g vertical heave  | 247        | 65         |
| 7° pitch and 0.3-g vertical heave  | 60         | 16         |
| Fore and aft acceleration of 0.25 g  | 95         | 25         |
| Ship on its side and with 2-g vertical heave                                     | 1140       | 300        |
| 30° roll, 0.7-g lateral heave, and 0.3-g vertical heave                          | 513        | 135        |
| 7° pitch, 0.3-g vertical heave, and 0.25-g fore and aft acceleration             | 155        | 41         |

#### Distribution of the Fuel-Element Loads for Frame Analyses

The concentrated loads  $R_2$  applied by the fuel elements to the container walls need to be distributed over some length. This length was established by assuming the deflection,  $\delta$ , of a flat rectangular plate of width  $L$  and length  $b$  (where  $b \rightarrow \infty$ ) simply supported on all four edges to be equal to the deflection of a simply supported beam of width  $a$  and span length  $L$  where both are loaded by a concentrated load normal to the undeflected surface at its midpoint (see Fig. A3). In the following

expressions,  $\alpha$  is a constant depending on the ratio of  $b/L$ ,  $E$  is the modulus of elasticity, and  $t$  is the plate thickness.

For the flat rectangular plate,<sup>1</sup>

$$\delta_{\max} = \alpha \frac{R_2 L^2}{Et^3},$$

where, for  $b/L \rightarrow \infty$ ,  $\alpha = 0.1849$ . For the beam<sup>2</sup>

$$\delta_{\max} = \frac{R_2 L^3}{48EI},$$

where

$$I = \frac{1}{12} at^3.$$

Hence,

$$\delta = \frac{R_2 L^3}{4aEt^3}.$$

Equating the two values of  $\delta$  yields

$$a = 1.355L.$$

For the fuel containers,  $L = 8.89$  in., and hence  $a = 12.0$  in. is the length over which to distribute the  $R_2$  loads.

---

<sup>1</sup>S. Timoshenko, Theory of Plates and Shells, p. 158, 1st Ed., McGraw-Hill, New York, 1940.

<sup>2</sup>P. G. Laurson and W. J. Cox, Mechanics of Materials, p. 407, 3rd Ed., John Wiley and Sons, New York, 1954.

UNCLASSIFIED  
ORNL-LR-DWG 77567

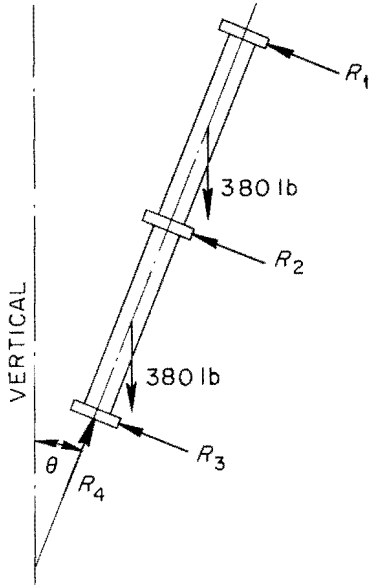


Fig. A1. Free-Body Diagram of a Core II Type Fuel Element.

UNCLASSIFIED  
ORNL-LR-DWG 77568

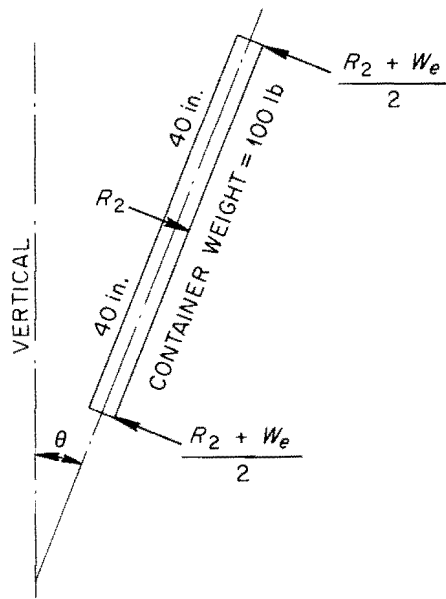


Fig. A2. Free-Body Diagram of a Fuel-Element Container as a Simple Beam.

UNCLASSIFIED  
ORNL-LR-DWG 77569

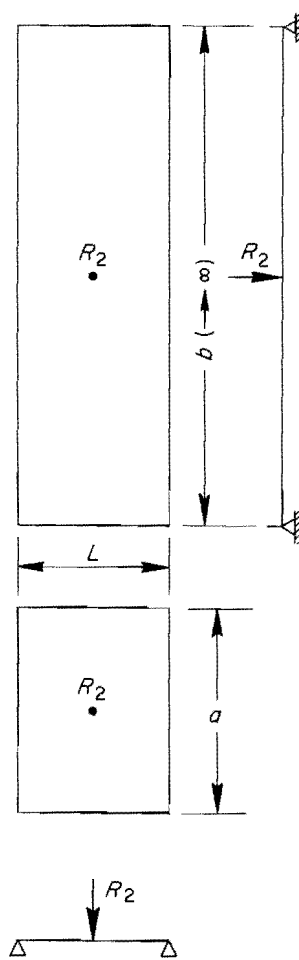


Fig. A3. A Plate Simply Supported on Four Sides Carrying a Concentrated Load at Mid-Point and a Simple Beam Carrying a Concentrated Load at Mid-Span.

Appendix B

## MISCELLANEOUS LOADINGS AND DEFLECTIONS

Dynamic Loads Resulting from Acceleration Caused by Ship's Roll

Dynamic loads may result as a consequence of the acceleration caused by the ship's roll. For the purpose of establishing this acceleration fairly closely, two approximations were made. In both approximations the angular velocity is a maximum when the angular displacement is zero, and the angular acceleration is a maximum when the angular displacement is a maximum.

Slender Rod Approximation

It was assumed that the roll of the ship approximated the motion of a long slender rod swinging in a vertical plane about a horizontal axis through its top end, as shown in Fig. B1. The length,  $L$ , consistent with the  $30^\circ$  roll in a 14-sec period must be established first. The angular acceleration,  $\alpha$ , may then be determined.

Let the bar rotate from the dashed line to the solid line shown in Fig. B1. By work and kinetic energy principles,

$$W \frac{L}{2} (\cos \theta - \cos \phi) = \frac{1}{2} \left( \frac{1}{3} \frac{W}{g} L^2 \right) \left( \frac{d\theta}{dt} \right)^2$$

and

$$\left( \frac{d\theta}{dt} \right)^2 = \frac{3g}{L} (\cos \theta - \cos \phi),$$

where

$\theta$  = angular displacement (in radians) at time  $t$ ,

$\phi$  = maximum angular displacement ( $\pi/6$ ),

$\alpha = \frac{d^2\theta}{dt^2}$  = angular acceleration (in radians/sec<sup>2</sup>),

$I_o$  = mass moment of inertia of rod with respect to horizontal axis at 0

$$= \frac{1}{3} \frac{W}{g} L^2,$$

W = weight of rod (in lb),

L = length of rod (in ft),

g = gravitational acceleration (32.2 ft/sec<sup>2</sup>),

t = time (in sec),

T = period of oscillation (14 sec).

The separation of variables and affixing of appropriate limits give

$$\left( \frac{3g}{L} \right)^{1/2} \int_0^{T/4} dt = \int_0^{\pi/6} \frac{d\theta}{(\cos \theta - \cos \phi)^{1/2}},$$

from which

$$\frac{T}{4} = \left( \frac{L}{3g} \right)^{1/2} \int_0^{\pi/6} \frac{d\theta}{(\cos \theta - \cos \phi)^{1/2}}.$$

From the procedure outlined by Sokolnikoff and Redheffer,<sup>1</sup>

$$T = 4 \frac{2L^{1/2}}{3g} \int_0^{\pi/2} \frac{d\beta}{(1 - K^2 \sin^2 \beta)^{1/2}}$$

is obtained where  $K = \sin 15^\circ$  and  $\sin \beta = \frac{\sin (\theta/2)}{K}$ .

From the C.R.C. Standard Mathematical Tables,<sup>2</sup>

$$\int_0^{\pi/2} \frac{d\beta}{(1 - K^2 \sin^2 \beta)^{1/2}} = 1.5981.$$

<sup>1</sup>I. S. Sokolnikoff and R. M. Redheffer, Mathematics of Physics and Modern Engineering, p. 49, McGraw-Hill, New York, 1958.

<sup>2</sup>C.R.C. Standard Mathematical Tables, p. 247, Chemical Rubber Publishing Co., Cleveland, Ohio, 1956.

Therefore,

$$T = 4 \left( \frac{2L}{3g} \right)^{1/2} (1.5981) .$$

For  $T = 14$  sec, it is calculated that  $L = 231.67$  ft, the length of rod required to have a 14-sec period and a maximum deflection angle of  $30^\circ$ .

From  $\Sigma M_O = I_O \alpha$ ,  $W \frac{L}{2} \sin \theta = -\frac{1}{3} \frac{W}{g} L^2 \alpha$ , and  $\alpha = -\frac{3g}{2L} \sin \theta$ , it is found that when  $\theta = 30^\circ$ ,

$$\alpha_{\max} = -0.104 \text{ radian/sec}^2 .$$

#### Harmonic Motion Approximation

If the roll of the ship is approximated by simple harmonic motion,

$$\frac{d^2\theta}{dt^2} + K^2\theta = 0 .$$

The general solution to this equation is

$$\theta = A \sin (Kt + B) ,$$

from which

$$\frac{d\theta}{dt} = AK \cos (Kt + B)$$

and

$$\frac{d^2\theta}{dt^2} = -AK^2 \sin (Kt + B) .$$

If it is assumed that  $\theta = 0$  when  $t = 0$ , and  $\theta = \pi/6$  and  $d\theta/dt = 0$  when  $t = T/4$ , it is found that  $B = 0$ ,  $K = 2\pi/T$ , and  $A = \pi/6$ . Hence,

$$\theta = \frac{\pi}{6} \sin \frac{2\pi}{T} t$$

and

$$\frac{d^2\theta}{dt^2} = -\frac{\pi}{6} \left(\frac{2\pi}{T}\right)^2 \sin \frac{2\pi}{T} t .$$

The period  $T$  is 14 sec and the maximum acceleration occurs when  $t = 3.5$  sec. Hence,

$$\frac{d^2\theta}{dt^2}_{\max} = -\frac{\pi}{6} \left(\frac{2\pi}{14}\right)^2 \sin \frac{2\pi}{14} (3.5) = \alpha_{\max}$$

and

$$\alpha_{\max} = -0.105 \text{ radian/sec}^2 .$$

With the center of roll 2 ft above the bottom of the core, the acceleration caused by roll of the top of a fuel element is approximately

$$a \cong 4\alpha .$$

Either value of  $\alpha$  (0.104 or 0.105) gives

$$a \cong 0.4 \text{ ft/sec}^2 ,$$

which may be ignored when compared with  $0.7 g = 22.54 \text{ ft/sec}^2$ . The dynamic loads from the angular acceleration are therefore negligible.

#### Thermal Deflection and Stresses of the Spacer Bar\*

Temperature gradients exist in the spacer bars that separate the fuel containers of the second and third coolant passes. The gradients are assumed to be identical and to cause each spacer bar to bow in the direction of the higher temperature. The spacer bars thus apply line

---

\*The author is indebted to S. E. Moore for the analysis contained in this section.

loads on the fuel containers. If a line load is appreciable, it must be considered in the design of the fuel container. Since the spacer bar is supported by the fuel container, it will behave as a beam on an elastic foundation loaded with a temperature distribution, where the foundation modulus is determined by the container wall thickness.

#### The Beam on an Elastic Foundation Loaded with a Temperature Distribution

The deflection of a beam on an elastic foundation with a temperature distribution linear through the thickness and arbitrary with the length,  $T = Ky f(z)$ , can be treated as the sum of the free deflection produced by the temperature  $w_t$  and the deflection caused by the resistance of the foundation  $w_f$ ,

$$w = w_t + w_f , \quad (1)$$

where the positive direction is downward (Fig. B2). The free deflection may be found by the method used in the analysis of the EGCR graphite columns,<sup>3</sup> where it was shown that the curvature of a beam with a linear temperature distribution is

$$\frac{d^2 w_t}{dz^2} = -\alpha \frac{\partial T}{\partial y} . \quad (2)$$

Integrating twice

$$w_t = -\alpha \iint \frac{\partial T}{\partial y} dz^2 + C_1 z + C_2 . \quad (3)$$

#### Deflections Caused by Temperature Distribution

The temperatures in the spacer bar were determined numerically for design conditions at points  $(x,y)$  for four cross sections 24 in. apart

---

<sup>3</sup>S. E. Moore and W. A. Shaw, "EGCR Core Structural Analysis, The Effects of Fast-Neutron Irradiation and the Bowing Characteristics of the Graphite Columns," USAEC Report ORNL CF-61-3-69, Oak Ridge National Laboratory, April 14, 1961.

along the spacer bar<sup>4</sup> (Fig. B3). For small deflections it can be assumed that plane sections remain plane and that nonlinear terms in the temperature distribution do not contribute to the deflection. Consequently, a plane was fitted to these data by the method of least squares, giving a linear temperature distribution through the beam at each cross section of the form

$$T_i = A_i x + B_i y + C_i ,$$

with  $A_i$  identically zero because of symmetry. The four planes define the following axial temperature function:

$$T = \frac{1}{l} \left\{ \left[ B_4 z + B_1 (l - z) - a l \sin \frac{2\pi z}{l} \right] y + \left[ C_4 z + C_1 (l - z) \right] \right\} . \quad (4)$$

The unrestrained temperature deflection for a beam with pinned ends is then

$$w_t = -\frac{\alpha}{l} \left[ \frac{B_4 z^3}{6} + B_1 \left( \frac{l z^2}{2} - \frac{z^3}{6} \right) + \frac{a l^3}{4\pi^2} \sin \frac{2\pi z}{l} \right] + \alpha l z \left( \frac{B_4}{6} + \frac{B_1}{3} \right) . \quad (5)$$

#### The Beam on an Elastic Foundation

The deflection caused by the resistance of the foundation may be found from the ordinary beam relations. For a beam that is loaded with a distributed force that is proportional to the deflection,

$$\frac{d^4 w_f}{dz^4} = -\frac{k}{EI_x} w . \quad (6)$$

Substituting the fourth derivatives of Eq. 1 and Eq. 5 into Eq. 6 results

---

<sup>4</sup>T. D. Anderson, "A Thermal Analysis of Zircaloy Fuel Element Containers for the N.S. Savannah Reactor," USAEC Report ORNL-TM-197, Oak Ridge National Laboratory, Nov. 16, 1962.

in the nonhomogeneous equation for the beam on an elastic foundation:

$$\frac{d^4 w}{dz^4} + \frac{k}{EI_x} w = - \frac{4\pi^2 a\alpha}{(\beta l)^2} \sin \frac{2\pi z}{l} . \quad (7)$$

The solution to this equation is

$$w = \sum_{n=1}^4 A_n N_n - \frac{\pi^2 (\beta l)^2 a\alpha}{\pi^4 + (\beta l)^4} \sin \frac{2\pi z}{l} , \quad (8)$$

where

$$\beta^4 = \frac{k}{4EI_x} ,$$

$$N_1 = e^{-\beta z} \sin \beta z \text{ (see ref. 5),}$$

$$N_2 = e^{-\beta z} \cos \beta z ,$$

$$N_3 = e^{\beta z} \sin \beta z ,$$

$$N_4 = e^{\beta z} \cos \beta z ,$$

$$A_n = \text{arbitrary coefficients.}$$

Since no stresses are produced by the temperature deflection, the moment,  $M$ , is a function of only the foundation deflection  $w_f$ ; thus,

$$M(z) = -EI_x \left\{ \beta^2 \sum_{n=1}^4 A_n N_n'' + \left[ \frac{4\pi^4 \beta^2}{\pi^4 + (\beta l)^4} - 1 \right] a\alpha \sin \frac{2\pi z}{l} + \frac{\alpha}{l} [B_4 z + B_1 (l - z)] \right\} , \quad (9)$$

where

$$N_n'' = \frac{d^2 N_n}{d(\beta z)^2} .$$

---

<sup>5</sup>These functions and their derivatives are tabulated for values of  $(\beta z)$  from 0 to 10 in "Stress Analysis of Cylindrical Shells," by F. J. Stanek, USAEC Report ORNL CF-58-9-2, Oak Ridge National Laboratory, July 22, 1959.

The Deflection of the Spacer Bar

Approximate physical dimensions of the stainless steel core, the materials properties of Zircaloy,<sup>6</sup> and the constants of the temperature function (Eq. 4) are listed below.

Temperature Constants

$$\begin{aligned} B_1 &= -0.49605 & B_4 &= 15.60867 \\ C_1 &= 514.08785 & C_4 &= 510.82823 \\ a &= 1.37692 & l &= 72 \end{aligned}$$

Material Constants

$$\begin{aligned} E &= 12.4 \times 10^6 \text{ psi, transverse at } 500^\circ\text{F,} \\ &= 11.2 \times 10^6 \text{ psi, longitudinal at } 500^\circ\text{F,} \\ \nu &= 0.4, \\ \alpha &= 3.71 \times 10^{-6} \text{ in./in. per } ^\circ\text{F.} \end{aligned}$$

Geometric Constants

$$\begin{aligned} k &= 1000 \text{ lb/in.}\cdot\text{in.} & I_x &= 0.0374 \text{ in.}^4 \\ \beta &= 0.156 \text{ in.}^{-1} & \beta l &= 11.25 \end{aligned}$$

Since the dimensionless quantity  $\beta l$  is greater than  $2\pi$ , the beam may be considered to be semi-infinite. Therefore the arbitrary constants for the pinned-end case are

$$A_1 = \frac{\alpha B_1}{2}$$

$$A_2 = A_3 = A_4 = 0 .$$

In order to consider the effect of the pin at  $z = l$ , the origin is translated to  $z = l$  by the variable change

$$\beta \eta = \beta l - \beta z .$$

---

<sup>6</sup>C. L. Whitmarsh, "Review of Zircaloy-2 and Zircaloy-4 Properties Relevant to N.S. Savannah Reactor Design," USAEC Report ORNL-3281, Oak Ridge National Laboratory, July 9, 1962.

The complete deflection equation is then

$$w = \frac{\alpha B_1}{2} N_1(\beta z) + \frac{\alpha B_4}{2} N_1(\beta \eta) - \frac{\pi^2 (\beta l)^2 a \alpha}{\pi^4 + (\beta l)^4} \sin \frac{2\pi z}{l} .$$

The maximum deflection is

$$w_{\max} = 9.3 \times 10^{-6} \text{ in.},$$

at  $z = 66.9$  in. This deflection is negligible.

The moment equation may be found in the same manner; however, since the deflections are small enough to be neglected, a conservative estimate can be obtained by assuming that the beam is completely restrained.

#### Stresses in the Spacer Bar

Using the second derivative of Eq. (5), the bending stress is

$$\sigma_b \cong \pm \frac{cE\alpha}{l} \left[ B_4 z + B_1(l - z) - a l \sin \frac{2\pi z}{l} \right] ,$$

where  $c$  is one-half the depth of the beam, from which the maximum  $\sigma_b = 240$  psi at  $z = 72$  in. Additional stresses are caused by the difference between the temperatures calculated by using Eq. 4 and the temperatures calculated in ref. 4. A conservative estimate is given by

$$\sigma_t = E\alpha \Delta T .$$

The maximum  $\Delta T = 6.04^\circ\text{F}$ ; thus the maximum stress is

$$\sigma_{t_{\max}} = 250 \text{ psi} .$$

The maximum stress in the spacer bar will be equal to or less than the sum

$$\sigma_{\max} \leq \sigma_b + \sigma_t \leq 490 \text{ psi} ,$$

which is less than 3% of the allowable primary stress of 17,600 psi and therefore was not considered further.

#### Torsional Deformation in Second-Pass Fuel-Element Containers

It may be seen in Figs. 1 and C4 (Appendix C) that the right-hand walls of the leftmost second pass fuel-element containers are supported through spacer bars by the third-pass fuel-element containers, whereas the left-hand walls are relatively unsupported, and only the bottoms of the fuel-element containers are fixed against rotation. Consequently excessive deflections and significant stresses may develop in the fuel-element containers during a 30° roll (as indicated in Fig. C4, which shows a cross section of the core with both spacer bars and fuel elements omitted) when the fuel elements impose loads on the fuel-element container walls.

To determine the magnitude of the torsional stresses and deflections caused by such action, it was assumed that each second-pass fuel-element container was fixed at one end, simply supported along one wall at the other end, and subjected to the load of 1140 lb imposed by the fuel element when the ship was on its side and subjected to a vertical upward acceleration of 2 g. This condition is shown in Fig. B4. The torque imposed is  $(4.445)(1140) = 5060$  lb-in.

The angle of twist per unit length of container is given by<sup>7</sup>

$$\theta_1 = \frac{M_t s}{4GA^2 h},$$

where

$M_t$  = torque (in lb-in.),

$s$  = length of perimeter of mid-surface of fuel-element container wall (in.),

$G$  = modulus of rigidity (in psi),

---

<sup>7</sup>S. Timoshenko, Strength of Materials, p. 249, Part II, 3rd Ed., D. Van Nostrand, New York, 1956.

$A$  = area enclosed by mid-surface of container wall ( $\text{in.}^2$ ),

$h$  = thickness of container wall ( $\text{in.}$ ).

For the container loaded as shown in Fig. B4,

$$M_t = 5060 \text{ lb-in.},$$

$h \sim 0.1 \text{ in.}$ , using the thickness of the existing stainless steel containers,

$$s \sim 4(8.8) = 35.2 \text{ in.},$$

$$A \sim 77.2 \text{ in.}^2,$$

$$G = 5.22 \times 10^6 \text{ psi.}$$

Therefore, the angle of twist in the 80-in. length is

$$\theta_{80 \text{ in.}} = 0.00114 \text{ radians.}$$

With this angle of twist the vertical deflection of B because of torsion is 0.010 in.

The shearing stress, and the consequent normal stresses, from torsion are<sup>8</sup>  $\tau = \sigma = M_t/2Ah$ , where the previous nomenclature holds. The normal stress is approximately 300 psi.

When it is considered that the top of a fuel-element container is not completely free to rotate, that there is some support from adjacent second-pass containers, and that the thickness of the container wall will be 0.14 in., the deflection of 0.010 for point B and the normal stress of 300 psi are conservative. Furthermore, during normal operation these values are approximately half as large. Stress and deflection because of torque were therefore not considered further.

---

<sup>8</sup>Ibid., p. 248.

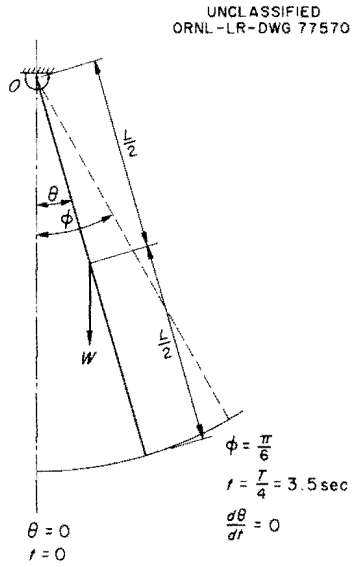


Fig. B1. A Rod Swinging in a Vertical Plane About an Axis at O.

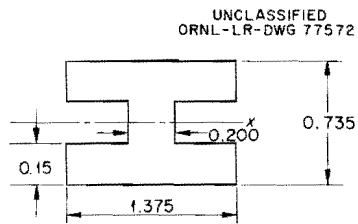


Fig. B3. Cross Section of Spacer Bar Used in Stainless Steel Fuel-Element Assembly.

ALL DIMENSIONS IN INCHES

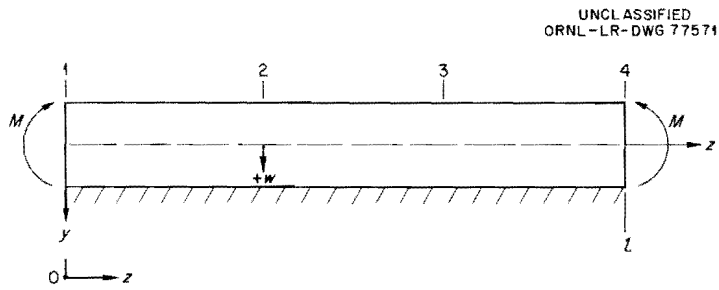


Fig. B2. A Beam of Finite Length on an Elastic Foundation.

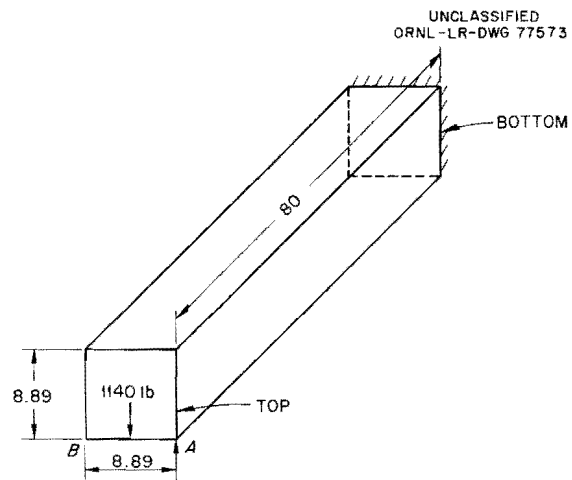


Fig. B4. Fuel-Element Container Loaded in Torsion.

Appendix C

## SELECTION OF MODELS FOR ANALYZING THE FUEL CONTAINERS

The significant stresses and deflections in the fuel-element containers are caused by the fuel-element loads imposed as a consequence of gravity and heaves and by pressure loadings, since it was shown in Appendix B that loads imposed by temperature gradients, twist caused by nonsymmetrical supports, and dynamic loads caused by the angular acceleration of the ship's roll are negligible. The selection of models for analyzing the fuel containers is discussed here.

Selection of a Model for Determining Stresses and Deflections  
Caused by Flexure of the Unit as a Whole

The data used in making the stress and deflection analyses necessary to select a conservative model are listed below:

1. The fuel containers were assumed to be 80 in. long. This is a conservative value, since Babcock and Wilcox Dwg. No. 10423F-4 indicates approximately 79 in. from center to center of supports where one end is fixed.
2. A modulus of elasticity of  $11 \times 10^6$  psi was assumed.<sup>1</sup>
3. Poisson's ratio,  $\mu$ , was assumed to be 0.4.
4. The weight of the fuel containers was assumed to be 100 lb.
5. The spacer bars and cover plates were assumed to weigh 9.5 lb each.
6. The cross-sectional dimensions used were those shown in Fig. C1, which were taken from Babcock and Wilcox drawing No. 10423F-4 and Massachusetts Institute of Technology drawing No. EPS-X-428.

Stresses and Deflections Obtained by Treating the Core Assembly as a Unit and Considering It To Be Simply Supported

The model requires that the 32 fuel containers shown in Fig. 1 be treated as a unit and considered as a builtup beam. The moment of inertia

---

<sup>1</sup>C. L. Whitmarsh, "Review of Zircaloy-2 and Zircaloy-4 Properties Relevant to N.S. Savannah Reactor Design," USAEC Report ORNL-3281, Oak Ridge National Laboratory, July 9, 1962.

of the cross section and the load of the whole assembly must therefore be determined.

The moment of inertia of the cross section with respect to its centroidal axis, which is the neutral axis, N.A., of the builtup section, is obtained by summing the moments of inertia of its several components with respect to the neutral axis. The basic dimensions are shown in Fig. C1. Minimum dimensions giving cross-sectional areas of 3,549 and 3,053 in.<sup>2</sup>, respectively, for the second- and third-pass fuel-element containers were used in calculating the required moment of inertia. The moment of inertia,  $I_x$ , of the cross section of a second-pass fuel-element container with respect to its own centroidal axis is obtained as follows:

$$\begin{aligned} I_x &= 2 \left[ \frac{1}{12} (0.106)(6.52)^3 \right] + 2[(6.52)(0.106)(4.438)^2] \\ &\quad + 4 \int_0^{\pi/2} (1.178 \sin \theta + 3.26)^2 (0.106)(1.178) d\theta \\ &= 44.8 \text{ in.}^4 . \end{aligned}$$

Similarly, for the third-pass fuel-element container,  $I_x = 38.7 \text{ in.}^4$ . Using these values for the moments of inertia of the fuel-element containers, the dimensions shown in Fig. C1, and neglecting the moments of inertia of the spacer bars, the moment of inertia of the cross section with respect to its neutral axis is

$$I = 27,200 \text{ in.}^4 .$$

The weight of the whole assembly, including the spacer bars, is 28,200 lb. The maximum shear in the builtup beam consisting of the fuel-element containers and separator bars is therefore

$$V = \frac{1}{2} (28,200)(3) = 42,300 \text{ lb}$$

when the ship is on its side and subjected to a vertical heave of 2 g.

The maximum shearing stress is given by<sup>2</sup>

$$\tau_{\max} = \frac{VQ}{Ib}, \quad (1)$$

where

$\tau_{\max}$  = shearing stress (in psi) at the neutral axis,

V = total force acting on the cross section parallel to the cross section (in lb),

Q = the first moment of that area of the cross section on either side of the neutral axis with respect to the neutral axis (in in.<sup>3</sup>),

I = moment of inertia of the cross section with respect to the neutral axis,

b = the width of the section at the neutral axis (in in.).

Here the values of V and I are those determined above,  $Q = 788 \text{ in.}^3$ ,  $b = 1.2 \text{ in.}$ , and therefore  $\tau_{\max} = 1020 \text{ psi}$ . This stress occurs in the spacer bars. For fuel-element containers having a wall thickness greater than 0.106 in., the stress will be less.

The maximum bending moment in the builtup beam will be at mid-span of the beam and will occur when core II type fuel elements are being used. Because of the load centrally imposed by the fuel elements, the mid-span bending moment will be  $R_2 \ell / 4$ , where  $\ell$  is the assumed length of 80 in. The bending moment from the loads imposed near the ends of the fuel-element containers by the fuel elements are assumed to be negligible because of the proximity of the supports. The bending moment at mid-span from the effective distributed total load,  $W_e$ , of the fuel-element containers and spacer bars is  $W_e \ell / 8$ . The resultant bending moment is

$$M = \left( R_2 + \frac{W_e}{2} \right) \frac{\ell}{4}.$$

---

<sup>2</sup>P. G. Laurson and W. J. Cox, Mechanics of Materials, p. 137, 3rd Ed., John Wiley and Sons, New York, 1954.

The resultant maximum flexure stress at mid-span is given by<sup>3</sup>

$$\sigma = \frac{Mc}{I},$$

where

$\sigma$  = flexure stress (in psi),

$M$  = resultant bending moment (in lb-in.),

$c$  = distance from the neutral axis of the cross section to the point in the cross section most distant from the neutral axis (in in.),

$I$  = moment of inertia, as previously defined.

Hence, the resultant bending stress for a simply supported beam subjected to a concentrated load,  $R_2$ , at mid-span and a total uniformly distributed effective load of  $W_e$  is

$$\sigma = \left( R_2 + \frac{W_e}{2} \right) \frac{lc}{4I}. \quad (2)$$

The maximum deflection will also occur at mid-span and is the sum<sup>4</sup>

$$\frac{R_2 l^3}{48EI} + \frac{5W_e l^3}{384EI},$$

that is, the sum of the deflections due respectively to the concentrated and the total uniformly distributed effective loads. The resultant deflection is

$$\delta = \left( R_2 + \frac{5W_e}{8} \right) \frac{l^3}{48EI}. \quad (3)$$

---

<sup>3</sup>Ibid., p. 129.

<sup>4</sup>Ibid., p. 407.

Here, for the ship on its side and subjected to a vertical heave of 2 g, where  $l$  and  $I$  are as previously noted,

$$R_2 = 1140(32) = 36,480 \text{ lb (from Appendix A, p. 17),}$$

$$W_e = (3850)3 = 11,500 \text{ lb, including 52 spacer bars and 16 cover plates,}$$

$$c = 28.78 \text{ in.,}$$

$$\sigma = 900 \text{ psi,}$$

$$\delta = 0.0015 \text{ in.}$$

Stresses and Deflections in a Single Fuel-Element Container Subjected to a Concentrated Load at Mid-Span and a Uniformly Distributed Load

For the beam shown in Fig. C2,

$$R_L = \frac{5}{8} W_e + \frac{11}{16} R_2$$

(see ref. 5),

$$R_R = \frac{3}{8} W_e + \frac{5}{16} R_2,$$

$$M_{\max} = \left( -\frac{3}{4} R_2 + \frac{W_e}{2} \right) \frac{l}{4},$$

$$\delta_{\max} = \left( 0.447R_2 + \frac{48}{185} W_e \right) \frac{l^3}{48EI},$$

if it is assumed that the maximum deflection from  $R_2$  and  $W_e$  are coincident.

For the beam shown in Fig. C3, the equations for the maximum bending moment and the maximum deflection are

$$M_{\max} = \left( R_2 + \frac{W_e}{2} \right) \frac{l}{4}$$

---

<sup>5</sup>American Institute of Steel Construction, Steel Construction, pp. 369-370, 5th Ed., New York, 1950.

and

$$\delta_{\max} = \left( R_2 + \frac{5}{8} W_e \right) \frac{\ell^3}{48EI} ,$$

as determined above.

Comparison of the values of  $M_{\max}$  and  $\delta_{\max}$  for the models shown in Figs. C2 and C3 indicates that the simple beam is the more conservative model of the two. With the ship on its side and with a vertical heave of 2 g, the maximum bending stress, the maximum deflection, and the maximum shearing stress in the fuel-element container considered as a simply supported beam and using third-pass dimensions are:

$$\sigma_{\max} = 3000 \text{ psi} ,$$

$$\delta_{\max} = 0.033 \text{ in.} ,$$

$$\tau_{\max} = 460 \text{ psi} .$$

#### Comparison of the Two Simply-Supported Models

The values of the stresses and deflections for the whole assembly and for a single fuel-element container treated as a simple beam are tabulated below for the condition when the ship is on its side and subjected to a vertical heave of 2 g:

| <u>Model</u>                  | <u>Bending<br/>Stress<br/>(psi)</u> | <u>Deflection<br/>(in.)</u> | <u>Shearing<br/>Stress<br/>(psi)</u> |
|-------------------------------|-------------------------------------|-----------------------------|--------------------------------------|
| Builtup beam                  | 900                                 | 0.00154                     | 1020                                 |
| Single fuel-element container | 3000                                | 0.033                       | 460                                  |

Thus, a comparison of the two models may be made.

It is obvious that insofar as these stresses and deflections are concerned, either model indicates that the core structure is satisfactory. There is doubtless some shear lag effect in both, but this will not be great, since the ratio of the length to the width of the fuel-element container is about 9. Shear lag was therefore neglected. Since the

bending stress and deflection of the single fuel-element container greatly exceed those of the assembly and since the shearing stress in the assembly is not critical, the single fuel-element container treated as a simple beam has been conservatively chosen as the model for dealing with deflections and stresses from beam action.

Comments on Stresses and Deflections Caused by Flexure of the Unit  
As a Whole

It is to be noted that the analysis thus far assumes core II type fuel elements and ignores the deflection and the bending stresses (which are small) caused by the loads applied by the fuel element near the ends of the fuel-element containers. The small values obtained for  $\sigma_{\max}$  and  $\delta_{\max}$  for the unusual condition of the ship on its side with a vertical heave of 2 g indicate that there is no need for concern because of this simplified approach. For core I type fuel elements, the values of  $\sigma_{\max}$  and  $\delta_{\max}$  at the core mid-height will be smaller than those computed above because there will be no concentrated load at the core mid-height.

Selection of a Model for Considering Stresses  
and Deflections Caused by Localized Action

Thus far in this appendix, consideration has been given only to the stresses and deflections from flexure of a unit as a whole. It was also necessary to select a model for determining the stresses and deflections from localized action. For orientation, it is assumed that the ship is in a 30° clockwise roll and that one is looking at Section A-A in Fig. C4. Column 1 consists of second-pass containers only, and column 2 consists of four intermediate third-pass containers with second-pass containers at top and bottom.

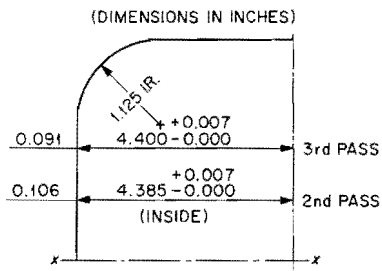
The second-pass containers are all subjected to a positive internal pressure and their left faces receive no support from an adjacent container. Simple supports at the upper corners have therefore been assumed for column 1 in order to allow the sides of the containers to deflect freely. The third-pass containers are subjected to a negative internal pressure, and each is supported by an adjacent container on every side. Furthermore,

the supports of these third-pass containers are such that there should be little, if any, rotation at the supports, and hence fixed supports were assumed on the third-pass containers. The right supports of the second-pass containers at the top and bottom of column 2 are likewise somewhat fixed against rotation by adjacent containers, but the left sides are more or less free; it was shown, however, on pages 30 to 31 that extreme nonsymmetrical loading in the form of torsion causes no appreciable stress or deformation in the fuel-element container wall. Therefore, the second-pass containers in column 2 were assumed to be symmetrically supported by simple supports at the mid-points of their sides. It is assumed that these simple supports are a reasonable symmetrical substitute for the nonsymmetrical supports they replace.

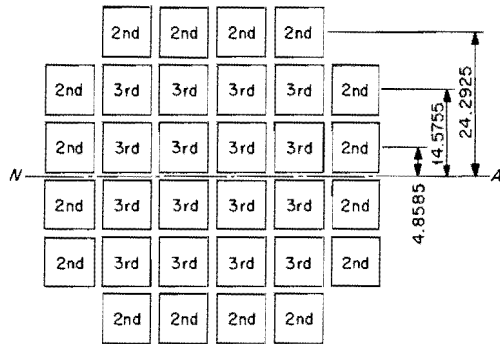
The intermediate frames in the respective columns were assumed to be identical in loading, stresses, and deflections. Therefore, the models selected consist of three containers each, as shown in Fig. C5.

It is seen in Fig. C1 that the existing third-pass container has a center-to-center wall dimension of 8.891 in. This is slightly more than that of the second-pass container and is used as the length of the sides of the rigid-frame models. The dimension  $a$  was assumed to be equal to 1.325 in. and was obtained from General Electric Sheets No. 101F544 entitled "Bottom Tie Plate" and No. 585D189 entitled "Top Tie Plate."

UNCLASSIFIED  
ORNL-LR-DWG 77574



(a) QUARTER SECTION OF FUEL-ELEMENT CONTAINER



(b) CROSS SECTION OF BUILT-UP BEAM  
(SPACER BARS OMITTED)

Fig. C1. Beam Sections.

UNCLASSIFIED  
ORNL-LR-DWG 77575

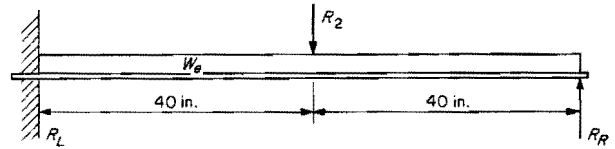


Fig. C2. Fuel-Element Container as a Beam Fixed at One End and Simply Supported at the Other.

UNCLASSIFIED  
ORNL-LR-DWG 77576

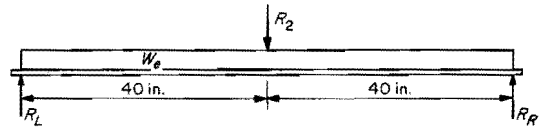


Fig. C3. Fuel-Element Container as a Simply Supported Beam.

UNCLASSIFIED  
ORNL-LR-DWG 64515A

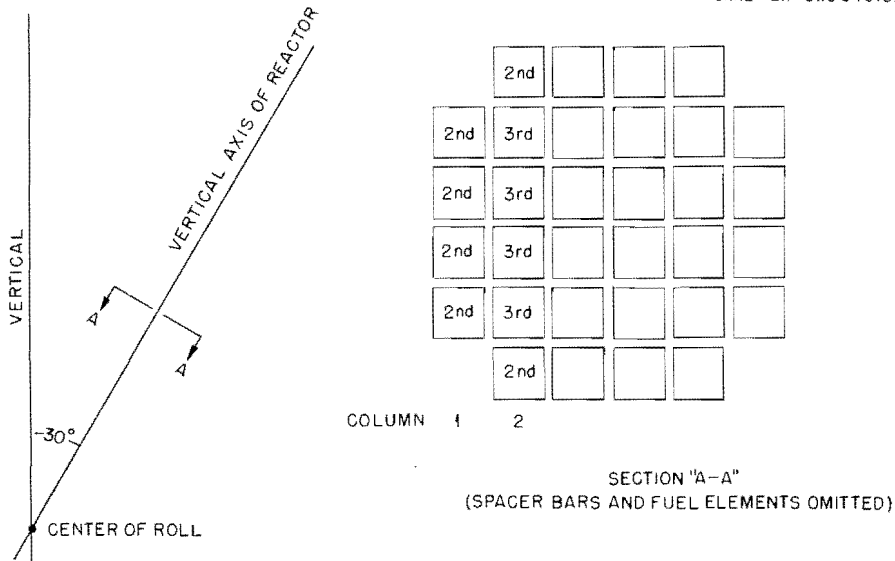


Fig. C4. Orientation of NS SAVANNAH Fuel-Element Containers Used in Analyzing Stresses Arising from Plate Action.

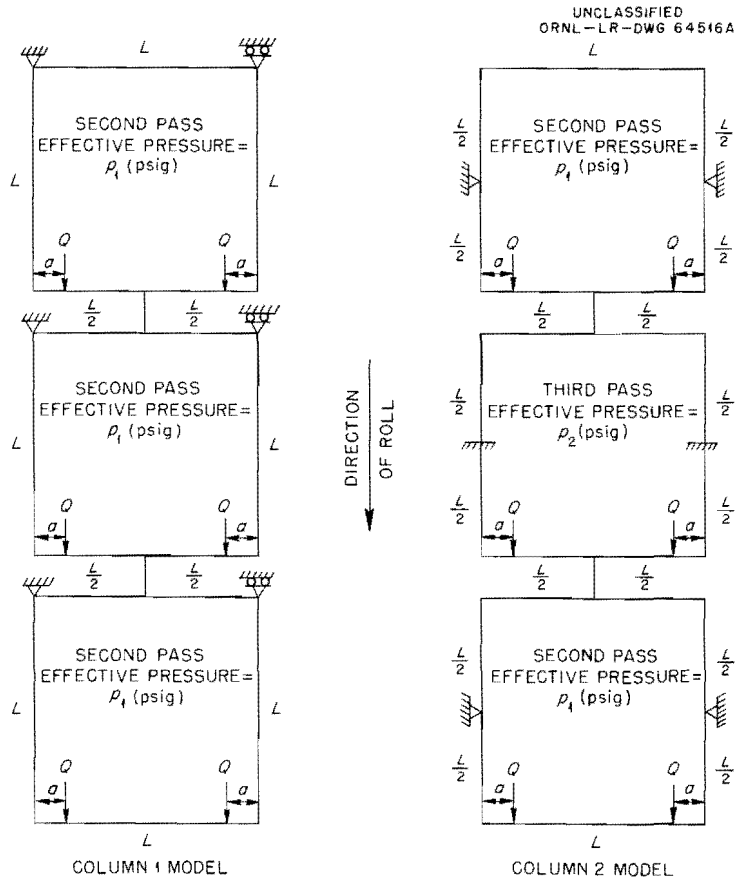


Fig. C5. Container Assembly Models Used in Analyzing Stresses from Plate Action of NS SAVANNAH Fuel-Element Containers.

Appendix D

## RIGID-FRAME ANALYSIS

Examination of the stresses and deflections in the models selected in Appendix C for localized action required analyses of three rigid basic frames. The three basic frames will be designated case I, case II, and case III, respectively, and are as shown in Fig. D1.

Method of Analysis

These frames were analyzed by the slope-deflection method wherein, by properly associating the rotations of the tangents to the elastic curve and the deflections at the ends of the individual members, standard equations for the end moments could be formulated in terms of the fixed-end moments, rotations, and deflections. The nomenclature and conventions used are those suggested by Carpenter.<sup>1</sup> Definitions of the nomenclature, conventions, and a brief outline of the method are given by utilizing Fig. D2, where

$M_{AB}^F$  = the bending moment at joint A in the beam AB, assuming both ends fixed; a clockwise moment on joint A is positive;

$M_{BA}^F$  = the bending moment at joint B in the beam AB, assuming both ends fixed; a clockwise moment on joint B is positive;

$\theta_A$  = the angle of rotation (in radians) of joint A; clockwise rotation of the joint is positive;

$\theta_B$  = the angle of rotation (in radians) of joint B; clockwise rotation of the joint is positive;

$M_{AB}$  = the actual bending moment at A in the beam AB after all relaxation has been accomplished;

---

<sup>1</sup>S. T. Carpenter, Structural Mechanics, pp. 189-198, John Wiley and Sons, New York, 1960.

$M_{BA}$  = the actual bending moment at B in the beam AB after all relaxation has been accomplished.

Since symmetrical supports were assumed (see p. 8), it is assumed that symmetrical deflections will occur. Consequently, there will be no relative vertical deflection of A with respect to B in Fig. D2. Development of the standard equation as it applies to the three basic frames involves the following three steps:

1. Assume that ends A and B of the member AB are momentarily locked against rotation. The loading on the member then produces the fixed end moments  $M_{AB}^F$  and  $M_{BA}^F$ , which are respectively positive and negative as shown in Fig. D2b.

2. With end B still locked and with  $M_{AB}^F$  still acting at A, a clockwise moment  $M'_{AB}$  is added at A to cause the assumed clockwise rotation  $\theta_A$  of the final configuration at A. It can be shown by area moment methods that the magnitude of  $M'_{AB} = 4EI\theta_A/L$  and that the moment at B is increased in magnitude by  $M'_{AB}/2$  or  $2EI\theta_A/L$ . The resultant moments at A and B are now

$$M_{AB}^F - M'_{AB}$$

and

$$-\left(M_{BA}^F + \frac{M'_{BA}}{2}\right),$$

as shown in Fig. D2c.

3. With the moments unchanged, B is unlocked. A clockwise moment  $M'_{BA}$  is then applied to cause the assumed clockwise rotation  $\theta_B$  of the final configuration at B. Again, by area moment methods, it can be shown that the magnitude of  $M'_{BA} = 4EI\theta_B/L$  and that the moment at A is decreased by  $M'_{BA}/2$  or  $2EI\theta_B/L$ , while  $\theta_A$  remains unchanged. The resultant moments at A and B are now

$$\begin{aligned}
 M_{AB} &= M_{AB}^F - M'_{AB} - \frac{M'_{BA}}{2} \\
 &= M_{AB}^F - \frac{4EI\theta_A}{L} - \frac{2EI\theta_B}{L},
 \end{aligned}$$

and

$$\begin{aligned}
 M_{BA} &= - \left( M_{BA}^F + \frac{M'_{AB}}{2} + M'_{BA} \right) \\
 &= - \left( M_{BA}^F + \frac{2EI\theta_A}{L} + \frac{4EI\theta_B}{L} \right).
 \end{aligned}$$

It is to be noted that the angles  $\theta_A$  and  $\theta_B$  are both assumed to be positive, as shown, so that the sign convention will be a general one and will ensure that any computed value of an angle may be interpreted correctly. For other members of the frame, the moments  $M_{ij}$  may also be expressed in terms of  $\theta_i$  and  $\theta_j$  in a similar way, and all moments are expressed in terms of fixed-end moments and angles of rotation. At A,  $M_{AC} + M_{AB} = 0$ . Corresponding equations may be written for other joints, and the method reduces to solving a system of  $n$  equations in  $n$  unknowns.

Attention is called to the fact that a positive value for  $M_{AB}$  indicates tension in the top of the member AB at A, whereas a positive value for  $M_{BA}$  indicates compression in the top of the member AB at B. In constructing the bending diagrams, the simply supported beam convention is used unless otherwise noted, that is, tension in the bottom fibers is considered positive. Hence, a negative value for  $M_{AB}$  (tension in bottom) is treated as positive in constructing the bending-moment diagrams.

#### Analyses of the Three Basic Frames

General equations for the three basic frames described at the first of this appendix are obtained by the method outlined briefly above. Because of symmetry, it is necessary to consider only half the frame in every case.

The fixed-end moments, which may be determined by elementary methods, are as follow (refer to Fig. D3):

Case I

$$M_{AF}^F = \frac{Qa(L-a)}{L} - \frac{PL}{8} + \frac{pL^2}{12},$$

$$M_{AB}^F = -\frac{pL^2}{48},$$

$$M_{BA}^F = +\frac{pL^2}{48},$$

$$M_{BC}^F = -\frac{pL^2}{48},$$

$$M_{CB}^F = +\frac{pL^2}{48},$$

$$M_{CD}^F = +\frac{RL}{8} - \frac{pL^2}{12}.$$

The expressions for the moments in terms of the slopes are the following:

$$M_{AB} = \frac{2EI}{L/2} (-2\theta_A - \theta_B) - \frac{pL^2}{48} = -\frac{8EI\theta_A}{L} - \frac{4EI\theta_B}{L} - \frac{pL^2}{48},$$

$$M_{BA} = \frac{2EI}{L/2} (-2\theta_B - \theta_A) + \frac{pL^2}{48} = -\frac{4EI\theta_A}{L} - \frac{8EI\theta_B}{L} + \frac{pL^2}{48},$$

$$M_{AF} = \frac{2EI}{L} (-2\theta_A - \theta_F) + \frac{Qa(L-a)}{L} - \frac{PL}{8} + \frac{pL^2}{12},$$

and, since  $\theta_F = -\theta_A$ ,

$$M_{AF} = -\frac{2EI\theta_A}{L} + \frac{Qa(L-a)}{L} - \frac{PL}{8} + \frac{pL^2}{12};$$

$$M_{BC} = \frac{2EI}{L/2} (-2\theta_B - \theta_C) - \frac{pL^2}{48} = -\frac{8EI\theta_B}{L} - \frac{4EI\theta_C}{L} - \frac{pL^2}{48},$$

$$M_{CB} = \frac{2EI}{L/2} (-2\theta_C - \theta_B) + \frac{pL^2}{48} = -\frac{4EI\theta_B}{L} - \frac{8EI\theta_C}{L} + \frac{pL^2}{48},$$

$$M_{CD} = -\frac{2EI}{L} (-2\theta_C - \theta_D) + \frac{RL}{8} - \frac{pL^2}{12},$$

and, since  $\theta_D = -\theta_C$ ,

$$M_{CD} = -\frac{2EI\theta_C}{L} + \frac{RL}{8} - \frac{pL^2}{12}.$$

By setting the sum of the moments at any joint equal to zero, three equations are obtained in terms of the slopes  $\theta_A$ ,  $\theta_B$ , and  $\theta_C$ :

For  $M_{AB} + M_{AF} = 0$ ,

$$-\frac{8EI\theta_A}{L} - \frac{4EI\theta_B}{L} - \frac{pL^2}{48} - \frac{2EI\theta_A}{L} + \frac{Qa(L-a)}{L} - \frac{PL}{8} + \frac{pL^2}{12} = 0,$$

$$5\theta_A + 2\theta_B = -\frac{PL^2}{16EI} + \frac{Qa(L-a)}{2EI} + \frac{pL^3}{32EI}. \quad (1)$$

For  $M_{BA} + M_{BC} = 0$ ,

$$\theta_A + 4\theta_B + \theta_C = 0. \quad (2)$$

For  $M_{CB} + M_{CD} = 0$ ,

$$2\theta_B + 5\theta_C = \frac{RL^2}{16EI} - \frac{pL^3}{32EI} \quad (3)$$

Simultaneous solution of Eqs. (1), (2), and (3) yields expressions for  $\theta_A$ ,  $\theta_B$ , and  $\theta_C$  in terms of the applied loads:

$$\theta_A = \frac{L^2}{640EI} \left[ -9P + R + \frac{72Qa(L-a)}{L^2} + 4pL \right], \quad (4)$$

$$\theta_B = \frac{L^2}{256EI} \left[ P - R - \frac{8Qa(L-a)}{L^2} \right], \quad (5)$$

$$\theta_C = \frac{L^2}{640EI} \left[ 9R - P - 4pL + \frac{8Qa(L-a)}{L^2} \right]. \quad (6)$$

With the slopes known, the expressions for the moments and deflections in terms of the applied loads are determined, as follows:

$$M_{AB} = \frac{L}{960} \left[ 93P + 3R - \frac{744Qa(L-a)}{L^2} - 68pL \right], \quad (7)$$

$$M_{AF} = -M_{AB}, \quad (8)$$

$$M_{BA} = \frac{L}{240} \left[ 6P + 6R - \frac{48Qa(L-a)}{L^2} - pL \right], \quad (9)$$

$$M_{BC} = -M_{BA}, \quad (10)$$

$$M_{CB} = \frac{L}{960} \left[ -3P - 93R + \frac{24Qa(L-a)}{L^2} + 68pL \right], \quad (11)$$

$$M_{CD} = -M_{CB} . \quad (12)$$

Use of these bending moments permits the determination of the end reactions and construction of the bending-moment diagrams, by parts, for the beams making up the frame. Because of the assumed symmetry of the whole frame, there is a horizontal tangent to the elastic curve at the mid-point of each of beams AF and CD, and the bending-moment diagrams, by parts, are needed for only the left halves of these beams. Beams AF and CD and their respective diagrams and elastic curves are shown in Figs. D4 and D5. The upward vertical displacement of end A of beam AF with respect to the horizontal tangent at K,  $\delta_{A/\tan K}$ , is equal in magnitude to the downward vertical deflection of K,  $\delta_K$ . A similar statement may be made for beam BC. Through use of the Second Area-Moment Proposition,<sup>2</sup> the vertical deflection of the mid-points of the beams may be determined.

From Fig. D4,

$$\begin{aligned}
 + \uparrow EI\delta_{A/\tan K} &= + \left( \frac{QL}{2} + \frac{pL^2}{4} - \frac{PL}{4} \right) \frac{L}{4} \frac{L}{3} - M_{AF} \frac{L}{2} \frac{L}{4} \\
 &\quad - \frac{Q[(L/2) - a]^2}{2} \frac{L+a}{3} - \frac{pL^2}{8} \frac{L}{6} \frac{3L}{8} , \\
 + \downarrow EI\delta_K &= \frac{1}{7680} (-67PL^3 + 216QaL^2 + 744Qa^2L \\
 &\quad - 1280Qa^3 + 32pL^4 + 3RL^3) . \quad (13)
 \end{aligned}$$

From Fig. D5,

$$\begin{aligned}
 + \uparrow EI\delta_{C/\tan N} &= + \frac{pL^2}{8} \frac{L}{6} \frac{3L}{8} - M_{CD} \frac{L}{2} \frac{L}{4} - \frac{pL^2}{4} \frac{L}{4} \frac{L}{3} + \frac{RL}{4} \frac{L}{4} \frac{L}{3} , \\
 + \downarrow EI\delta_N &= \frac{1}{7680} (-3PL^3 + 67RL^3 + 24QaL^2 - 24Qa^2L - 32pL^4) . \quad (14)
 \end{aligned}$$

<sup>2</sup>P. G. Laurson and W. J. Cox, Mechanics of Materials, p. 169, 3rd Ed., John Wiley and Sons, 1954.

Case II

The procedure of case I was followed in the analysis of case II. Only the final forms of the slope, moment, and deflection equations are listed. For the frame shown in Fig. D6,

$$\theta_B = 0, \quad (15)$$

$$\theta_A = \frac{L^2}{160EI} \left[ \frac{16Qa(L-a)}{L^2} - 2P + pL \right], \quad (16)$$

$$M_{AB} = \frac{L}{240} \left[ 24P - \frac{192Qa(L-a)}{L^2} - 17pL \right], \quad (17)$$

$$M_{AF} = -M_{AB}, \quad (18)$$

$$M_{BA} = \frac{L}{240} \left[ 12P - \frac{96Qa(L-a)}{L^2} - pL \right], \quad (19)$$

$$+ \delta_J = \frac{1}{240} (-2PL^3 + 6QaL^2 + 24Qa^2L - 40Qa^3 + pL^4). \quad (20)$$

Case III

The procedure used for case III was the same or similar to that for the previous two cases, and therefore only equations in their final form are listed. For the frame of Fig. D7,

$$\theta_A = \frac{L^2}{128EI} \left[ -3P - R + \frac{24Qa(L-a)}{L^2} \right], \quad (21)$$

$$\theta_B = \frac{L^2}{128EI} \left[ P + 3R - \frac{3Qa(L-a)}{L^2} \right], \quad (22)$$

$$M_{AB} = \frac{L}{192} \left[ 15P - 3R - \frac{120Qa(L-a)}{L^2} - 16pL \right], \quad (23)$$

$$M_{AD} = -M_{AB}, \quad (24)$$

$$M_{BA} = \frac{L}{192} \left[ 3P - 15R - \frac{24Qa(L-a)}{L^2} + 16pL \right], \quad (25)$$

$$M_{BC} = -M_{BA}, \quad (26)$$

$$+ \uparrow EI\delta_G = \frac{1}{1536} (-17PL^3 + 72QaL^2 + 120Qa^2L - 3RL^3 - 256Qa^3 + 4pL^4), \quad (27)$$

$$+ \downarrow EI\delta_H = \frac{1}{1536} [17RL^3 + 3PL^3 - 24Qa(L-a)L - 4pL^4], \quad (28)$$

$$+ \uparrow EI\delta_E = \frac{1}{1536} [6PL^3 + 6RL^3 - 48Qa(L-a)L + 4pL^4]. \quad (29)$$

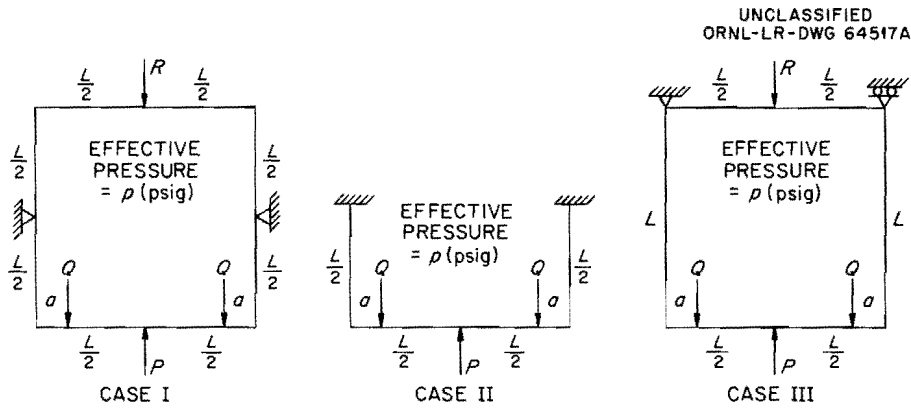


Fig. D1. Basic Rigid-Frame Models Used in Stress Analysis of NS SAVANNAH Fuel-Element Containers.

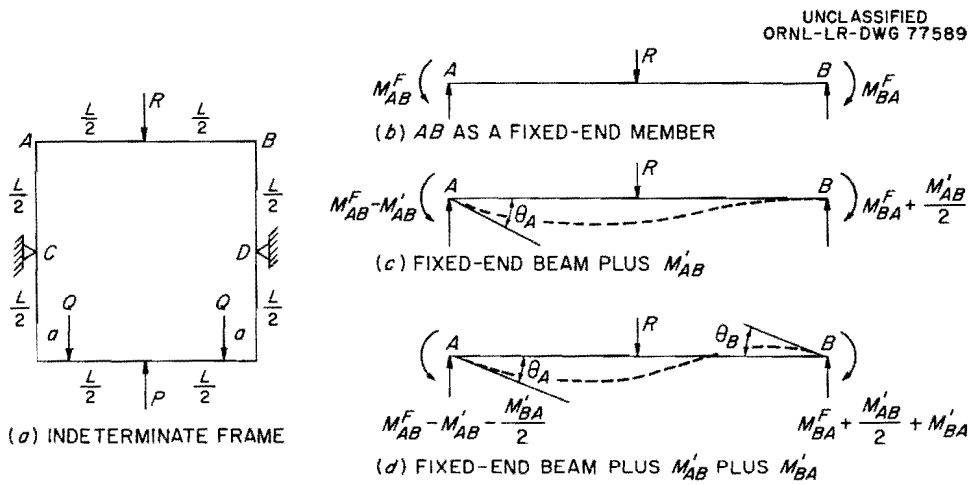


Fig. D2. Steps in Developing the Slope -Deflection Method.

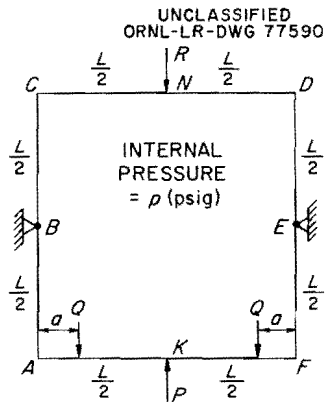


Fig. D3. Basic Frame of Case I.

UNCLASSIFIED  
ORNL-LR-DWG 77591

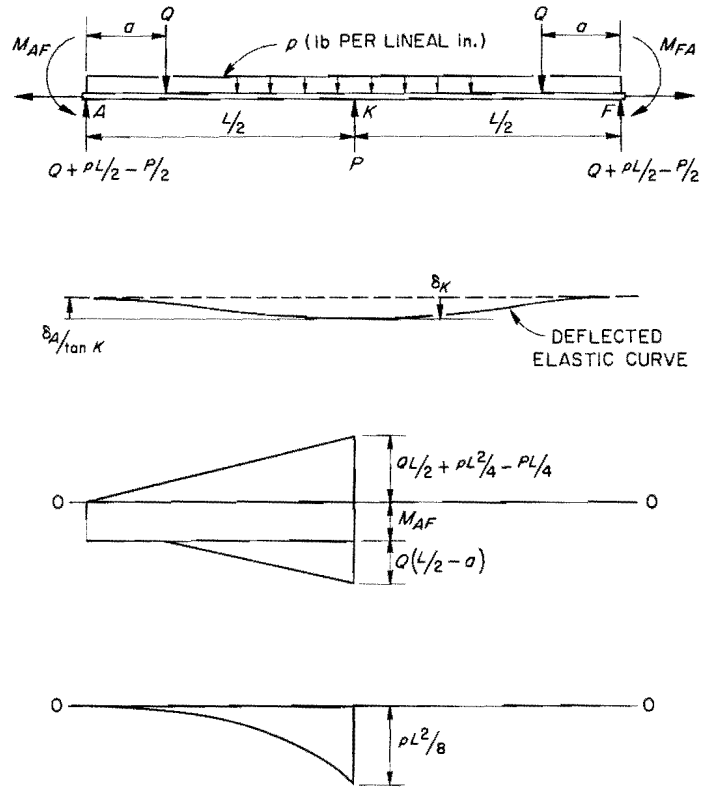


Fig. D4. Bending Moment Diagram by Parts for Half of Beam AF for Basic Frame of Case I.

UNCLASSIFIED  
ORNL-LR-DWG 77592

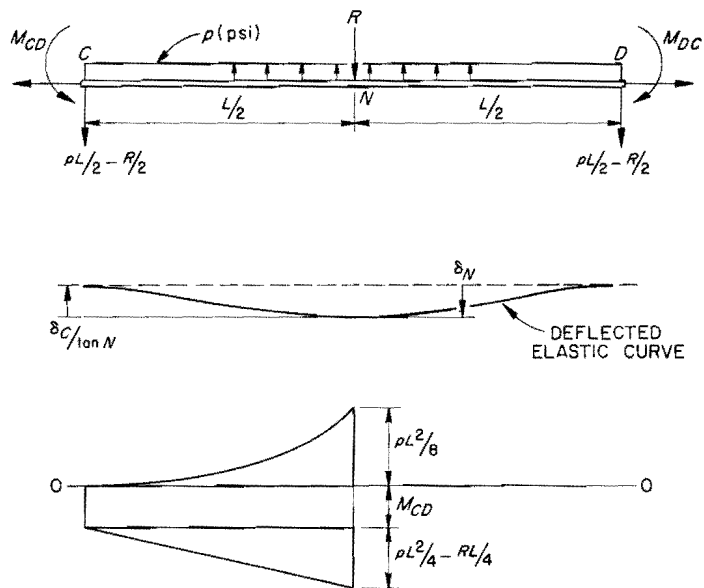


Fig. D5. Bending Moment Diagram by Parts for Half of Beam CD for Basic Frame of Case I.

$$\frac{dy}{dx} = \pm \frac{P\lambda^2}{k} B_{\lambda|x-e|} + \frac{q\lambda}{2k} [A_{\lambda x} - A_{\lambda(l-x)}] + \frac{q_0}{2k\ell} [D_{\lambda(l-x)} + D_{\lambda x} + \lambda\ell A_{\lambda x} - 2],$$

$$M = \frac{P}{4\lambda} C_{\lambda|x-e|} + \frac{q}{4\lambda^2} [B_{\lambda x} + B_{\lambda(l-x)}] + \frac{q_0}{8\lambda^3\ell} [A_{\lambda x} - A_{\lambda(l-x)} + 2\lambda\ell B_{\lambda x}],$$

and

$$Q = \pm \frac{P}{2} D_{\lambda|x-e|} + \frac{q}{4\lambda} [C_{\lambda x} - C_{\lambda(l-x)}] - \frac{q_0}{4\lambda^2\ell} [B_{\lambda x} + B_{\lambda(l-x)} - \lambda\ell C_{\lambda x}].$$

The first terms in the equations for  $dy/dx$  and  $Q$  are positive for  $x < e$  and negative for  $x \geq e$ . In these expressions,

$$\begin{aligned} A_{\lambda x} &= e^{-\lambda x} (\cos \lambda x + \sin \lambda x) \\ A_{\lambda|x-e|} &= e^{-\lambda|x-e|} (\cos \lambda|x-e| + \sin \lambda|x-e|) \\ B_{\lambda x} &= e^{-\lambda x} \sin \lambda x \\ B_{\lambda|x-e|} &= e^{-\lambda|x-e|} \sin \lambda|x-e| \\ C_{\lambda x} &= e^{-\lambda x} (\cos \lambda x - \sin \lambda x) \\ C_{\lambda|x-e|} &= e^{-\lambda|x-e|} (\cos \lambda|x-e| - \sin \lambda|x-e|) \\ D_{\lambda x} &= e^{-\lambda x} \cos \lambda x \\ D_{\lambda|x-e|} &= e^{-\lambda|x-e|} \cos \lambda|x-e| \end{aligned}$$

$$\lambda = \left( \frac{k}{4EI} \right)^{1/4}$$

$k$  = the foundation modulus (in pounds per lineal inch of beam per inch of deflection).

The functions  $A_x$ ,  $B_x$ ,  $C_x$ , and  $D_x$  have been evaluated and tabulated<sup>2</sup> for  $0 \leq x \leq 8$ . Use of these values greatly facilitates the longhand numerical evaluation of a beam on an elastic foundation.

The deflection, slope, moment, and shear at point A of the infinite beam are obtained by setting  $x = 0$ . For  $x = 0$ ,  $A_0 = C_0 = D_0 = 1$  and  $B_0 = 0$ . Therefore,

$$y_A = \frac{P\lambda}{2k} A_{\lambda e} + \frac{q}{2k} (1 - D_{\lambda l}) + \frac{q_0}{4\lambda k l} (C_{\lambda l} - 1 + 2\lambda l),$$

$$\frac{dy}{dx}_A = \frac{P\lambda^2}{k} B_{\lambda e} + \frac{q\lambda}{2k} (1 - A_{\lambda l}) + \frac{q_0}{2k l} (D_{\lambda l} - 1 + \lambda l),$$

$$M_A = \frac{P}{4\lambda} C_{\lambda e} + \frac{q}{4\lambda^2} B_{\lambda l} + \frac{q_0}{8\lambda^3 l} (1 - A_{\lambda l}),$$

and

$$Q_A = \frac{P}{2} + \frac{q}{4\lambda} (1 - C_{\lambda l}) - \frac{q_0}{4\lambda^2 l} (B_{\lambda l} - \lambda l).$$

#### The Semi-Infinite Beam with Hinged End

To convert the infinite beam to a semi-infinite beam simply supported at A, it is necessary to apply an end-conditioning force and moment at A such that the resulting deflection and moment at A will be zero.<sup>3</sup> In

<sup>2</sup>Ibid., pp. 219-239.

<sup>3</sup>Ibid., pp. 22-23.

other words, it is necessary to add a force,  $P_o$ , and a moment,  $M_o$ , at A, as indicated by the dashed force and couple in Fig. E1, so that

$$y_A + \frac{P_o \lambda}{2k} = 0$$

and

$$M_A + \frac{P_o}{4\lambda} + \frac{M_o}{2} = 0 .$$

Solution of these two equations for  $P_o$  and  $M_o$  yields

$$P_o = -PA_{\lambda e} - \frac{q_o}{2\lambda^2 l} (C_{\lambda l} - 1 + 2\lambda l) - \frac{q}{\lambda} (1 - D_{\lambda l})$$

and

$$M_o = \frac{P}{\lambda} B_{\lambda e} + \frac{q_o}{2\lambda^3 l} (D_{\lambda l} + \lambda l - 1) + \frac{q}{2\lambda^2} (1 - A_{\lambda l}) .$$

The addition of these loads to the infinite beam of Fig. E1 converts it to the semi-infinite beam shown in Fig. E2. The deflection, slope, moment, and shear are now due to the three original loads plus the effect of  $P_o$  and  $M_o$  and by superposition are given as functions of  $x$  and  $|x - e|$ ; they are

$$y = \frac{P\lambda}{2k} A_{\lambda|x-e|} + \frac{P_o \lambda}{2k} A_{\lambda x} + \frac{M_o \lambda^2}{k} B_{\lambda x} + \frac{q}{2k} [2 - D_{\lambda x} - D_{\lambda(l-x)}] \\ + \frac{q_o}{4\lambda k l} [C_{\lambda(l-x)} - C_{\lambda x} - 2\lambda l D_{\lambda x} + 4\lambda(l-x)] ,$$

$$\frac{dy}{dx} = \pm \frac{P\lambda^2}{k} B_{\lambda|x-e|} - \frac{P_0\lambda^2}{k} B_{\lambda x} + \frac{M_0\lambda^3}{k} C_{\lambda x} + \frac{q\lambda}{2k} [A_{\lambda x} - A_{\lambda(\ell-x)}] \\ + \frac{q_0}{2k\ell} [D_{\lambda(\ell-x)} + D_{\lambda x} + \lambda\ell A_{\lambda x} - 2] ,$$

$$M = \frac{P}{4\lambda} C_{\lambda|x-e|} + \frac{P_0}{4\lambda} C_{\lambda x} + \frac{M_0}{2} D_{\lambda x} + \frac{q}{4\lambda^2} [B_{\lambda x} + B_{\lambda(\ell-x)}] \\ + \frac{q_0}{8\lambda^3\ell} [A_{\lambda x} - A_{\lambda(\ell-x)} + 2\lambda\ell B_{\lambda x}] ,$$

and

$$Q = \pm \frac{P}{2} D_{\lambda|x-e|} - \frac{P_0}{2} D_{\lambda x} - \frac{M_0\lambda}{2} A_{\lambda x} + \frac{q}{4\lambda} [C_{\lambda x} - C_{\lambda(\ell-x)}] \\ - \frac{q_0}{4\lambda^2\ell} [B_{\lambda x} + B_{\lambda(\ell-x)} - \lambda\ell C_{\lambda x}] .$$

The first terms in the equations for  $dy/dx$  and  $Q$  are positive for  $x < e$  and negative for  $x \geq e$ .

#### The Semi-Infinite Beam with Fixed End

To convert the infinite beam of Fig. E1 to a semi-infinite beam fixed at A, it is necessary to apply an end-conditioning force and moment at A such that the resulting deflection and slope at A will be zero. In other words, the magnitudes of the force  $P_0$  and moment  $M_0$  in this case must satisfy the following two equations:

$$y_A + \frac{P_0\lambda}{2k} = 0 ,$$

and

$$\frac{dy}{dx_A} + \frac{M_o \lambda^3}{k} = 0 .$$

Simultaneous solution of these two equations yields

$$P_o = -PA_{\lambda e} - \frac{q_o}{2\lambda^2 l} (C_{\lambda l} - 1 + 2\lambda l) - \frac{q}{\lambda} (1 - D_{\lambda l}) .$$

and

$$M_o = -\frac{P}{\lambda} B_{\lambda e} - \frac{q}{2\lambda^2} (1 - A_{\lambda l}) - \frac{q_o}{2\lambda^3 l} (D_{\lambda l} - 1 + \lambda l) .$$

The expressions above for  $P_o$  and  $M_o$  are respectively identical to and the negative of the corresponding expressions for the previous case. The addition of these loads to the infinite beam of Fig. E1 converts it to the semi-infinite beam shown in Fig. E3. The deflection, slope, moment, and shear are again due to the three original loads plus the effect of  $P_o$  and  $M_o$ . The expressions for them differ from those for a beam with a hinged end only because of the difference in the expression for the moment  $M_o$ .

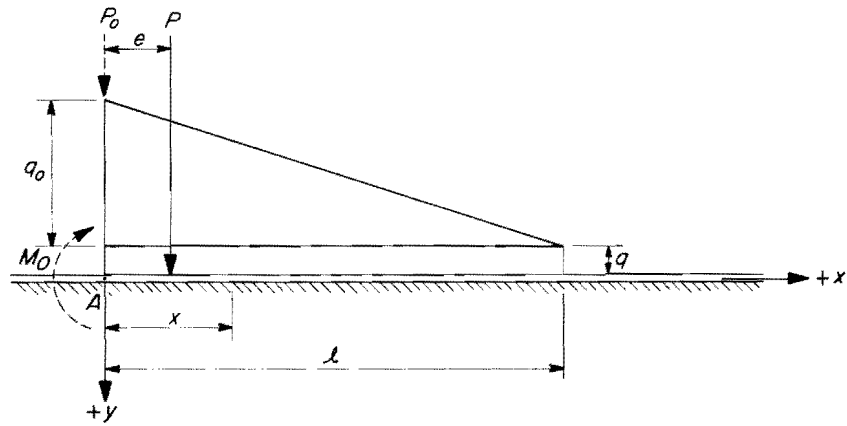


Fig. E1. A Beam of Infinite Length on an Elastic Foundation.

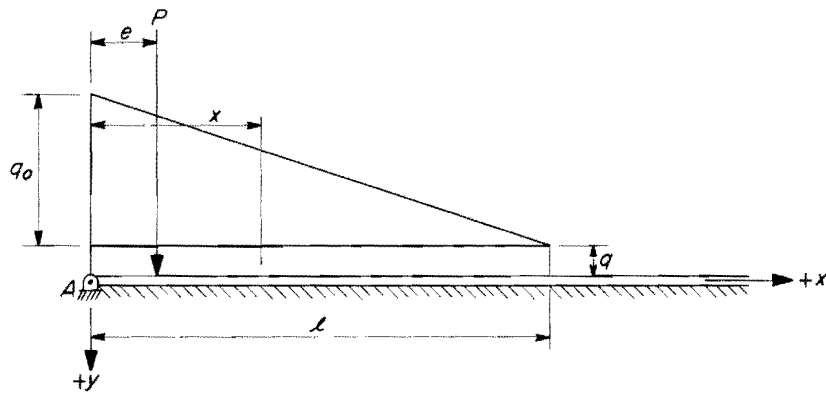


Fig. E2. A Beam of Semi-Infinite Length, Hinged at One End, and on an Elastic Foundation.

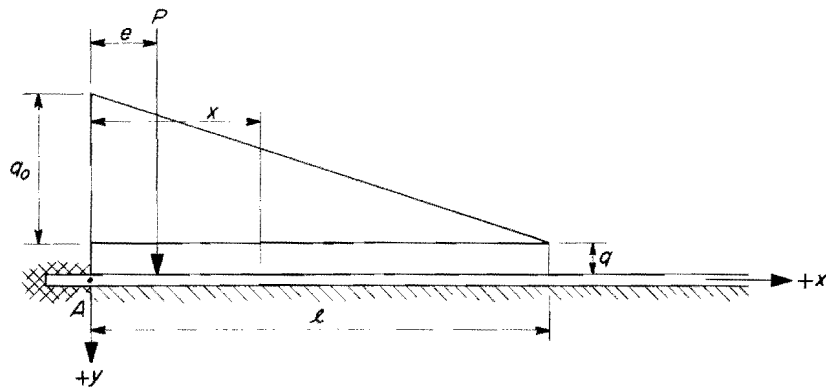


Fig. E3. A Beam of Semi-Infinite Length, Fixed at One End, and on an Elastic Foundation.

Appendix FANALYSES OF THE FUEL-ELEMENT CONTAINERS AT MID-HEIGHT  
OF THE CORE FOR FUEL ELEMENTS OF CORE II TYPE

The  $R_2$  values tabulated on page 17 for ship motions indicate that the most severe combination of normal motions is that of the  $30^\circ$  roll, 0.7-g lateral heave (assumed normal to the ship's longitudinal vertical plane of symmetry), and 0.3-g vertical heave. This is the normal condition assumed in this appendix. In the analyses that follow, a 1-in. length of the fuel-element container is assumed to constitute the rigid frame under consideration.

Rigid-Frame Calculations for Column 2 when Subjected to Simultaneous  
 $30^\circ$  Roll, 0.7-g Lateral Heave, and 0.3-g Vertical Heave

The deflection of the spacer bar between the top and intermediate fuel-element containers (see Fig. F1) may be expressed in terms of the deflection of either container at the point of contact with the spacer bar. Therefore,

$$\delta_{K_T} = \delta_{J_U}$$

In evaluating this equation, the deflection caused by beam action was neglected, because, as shown on page 38, with the ship on its side and subjected to a vertical acceleration of 2 g, the deflection amounts to only 0.033 in. with the spacer bars neglected. Furthermore this approximate value would appear in both members of the equation and tend to cancel out. From D(13)\*,

$$+ \downarrow EI \delta_{K_T} = - \frac{67PL^3}{7680} + \frac{9}{320} QaL^2 + \frac{31}{320} Qa^2L - \frac{Qa^3}{6} + \frac{p_1L^4}{240} + \frac{RL^3}{2560},$$

---

\*The letter indicates the appropriate appendix; the number in parenthesis, the equation in that appendix.

where  $p_1 = +7$  psi. Since there is no load at  $N_T$ ,  $R = 0$  in this equation. From D(20),

$$+ \downarrow EI\delta_{JU} = + \frac{PL^3}{120} - \frac{QaL^2}{40} - \frac{Qa^2L}{10} + \frac{Qa^3}{6} - \frac{p_2L^4}{240},$$

where  $p_2 = -4$  psi. Since there are no fuel element loads on the upper part of the intermediate fuel-element container,  $Q = 0$  in this equation. The term  $EI$ , which actually should be  $D = EI/(1 - \mu^2)$ , is the same in both expressions above, and the solution of the equation  $D\delta_{KT} = D\delta_{JU}$  for  $P$  follows.

From page 17 the load applied by the fuel bundle on the container walls is  $R_2 = 513$  lb. As shown on pages 18 and 19, this is distributed over a 12-in. length of the container wall. The result is then divided between the two "pads" in contact with the deflected container wall to obtain the value  $Q = 21.375$  lb. The wall dimensions  $L$  and  $a$  were obtained as explained on pages 33 and 40. Equating the deflections gives

$$-\frac{67PL^3}{7680} + \frac{9QaL^2}{320} + \frac{31Qa^2L}{320} - \frac{Qa^3}{6} + \frac{p_1L^4}{240} = + \frac{PL^3}{120} - \frac{p_2L^4}{240} \quad (1)$$

or

$$P = \frac{(165.061)(7680)}{(131)(702.595)} = 13.8 \text{ lb.}$$

With the value of  $P$  thus determined, Eqs. D(7) and D(8) are used to determine  $M_{AF}$  in the bottom of the top container:

$$\begin{aligned} M_{AF} &= -\frac{31}{320} PL + \frac{31}{40} \frac{Qa(L-a)}{L} + \frac{17p_1L^2}{240} \\ &= 46 \text{ lb-in.} \end{aligned}$$

In line with the sign conventions explained on page 43, this moment produces tension in the top fibers of the beam and hence is negative

according to the usual beam conventions. The model beam and bending-moment diagram are shown in Fig. F2. The bending-moment diagram shows the maximum moment to be approximately -46 lb-in. and indicates that the maximum deflection is at  $K_T$ , the mid-point of the span.

The deflection of  $K_T$  (or of  $J_U$ ) is due to the deflection of the container as a unit, which will be called beam action and designated  $\delta_1$ , plus the additional deflection caused by plate action of the container wall, which will be designated  $\delta_2$ . The term  $\delta_1$  is given by the equation

$$EI\delta_1 = \left( R_2 + \frac{5}{8} W_e \right) \frac{(\text{beam length})^3}{48},$$

as developed on page 36. Using the appropriate values for  $R_2$  and  $W_e$  as tabulated on page 18,

$$EI\delta_1 = \left[ 513 + \frac{5}{8} (135) \right] \frac{80^3}{48}.$$

If it is assumed that the moment of inertia  $I$  is directly proportional to the thickness  $t$  of the container wall,  $I = 423t \text{ in.}^4$ , since it was shown on page 34 that  $I = 44.8 \text{ in.}^4$  when  $t = 0.106 \text{ in.}$  Hence,

$$\downarrow \delta_1 = \frac{0.00137}{t} \text{ in.}$$

It is to be noted that this neglects the  $l2P = 165.6 \text{ lb}$  upward force and is therefore conservative.

From D(20),

$$EI\delta_{J_U} = EI\delta_2 = \frac{PL^3}{120} - \frac{p_2L^4}{240},$$

since  $Q = 0$ . Here the  $EI$  is replaced by

$$D = \frac{EI}{1 - \mu^2} = 1,091,270t^3 ,$$

since the bending of a plate is involved. Consequently,

$$\begin{aligned} D\delta_2 &= \frac{PL^3}{120} - \frac{p_2L^4}{240} \\ &= 184.896 \text{ lb-in.}^3 , \end{aligned}$$

and

$$\downarrow \delta_2 = \frac{184.896}{1,091,270t^3} = \frac{0.000169}{t^3} \text{ in.}$$

The total deflection in inches of either  $K_T$  or  $J_U$  is therefore

$$+ \downarrow \delta_{K_T} = \frac{0.00137}{t} + \frac{0.000169}{t^3} .$$

It is to be noted that this neglects the deflection caused by the dynamic effect of the plate weight, but this is  $<0.00000353/t^2$  in. and therefore negligible if  $t \geq 0.1$ .

With due regard for signs, the value  $P = 13.8$  lb and  $D(17)$  and  $D(18)$  are again used to determine  $M_{AF}$  in the top of the third-pass container:

$$\begin{aligned} M_{AF} &= \frac{PL}{10} - \frac{17}{240} p_2L^2 \\ &= 34.660 \text{ lb-in.} \end{aligned}$$

It is again noted that the positive value indicates tension in the top at A. The model beam and bending-moment diagram are shown in Fig. F3.

Data for the top of the upper second-pass container are of interest because the predominant effect is, by far, that from pressure, as can be seen by observing the relative magnitudes of the terms in the

equation D(14) following. For all practical purposes it may be said that pressure alone determines the shears, moments, and deflections here. The value  $P = 13.8$  lb, previously determined, is used to obtain data which follow for the member CD of the top frame. The model beam and bending-moment diagram are shown in Fig. F4.

For member CD of the top frame,

$$\begin{aligned}
 + \downarrow D\delta_2 &= -\frac{PL^3}{2560} + \frac{QaL^2}{320} - \frac{Qa^2L}{320} - \frac{p_1L^4}{240} & D(14) \\
 &= -3.787 + 6.995 - 1.043 - 182.177 \\
 &= -180.012 \text{ lb-in.}^3,
 \end{aligned}$$

and it was indicated above that  $D = 1,091,270t^3$ ; therefore,

$$\delta_2 = -\frac{180.012}{1,091,270t^3} = -\frac{0.000165}{t^3} \text{ in.}$$

As on page 64,

$$\downarrow \delta_1 = \frac{0.00137}{t} \text{ in.}$$

Hence,

$$+ \downarrow \delta_{N_T} = \frac{0.00137}{t} - \frac{0.000165}{t^3} \text{ in.}$$

Also

$$\begin{aligned}
 M_{CD} &= \frac{PL}{320} - \frac{Qa(L-a)}{40L} - \frac{17}{240} p_1L^2, & D(12) \\
 &= -39.4 \text{ lb-in.},
 \end{aligned}$$

which indicates tension in the bottom.

The procedure described above is then used to analyze the container walls adjacent to the lower spacer bar. Again, the deflection of the spacer bar between the intermediate and bottom fuel-element containers may be expressed in terms of the deflection of either container at the point of contact with the spacer bar. Therefore,  $\delta_{J_L} = \delta_{N_B}$ . From D(20),

$$+ \downarrow EI\delta_{J_L} = -\frac{PL^3}{120} + \frac{QaL^2}{40} + \frac{Qa^2L}{10} - \frac{Qa^3}{6} + \frac{p_2L^4}{240},$$

where  $p_2 = -4$  psi. From D(14),

$$+ \downarrow EI\delta_{N_B} = +\frac{67PL^3}{7680} + \frac{QaL^2}{320} - \frac{Qa^2L}{320} - \frac{p_1L^4}{240},$$

where  $p_1 = +7$  psi. As before,  $EI$ , which actually should be  $D = EI/(1 - \mu^2)$ , is the same in both expressions, and the solution of  $D\delta_{J_L} = D\delta_{N_B}$  for  $P$  gives

$$P = \frac{153.157}{11.984} = 12.8 \text{ lb.}$$

This value of  $P$  is used to obtain the data of the following four items.

1. For the bottom of the third-pass container (see Fig. F5),

$$\begin{aligned} M_{AF} &= -\frac{PL}{10} + \frac{8Qa(L-a)}{10L} + \frac{17}{240} p_2L^2 & D(18) \\ &= -14.5 \text{ lb-in.}, \end{aligned}$$

which indicates tension in the bottom.

2. For the deflection of the spacer bar,

$$\downarrow \delta_1 = \frac{0.00137}{t} \text{ in.},$$

as on page 64,

$$\begin{aligned}
 + \downarrow D\delta_2 &= \frac{67PL^3}{7680} + \frac{QaL^2}{320} - \frac{Qa^2L}{320} - \frac{7L^4}{240} & D(14) \\
 &= -98 \text{ lb-in.}^3,
 \end{aligned}$$

$$\delta_2 = -\frac{98}{1,091,270t^3} = -\frac{0.00009}{t^3} \text{ in.}$$

(see p. 65 for value of D),

$$+ \downarrow \delta_{J_L} = \frac{0.00137}{t} - \frac{0.00009}{t^3} \text{ in.}$$

3. For the top of the lower second-pass container (see Fig. F6),

$$\begin{aligned}
 M_{CD} &= -\frac{1}{40} \frac{Qa(L-a)}{L} + \frac{31PL}{320} - \frac{17p_1L^2}{240} & D(12) \\
 &= -28.8 \text{ lb-in.},
 \end{aligned}$$

which indicates tension in the bottom.

4. For the bottom of the lower second-pass container (see Fig. F7),

$$\begin{aligned}
 M_{AF} &= \frac{31}{40} \frac{Qa(L-a)}{L} - \frac{PL}{320} + \frac{17}{240} p_1L^2 & D(8) \\
 &= 57.5 \text{ lb-in.},
 \end{aligned}$$

which indicates tension in the top,

$$\downarrow \delta_1 = \frac{0.00137}{t} \text{ in.},$$

as on page 64,

$$\begin{aligned}
 + \downarrow D\delta_2 &= \frac{PL^3}{2560} + \frac{9}{320} QaL^2 + \frac{31}{320} Qa^2L - \frac{Qa^3}{6} + \frac{p_1L^4}{240} & D(13) \\
 &= 3.507 + 62.953 + 32.318 - 8.287 + 182.177 \\
 &= 273 \text{ lb-in.}^3,
 \end{aligned}$$

$$\delta_2 = \frac{273}{1,091,269t^3} \cdot \frac{0.000250}{t^3} \text{ in.}$$

(see p. 65 for value of D),

$$\downarrow \delta_{KB} = \frac{0.00137}{t} + \frac{0.000250}{t^3} \text{ in.}$$

The results of this section, along with the bending-moment diagrams of the vertical walls (Fig. F1) of the fuel-element containers were summarized in Fig. 4. The significant maximum values are shown in Fig. F16 (see page 100).

Rigid-Frame Calculations for Column 1 when Subjected to Simultaneous 30° Roll, 0.7-g Lateral Heave, and 0.3-g Vertical Heave

The analysis of the column 1 model parallels that of the column 2 model, with the exception that a different basic frame analysis is employed. The deflection of the top spacer bar (see Fig. F8) equals  $\delta_{GT} = \delta_{HT}$ . The expressions for  $D\delta_{GT}$  and  $D\delta_{HT}$  are given by Eqs. D(27) and D(28), respectively. If it is assumed that the spacer bars are subjected to the same compressive load P, the equation  $D\delta_{GT} = D\delta_{HT}$  follows:

$$\begin{aligned}
 -\frac{17PL^3}{1536} + \frac{3}{64} QaL^2 + \frac{5}{64} Qa^2L - \frac{Qa^3}{6} + \frac{pL^4}{384} &= \\
 &= \frac{17PL^3}{1536} + \frac{PL^3}{512} - \frac{QaL^2}{64} + \frac{Qa^2L}{64} - \frac{pL^4}{384}.
 \end{aligned}$$

The solution of this equation yields

$$P = 22.5 \text{ lb.}$$

This value of P is used to obtain the data of the following four items.

1. For the bottom of the top container (see Fig. F9),

$$\begin{aligned} M_{AD} &= -\frac{5PL}{64} + \frac{5Qa(L-a)}{8L} + \frac{pL^2}{12} & D(24) \\ &= 45.6 \text{ lb-in.}, \end{aligned}$$

which indicates tension in the top. The bending-moment diagram shows the maximum moment to be 45.6 lb-in. and indicates that the maximum deflection is at G.

2. For the deflection of the spacer bar,

$$\downarrow \delta_1 = \frac{0.00137}{t} \text{ in.},$$

as on page 64,

$$\begin{aligned} + \downarrow D\delta_2 &= -\frac{17PL^3}{1536} + \frac{3QaL^2}{64} + \frac{5Qa^2L}{64} - \frac{Qa^3}{6} + \frac{pL^4}{384} & D(27) \\ &= 55.7 \text{ lb-in.}^3, \end{aligned}$$

$$\delta_2 = \frac{55.7}{1,091,269t^3} = \frac{0.000051}{t^3} \text{ in.}$$

(see p. 65 for value of D),

$$\downarrow \delta_{GT} = \frac{0.00137}{t} + \frac{0.000051}{t^3} \text{ in.}$$

3. For the top of the intermediate second-pass container (see Fig. F10),

$$M_{BC} = -\frac{PL}{64} + \frac{5}{64} RL + \frac{Qa(L-a)}{8L} - \frac{pL^2}{12} \quad D(26)$$

$$= -30.6 \text{ lb-in. ,}$$

which indicates tension in the bottom.

4. For the top of the top second-pass container (see Fig. F11),

$$\downarrow \delta_1 = \frac{0.00137}{t} \text{ in. ,}$$

as on page 64,

$$+ \downarrow D\delta_2 = \frac{PL^3}{512} - \frac{QaL^2}{64} + \frac{Qa^2L}{64} - \frac{pL^4}{384} \quad D(28)$$

$$= -113 \text{ lb-in.}^3 \text{ ,}$$

$$+ \downarrow \delta_2 = -\frac{113}{1,091,270t^3} = -\frac{0.000104}{t^3} \text{ in.}$$

(see p. 65 for value of D),

$$+ \downarrow \delta_{HT} = \frac{0.00137}{t} - \frac{0.000104}{t^3} \text{ in. ,}$$

$$M_{BC} = -\frac{PL}{64} + \frac{Qa(L-a)}{8L} - \frac{pL^2}{12} \quad D(26)$$

$$= -46.2 \text{ lb-in. ,}$$

which indicates tension in the bottom.

The deflection of the lower spacer bar equals  $\delta_{G_I} = \delta_{H_B}$ . The expressions for  $D\delta_{G_I}$  and  $D\delta_{H_B}$  are given by D(27) and D(28), respectively. The solution of  $D\delta_{G_I} = D\delta_{H_B}$  for P, where  $R = P$ , gives

$$P = 22.5 \text{ lb.}$$

By using this value of P, data were obtained for the following five items.

1. For the bottom of the intermediate container (see Fig. F12),

$$\begin{aligned} M_{AD} &= \frac{5PL}{64} + \frac{RL}{64} + \frac{5Qa(L-a)}{8L} + \frac{pL^2}{12} & D(24) \\ &= 48.7 \text{ lb-in.}, \end{aligned}$$

which indicates tension in the top. The bending-moment diagram in Fig. F12 indicates that the maximum deflection is not at the mid-point,  $G_I$ . The point of maximum deflection will be at the point of zero slope, which was found to be 0.23 in. from  $G_I$ . The maximum deflection was found to be larger than the mid-point deflection by a negligible amount, if  $t \geq 0.14$  in. The deflection at  $G_I$  was therefore computed.

2. For the deflection of the spacer bar,

$$\begin{aligned} + \downarrow D\delta_2 &= -\frac{17PL^3}{1536} + \frac{3}{64} QaL^2 + \frac{5}{64} Qa^2L - \frac{RL^3}{512} - \frac{Qa^3}{6} + \frac{pL^4}{384} & D(27) \\ &= 29.8 \text{ lb-in.}^3, \end{aligned}$$

$$\delta_2 = \frac{29.8}{1,091,270t^3} = \frac{0.000027}{t^3} \text{ in.}$$

(see p. 65 for value of D),

$$\downarrow \delta_1 = \frac{0.00137}{t} \text{ in.},$$

as on page 64,

$$\downarrow \delta_{G_I} = \frac{0.00137}{t} + \frac{0.000027}{t^3} \text{ in.}$$

3. For the top of the bottom container (see Fig. F13),

$$\begin{aligned} M_{BC} &= \frac{5}{64} RL + \frac{Qa(L-a)}{8L} - \frac{pL^2}{12} & D(26) \\ &= -27.46 \text{ lb-in. ,} \end{aligned}$$

which indicates tension in the bottom. Calculations proved that the maximum deflection occurs at the mid-point,  $H_B$ , even though the bending-moment diagram indicates that this is not necessarily so. The maximum deflection is the same as that calculated for  $\delta_{G_I}$  above.

4. For the bottom of the bottom container (see Fig. F14),

$$\begin{aligned} M_{AD} &= \frac{RL}{64} + \frac{5Qa(L-a)}{8L} + \frac{pL^2}{12} & D(24) \\ &= 64.28 \text{ lb-in. ,} \end{aligned}$$

which indicates tension in the top,

$$\downarrow \delta_1 = \frac{0.00137}{t} \text{ in. ,}$$

as on page 64 ,

$$\begin{aligned} + \downarrow D\delta_2 &= \frac{3}{64} QaL^2 + \frac{5}{64} Qa^2L - \frac{RL^3}{512} - \frac{Qa^3}{6} + \frac{pL^4}{384} & D(27) \\ &= 104.922 + 26.06 - 30.87 - 8.287 + 113.86 \\ &= 205.68 \text{ lb-in.}^3 \text{ ,} \end{aligned}$$

$$\delta_2 = \frac{205.68}{1,091,270t^3} = \frac{0.000188}{t^3} \text{ in.}$$

(see p. 65 for value of D),

$$\downarrow \delta_{G_B} = \frac{0.00137}{t} + \frac{0.000188}{t^3} \text{ in.}$$

5. For the sides of the containers (see Fig. F8),

$$D\delta_E^+ = \frac{PL^3}{256} + \frac{RL^3}{256} - \frac{Qa(L-a)L}{32} + \frac{pL^4}{384}. \quad D(29)$$

For the top container,  $R = 0$ , and therefore

$$D\delta_{E_T}^{\leftarrow} = 116.1 \text{ lb-in.}^3$$

and

$$\delta_{E_T}^{\leftarrow} = \frac{116.1}{1,091,270t^3} = \frac{0.000106}{t^3} \text{ in.}$$

(see p. 65 for value of D). For the intermediate container,

$$\delta_{E_I}^{\leftarrow} = \frac{0.000163}{t^3},$$

and for the bottom container

$$\delta_{E_B}^{\leftarrow} = \frac{0.000106}{t^3},$$

as for the top container.

Although the above values for  $\delta_{ET}$ ,  $\delta_{EI}$ , and  $\delta_{EB}$  are not necessarily the maximum horizontal deflections for the respective container walls, they do indicate that the maximum horizontal deflection will be approximately 0.06 in., which is not excessive. These quantities were not considered further.

The results of this section, along with the bending-moment diagrams of the vertical walls (Fig. F8) of the fuel-element containers are summarized in Fig. 3. The significant maximum values are shown in Fig. F15.

Determination of Fuel-Element Container Wall Thicknesses Based on Bending Moments in the Intermediate Fuel-Element Container

By referring to Figs. F15 and F16 it may be seen that the maximum bending moments at the corners and mid-spans of the walls of the intermediate containers are 48.7 and 35.5 lb-in. per unit width, respectively. These moments will be used in establishing the wall thickness, since additional support can be provided for the peripheral walls. With an assumed allowable stress of 17,000 psi, the required thickness is approximated by the elementary flexure formula

$$\sigma = \frac{Mc}{I} ,$$

where the nomenclature is as given in Appendix C. At the corner of the intermediate container of the column 1 model,

$$17,000 = \frac{(48.7)(t/2)}{(1/12)(1)t^3} = \frac{292.2}{t^3} ,$$

and  $t = 0.1311$  in. A thickness of 0.14 in. was assumed.

The properties of a repeating section of the container wall at mid-span were calculated using this assumed thickness. The mid-span section is shown in Fig. F17. The neutral axis of the cross section is located by  $\bar{y}$ , which was found to be 0.0672 in. The moment of inertia  $I$  of section A-A with respect to the neutral axis was found to be 0.000156 in.<sup>4</sup>.

In order to check the adequacy of the wall thickness of 0.14 in., the three principal stresses were determined. The direct pressure stresses are negligible throughout the core. The primary stress in the longitudinal direction is found from Eq. C(2),

$$\sigma_{\ell} = \left( R_2 + \frac{W_e}{2} \right) \frac{\ell c}{4I} .$$

From page 18,  $W_e = 135$  lb for  $t \sim 0.10$  in. and  $R_2 = 513$  lb. Since  $t$  will be  $\sim 0.14$  in.,  $W_e$  was assumed to be 190 lb. The moment of inertia  $I$  was assumed to be  $423t = 59.2$  in.<sup>4</sup> (see page 64), and  $\ell$  was assumed to be 80 in. while  $c$  was 4.445 in. Use of these values gives  $\sigma_{\ell} = \pm 913$  psi; say, 900 psi. These are principal stresses, as are the transverse stresses determined later, since, at mid-height of the core, the total shear and consequent shearing stresses are zero.

The symbols  $\sigma_p$ ,  $\sigma_{\ell}$ , and  $\sigma_t$  are used to represent, respectively, the stresses from pressure, from bending in the longitudinal direction, and from bending plus the axial load in the transverse direction.

#### Point A of Member AD in the Intermediate Fuel-Element Container of the Column 1 Model

A free body of the member AD of the intermediate container of the column 1 model for the 30° clockwise roll is shown in Fig. F12. For the 30° counterclockwise roll, the free-body diagram is the same as that obtained by inverting Fig. F10.

The primary stress in the transverse direction on the interior surface is the sum of the bending stress  $Mc/I$  and the axial stress  $P/A$ . At A, the maximum primary stress in the transverse direction is

$$\sigma_{\max} = \frac{(48.7)(0.07)}{(1/12)(1)(0.14)^3} + \frac{33.1}{0.14} = 14,900 + 236 \sim 15,100 \text{ psi} .$$

Similarly, at A, the minimum primary stress in the transverse direction on the interior surface is

$$\sigma_{\min} = \frac{(30.6)(6)}{(0.14)^2} + \frac{29.1}{0.14} = 9360 + 208 \sim 9600 \text{ psi.}$$

The values 33.1 and 29.1 used above were obtained by considering free-body diagrams of appropriate portions of Fig. 4.

Primary Stress Intensity. The principal stresses and the stress differences,  $S_{xy} = \sigma_x - \sigma_y$ , are tabulated below:

| Fuel-Element<br>Container<br>Surface | Angle<br>of<br>Roll | Principal Stresses<br>(psi) |            |            | Stress Differences<br>(psi) |          |          |
|--------------------------------------|---------------------|-----------------------------|------------|------------|-----------------------------|----------|----------|
|                                      |                     | $\sigma_p$                  | $\sigma_l$ | $\sigma_t$ | $S_{pl}$                    | $S_{lt}$ | $S_{tp}$ |
| Interior                             | 30° ↓               | 0                           | 900        | 15,100     | -900                        | -14,200  | 15,100   |
|                                      | 30° ↗               | 0                           | -900       | 9,600      | 900                         | -10,500  | 9,600    |
| Exterior                             | 30° ↓               | 0                           | 900        | -14,700    | -900                        | 15,600   | -14,700  |
|                                      | 30° ↗               | 0                           | -900       | -9,200     | 900                         | 8,300    | -9,200   |

The primary stress intensity is seen to be 15,600 psi. This is less than the allowable  $S_m$  value of 17,600 psi and is therefore acceptable.

Combinations of Steady-State and Transient Conditions. Stress quantities needed other than those listed above are the stress ranges,  $S_{rxy}$ , the alternating stress differences,  $S_{\text{alt } xy} = S_{rxy}/2$ , and the basic mean stress differences,  $S'_{\text{mean } xy}$ . These are given below:

|                        | Interior Surface<br>Stresses (psi) |        |        | Exterior Surface<br>Stresses (psi) |        |        |
|------------------------|------------------------------------|--------|--------|------------------------------------|--------|--------|
|                        | $pl$                               | $lt$   | $tp$   | $pl$                               | $lt$   | $tp$   |
| $S_{rxy}$              | 1800                               | 3,700  | 5,500  | 1800                               | 7,300  | 5,500  |
| $S_{\text{alt } xy}$   | 900                                | 1,850  | 2,750  | 900                                | 3,650  | 2,750  |
| $S'_{\text{mean } xy}$ | 0                                  | 12,350 | 12,350 | 0                                  | 11,950 | 11,950 |

Since  $S'_{\text{mean } xy} + S_{\text{alt } xy} < 48,500 \text{ psi} = S_b = S_y$  of cold-worked Zircaloy,

$$S'_{\text{mean } xy} = S_{\text{mean } xy}$$

Obviously,  $S_{\text{mean}} = 11,950$  psi and  $S_{\text{alt}} = 3650$  psi constitute the significant set of values. This point is in the "safe" area of Fig. H3b (see Appendix H), and the wall thickness of 0.14 in. is adequate for the corners of the intermediate fuel containers.

Point  $J_L$  of Member AF in the Intermediate Fuel-Element Container of the Column 2 Model

A free-body diagram of the member AF of the third pass of the column 2 model for the  $30^\circ$  clockwise roll is shown in Fig. F5. For the  $30^\circ$  counterclockwise roll, the free-body diagram is the same as that obtained by inverting Fig. F3.

At  $J_L$ , the maximum primary stress on the interior surface in the transverse direction for a wall thickness of 0.14 in. is

$$\begin{aligned}\sigma_{\text{max}} &= \frac{(35.5)(0.0728)}{0.000156} - \frac{18.4}{0.0985} \\ &= 16,566 - 187 \sim 16,400 \text{ psi} .\end{aligned}$$

The corresponding minimum primary stress at  $J_L$  on the interior surface in the transverse direction is

$$\begin{aligned}\sigma_{\text{min}} &= \frac{(25.1)(0.0728)}{0.000156} - \frac{11.6}{0.0985} \\ &= 11,713 - 118 \sim 11,600 \text{ psi} .\end{aligned}$$

The stresses for the exterior surface are obtained by replacing 0.0728 with 0.0672.

Primary Stress Intensity. The principal stresses and the stress differences,  $S_{xy} = \sigma_x - \sigma_y$ , are tabulated below:

| Fuel-Element<br>Container<br>Surface | Angle<br>of<br>Roll | Principal Stresses<br>(psi) |            |            | Stress Differences<br>(psi) |          |          |
|--------------------------------------|---------------------|-----------------------------|------------|------------|-----------------------------|----------|----------|
|                                      |                     | $\sigma_p$                  | $\sigma_l$ | $\sigma_t$ | $S_{pl}$                    | $S_{lt}$ | $S_{tp}$ |
| Interior                             | 30° ↓               | 0                           | 900        | 16,400     | -900                        | -15,500  | 16,400   |
|                                      | 30° ↑               | 0                           | -900       | 11,600     | +900                        | -12,500  | 11,600   |
| Exterior                             | 30° ↓               | 0                           | +900       | -15,500    | -900                        | +16,400  | -15,500  |
|                                      | 30° ↑               | 0                           | -900       | -11,000    | +900                        | +10,100  | -11,000  |

The primary stress intensity is 16,400 psi (for  $t = 0.14$  in.). This is less than the allowable  $S_m$  value of 17,600 psi and is therefore acceptable.

Combinations of Steady-State and Transient Conditions. Stress quantities needed in addition to those listed above are  $S_{rxy}$ ,  $S_{alt\ xy}$ , and  $S'_{mean\ xy}$ , as for the previous case. These are shown below:

|                 | Interior Surface<br>Stresses (psi) |        |        | Exterior Surface<br>Stresses (psi) |        |        |
|-----------------|------------------------------------|--------|--------|------------------------------------|--------|--------|
|                 | $pl$                               | $lt$   | $tp$   | $pl$                               | $lt$   | $tp$   |
| $S_{rxy}$       | 1800                               | 3,000  | 4,800  | 1800                               | 6,300  | 4,500  |
| $S_{alt\ xy}$   | 900                                | 1,500  | 2,400  | 900                                | 3,150  | 2,250  |
| $S'_{mean\ xy}$ | 0                                  | 14,000 | 14,000 | 0                                  | 13,250 | 13,250 |

Since  $S'_{mean\ xy} + S_{alt\ xy} < 48,500$  psi =  $S_b = S_y$  of cold-worked Zircaloy,

$$S'_{mean\ xy} = S_{mean\ xy}$$

The most critical set of values above is  $S_m = 13,250$  psi and  $S_{alt} = 3150$  psi. This point is within the "safe" area of Fig. H3a and is acceptable. A thickness of 0.14 in. is sufficient here.

#### Transverse Sections of the Peripheral Fuel-Element Container Walls

The summaries of Figs. F15 and F16 show that the corners of the "bottom" frames of column 1 and column 2 models are subjected to bending moments of 64.3 and 57.5 lb-in., respectively. The corresponding mid-span moments are -34.2 and -41.0 lb-in., respectively.

|                 | Interior Surface<br>Stresses (psi) |           |           | Exterior Surface<br>Stresses (psi) |           |           |
|-----------------|------------------------------------|-----------|-----------|------------------------------------|-----------|-----------|
|                 | <u>pl</u>                          | <u>lt</u> | <u>tp</u> | <u>pl</u>                          | <u>lt</u> | <u>tp</u> |
| $S_{rxy}$       | 1800                               | 1,500     | 300       | 1800                               | 2,100     | 300       |
| $S_{alt\ xy}$   | 900                                | 750       | 150       | 900                                | 1,050     | 150       |
| $S'_{mean\ xy}$ | 0                                  | 12,450    | 12,450    | 0                                  | 12,050    | 12,050    |

Since  $S'_{mean\ xy} + S_{alt\ xy} < 48,500$  psi, the significant point ( $S_{mean} = 12,100$  psi, and  $S_{alt} = 1100$  psi) lies in the "safe" area of Fig. H3b, and the 0.14 in. thickness is adequate for point A.

Point  $K_B$  of Member AF,  $t = 0.14$  in. Shown To Be Inadequate. The transverse principal stresses at point  $K_B$  were obtained through the use of the bending moments of 13.4 and 29.7 lb-in. shown in Figs. F19 and F4 (or F16), respectively. The principal stresses and stress differences are as follow:

| Fuel-Element<br>Container<br>Surface | Angle<br>of<br>Roll | Principal Stresses<br>(psi)  |                              |                              | Stress Differences<br>(psi) |                            |                            |
|--------------------------------------|---------------------|------------------------------|------------------------------|------------------------------|-----------------------------|----------------------------|----------------------------|
|                                      |                     | <u><math>\sigma_p</math></u> | <u><math>\sigma_l</math></u> | <u><math>\sigma_t</math></u> | <u><math>S_{pl}</math></u>  | <u><math>S_{lt}</math></u> | <u><math>S_{tp}</math></u> |
| Interior                             | 30°                 | 0                            | +900                         | -6,100                       | -900                        | 7,000                      | -6,100                     |
|                                      | 30°                 | 0                            | -900                         | -13,700                      | +900                        | 12,800                     | -13,700                    |
| Exterior                             | 30°                 | 0                            | +900                         | +6,000                       | -900                        | -5,100                     | +6,000                     |
|                                      | 30°                 | 0                            | -900                         | 13,000                       | +900                        | -13,900                    | +13,000                    |

The primary stress intensity is 13,900 psi (i.e., <17,600 psi) and is satisfactory. Other stress quantities needed for the combinations of steady-state and transient conditions are:

|                 | Interior Surface<br>Stresses (psi) |           |           | Exterior Surface<br>Stresses (psi) |           |           |
|-----------------|------------------------------------|-----------|-----------|------------------------------------|-----------|-----------|
|                 | <u>pl</u>                          | <u>lt</u> | <u>tp</u> | <u>pl</u>                          | <u>lt</u> | <u>tp</u> |
| $S_{rxy}$       | 1800                               | 5800      | 7600      | 1800                               | 8800      | 7000      |
| $S_{alt\ xy}$   | 900                                | 2900      | 3800      | 900                                | 4400      | 3500      |
| $S'_{mean\ xy}$ | 0                                  | 9900      | 9900      | 0                                  | 9500      | 9500      |

Since  $S'_{\text{mean } xy} + S_{\text{alt } xy} = 16,000 \text{ psi}$  (i.e.,  $< 48,500 \text{ psi}$ ),  $S'_{\text{mean } xy} = S_{\text{mean } xy}$ . The critical point ( $S_{\text{mean}} = 9500 \text{ psi}$ ,  $S_{\text{alt}} = 4400 \text{ psi}$ ) lies outside the "safe" area of Fig. H3a, and a wall thickness of 0.14 in. is not adequate here.

Point  $K_B$  of Member AF,  $t = 0.22 \text{ in.}$  Subsequent to the preceding analyses of the fuel-element container walls, it was decided to use a wall thickness of 0.22 in. (see p. 118, Appendix G) at the points of fuel-element container wall attachment to the spacer bars and connecting members, since the 0.14 in. thickness was found inadequate in the preceding paragraph and on page 117. For a thickness of 0.22 in., the 0.06-in. dimension in Fig. F17 becomes 0.14 in.,  $\bar{y}$  is 0.107 in., and  $I = 0.000617 \text{ in.}^4$ . The transverse bending moments and stresses are:

| Angle of Roll    | Bending Moment (lb-in.) | Container Surface Stress (psi) |          |
|------------------|-------------------------|--------------------------------|----------|
|                  |                         | Interior                       | Exterior |
| 30° <sub>l</sub> | 13.4                    | -2450                          | 2320     |
| 30° <sub>r</sub> | 29.7                    | -5430                          | 5150     |

These values must be combined with the ~200-psi axial stress, as was done on page 76. The resultant transverse stresses were rounded off and all principal stresses and stress differences are listed below:

| Fuel-Element Container Surface | Angle of Roll    | Principal Stresses (psi) |            |            | Stress Differences (psi) |          |          |
|--------------------------------|------------------|--------------------------|------------|------------|--------------------------|----------|----------|
|                                |                  | $\sigma_p$               | $\sigma_l$ | $\sigma_t$ | $S_{pl}$                 | $S_{lt}$ | $S_{tp}$ |
| Interior                       | 30° <sub>l</sub> | 0                        | 900        | -2300      | -900                     | 3200     | -2300    |
|                                | 30° <sub>r</sub> | 0                        | -900       | -5400      | 900                      | 4500     | -5400    |
| Exterior                       | 30° <sub>l</sub> | 0                        | 900        | 2500       | -900                     | -1600    | 2500     |
|                                | 30° <sub>r</sub> | 0                        | -900       | 5400       | 900                      | -6300    | 5400     |

The primary stress intensity is 6300 psi and is acceptable.

The stress quantities needed for the combinations of steady-state and transient conditions are:

|                 | Interior Surface<br>Stresses (psi) |           |           | Exterior Surface<br>Stresses (psi) |           |           |
|-----------------|------------------------------------|-----------|-----------|------------------------------------|-----------|-----------|
|                 | <u>pl</u>                          | <u>lt</u> | <u>tp</u> | <u>pl</u>                          | <u>lt</u> | <u>tp</u> |
| $S_{rxy}$       | 1800                               | 1300      | 3100      | 1800                               | 4700      | 2900      |
| $S_{alt\ xy}$   | 900                                | 650       | 1550      | 900                                | 2350      | 1450      |
| $S'_{mean\ xy}$ | 0                                  | 3850      | 3850      | 0                                  | 3950      | 3950      |

Since  $S'_{mean\ xy} + S_{alt\ xy} < 48,500\ psi = S_b$ ,  $S'_{mean\ xy} = S_{mean\ xy}$ . The significant point ( $S_{mean} = 3950\ psi$ ,  $S_{alt} = 2350\ psi$ ) falls well within the "safe" area of Fig. H3a, and the 0.22-in. thickness is quite adequate. As a matter of fact, the 0.22-in. thickness at  $K_B$  is adequate to carry the normal mid-span moments without any support, and only minor support is required at mid-span in order to assure that the stresses at the ends of the span are within limits.

#### Unusual Ship Motion

The unusual condition of the ship being on its side and being subjected to a vertical heave of 2 g was investigated in a manner similar to that used in the first part of this appendix. Since it was stated that control rod insertion would be the only concern in such a condition, the deflections were the primary interest. Inspection of Figs. F15 and F16 shows that the column 2 model exhibits the greatest deflections. This particular investigation was therefore limited to the column 2 model. The results are summarized in Fig. F20, where it may be seen that the maximum deflection in a control rod region is 0.10 in. This is well within the limits set (see p. 2) and is therefore satisfactory.

#### The Connecting Members

It was shown on pages 80 and 81 that limiting the mid-span deflection to 0.05 in. in the member AD of the bottom frame of the column 1 model gives a primary stress of 18,100 psi at the corner of the frame. Therefore the connecting member must be either rigid enough to restrict the mid-span deflection of the member of 0.05 in. or strong enough to

carry additional load in the event of yielding at the corners of the frame. The connecting member extending the full length of the fuel-element container was therefore designed as a structural component. This was done by treating this component as a beam on an elastic foundation.

The deflection of either  $G_B$  (see Fig. F15) or  $K_B$  (see Fig. F16) may be resolved into three parts, as follow: (1) the deflection caused by the longitudinal bending of the fuel-element container as a unit when subjected to fuel-element loads, (2) the deflection caused by transverse bending of the fuel-element container wall as a result of pressure, and (3) the deflection caused by the transverse bending of the fuel-element container wall when subjected to fuel-element loads. It was assumed for the analysis below that the elastic foundation provided by the fuel-element container wall was perfectly straight after the application of loads (1) and (2) above and that the deflection caused by load (3) was due solely to the deflection of the beam on an elastic foundation.

#### Connecting Member for AD, Bottom Frame, Column 1 Model

From Eq. D(27) on page 73, it may be seen that removal of the fuel-element loads (Q's) gives  $D\delta_2 = 83 \text{ lb-in.}^3$ . With  $D = 3000 \text{ lb-in.}^2$  for  $t = 0.14 \text{ in.}$  (see p. 65),  $\delta_2 = 0.0277 \text{ in.}$  On page 64, however, it may be seen that for  $t = 0.14 \text{ in.}$ ,  $\delta_1 = 0.00137/t = 0.0098 \text{ in.}$  with the fuel-element loads (Q's) on the fuel-element containers. Thus, the deflection of part (3) above must be restricted to  $[0.05 - (0.0098 + 0.0277)] = 0.0125 \text{ in.}$  in order to meet the deflection limit of 0.05 in.

The modulus  $k$  of the elastic foundation is defined as the force per unit length required to cause a deflection of 1 in. From Eq. D(27),

$$EI\delta_G = -\frac{17PL^3}{1536};$$

substitution of  $EI = D = 3000 \text{ lb-in.}^2$ ,  $L^3 = 702.6 \text{ in.}^3$ , and  $\delta = 1 \text{ in.}$  gives  $-P = 386 \text{ lb.}$  Thus,  $k = 386 \text{ lb/in.}\cdot\text{in.}$  If it is assumed that this "beam" carries the 154-lb load, as determined on page 110, for an infinite beam on an elastic foundation the deflection under a concentrated load is  $PL/2k$  (see Appendix E). Hence,

$$0.0125 = \frac{154\lambda}{2(386)}$$

and

$$\lambda = 0.0627 \text{ in.}^{-1} .$$

Now,  $\lambda^4 = k/4EI$ . Since the area in which this member is to be used is outside the active core area, stainless steel was assumed for the member. Therefore,  $I = k/4E\lambda^4$ , where  $k = 386 \text{ lb/in.}\cdot\text{in.}$ ,  $E = 29,000,000 \text{ psi}$ , and  $\lambda = 0.0627 \text{ in.}^{-1}$ . Substitution of these values gives  $I = 0.216 \text{ in.}^4$ . Any section having a moment of inertia of  $0.216 \text{ in.}^4$  would be satisfactory, but one having an I section is more economical. A possible section is shown in Fig. F21.

Since this is a beam of two materials, the section shown is transformed into an equivalent steel section<sup>1</sup> for analysis purposes. The transformed section is shown in Fig. F22, in which the width of the Zircaloy is one-third of its actual width, since its modulus of elasticity is about one-third that of steel. For the equivalent transformed steel section,  $\bar{y} = 0.775 \text{ in.}$ ,  $\bar{I} = 0.32 \text{ in.}^4$ , and  $\lambda = 0.0567 \text{ in.}^{-1}$ .

From Appendix E it may be seen that the maximum bending moment in the connecting member is

$$M = \frac{P}{4\lambda} = \frac{154}{4(0.0567)} = 680 \text{ lb-in.}$$

The longitudinal bending stress at any point in the transformed section is given by  $\sigma_{\ell} = My/\bar{I}$ , where  $y$  is the distance from the neutral axis, N.A., in Fig. F22, to the point under consideration. Values of  $\sigma_{\ell}$  at elevations marked 1, (2), and 4) on Fig. F23 are, respectively, -2010, -1540, and +1650 psi. Use of the bending moments of 16.5 and 22.9 lb-in. shown in Figs. F18 and F11 and the properties of the 0.22-in.-thick

---

<sup>1</sup>S. Timoshenko, Strength of Materials, p. 217, Part I, 3rd Ed., D. Van Nostrand, New York, 1955.

repeating section listed on page 85 gives the transverse stresses listed below in a fatigue analysis tabulation:

|             |      | Container Interior<br>Wall Stresses (psi) |            |            | Container Exterior<br>Wall Stresses (psi) |            |            |
|-------------|------|---|------------|------------|---|------------|------------|
|             |      | $\sigma_p$                                | $\sigma_l$ | $\sigma_t$ | $\sigma_p$                                | $\sigma_l$ | $\sigma_t$ |
| 30°↓        | Roll | 0   | -2010      | -2800      | 0   | -1540      | +3100      |
| 30°↑        | Roll | 0   | 0          | -4000      | 0   | 0          | +4200      |
|             |      | $S_{pl}$                                  | $S_{lt}$   | $S_{tp}$   | $S_{pl}$                                  | $S_{lt}$   | $S_{tp}$   |
| 30°↓        | Roll | 2010                                      | +790       | -2800      | 1540                                      | -4640      | 3100       |
| 30°↑        | Roll | 0   | +4000      | -4000      | 0   | -4200      | 4200       |
|             |      | $p_l$                                     | $l_t$      | $t_p$      | $p_l$                                     | $l_t$      | $t_p$      |
| $S_r$       |      | 2010                                      | 3210       | 1200       | 1540                                      | 440        | 1100       |
| $S_{alt}$   |      | 1005                                      | 1605       | 600        | 770                                       | 220        | 550        |
| $S'_{mean}$ |      | 1005                                      | 2395       | 3400       | 770                                       | 4420       | 4750       |

The primary stress intensity shown above is 4640 psi. In all cases,  $S'_{mean} + S_{alt} < 48,500$  psi and hence  $S_{mean} = S'_{mean}$ . All points ( $S_{mean}$ ,  $S_{alt}$ ) fall well within the "safe" zone of Fig. H3a, and the design appears to be ultraconservative.

As a check on this apparent ultraconservatism in the design of the connecting member, the problem was considered in another way. The terms  $P$  and  $M_{AD}$  for a pressure load of 7 psi alone were calculated and found to be 13.5 lb and 48 lb-in., respectively. It was shown on page 80 that a bending moment of approximately 54 lb-in. causes no difficulty in the corners of the fuel-element containers. The fuel-element container connecting member design is obviously adequate if any loads in addition to the 7-psi load are carried by a structural member. The connecting member was therefore assumed loaded as shown in Fig. F23. The 10-lb/in. triangularly distributed loading was obtained by the same procedure used on page 109 to obtain the 36 lb per lineal inch value, and the 154-lb load is taken from page 110. The 77-lb load is the fuel element load near the top. There is also a 77-lb fuel-element load near the bottom, but it has been omitted because the reduced pressure loading enables

the fuel-element container to carry it without difficulty. The connecting member has been considered as a simple beam because this gives the maximum bending moment and deflection in the central portion of the span, since the top end will be only partially fixed and, also, excessive yielding at the ends of a fixed ended beam causes it to function as a simple beam.

Values of  $R_L$  and  $R_R$  were calculated and found to be 317 and 114 lb, respectively. The maximum longitudinal bending moment occurs at mid-span and is 4580 lb-in. With  $\bar{y} = 0.775$  in. and  $\bar{I} = 0.32$  in.<sup>4</sup>, values of  $\sigma_\ell$  at elevations marked (1), (2), and (3) on Fig. 22, are, respectively, -13,500, -10,350, and -6800 psi.

The stresses of -13,500 and -10,350 psi in the transformed section are equivalent to -4500 and -3450 psi, respectively, in the Zircaloy. The transverse bending moments of 34.2 and 22.9 lb-in., as shown in Fig. F15 for unrestrained deflection, and the properties of the 0.22-in.-thick section were used to determine the  $\sigma_t$  stresses listed below in the fatigue analysis of the Zircaloy portion of the section shown in Fig. F21 when this section is used as the simple beam of Fig. F23:

|                 | Container Interior<br>Wall Stresses (psi) |               |            | Container Exterior<br>Wall Stresses (psi) |               |            |
|-----------------|---|---------------|------------|---|---------------|------------|
|                 | $\sigma_p$                                | $\sigma_\ell$ | $\sigma_t$ | $\sigma_p$                                | $\sigma_\ell$ | $\sigma_t$ |
| 30° Roll        | 0   | -4500         | -6100      | 0   | -3450         | +6100      |
| 30° Roll        | 0   | 0             | -4000      | 0   | 0             | +4200      |
|                 | $S_{p\ell}$                               | $S_{\ell t}$  | $S_{tp}$   | $S_{p\ell}$                               | $S_{\ell t}$  | $S_{tp}$   |
| 30° Roll        | 4500                                      | 1600          | -6100      | +3450                                     | -9550         | +6100      |
| 30° Roll        | 0   | 4000          | -4000      | 0   | -4200         | +4200      |
| $S_{rxy}$       | 4500                                      | 2400          | 2100       | 3450                                      | 5350          | 1900       |
| $S_{alt\ xy}$   | 2250                                      | 1200          | 1050       | 1725                                      | 2675          | 950        |
| $S'_{mean\ xy}$ | 2250                                      | 2800          | 5050       | 1725                                      | 6875          | 5150       |

The primary stress intensity in the Zircaloy is 9550 psi, which is less than 17,600 psi, and is therefore satisfactory. The significant point for the fatigue analysis is  $S_{mean} = 6900$  psi and  $S_{alt} = 2700$  psi (rounded up to the next hundred). This falls in the "safe" zone of Fig. H3a and is satisfactory.

In the upper flange of the steel I section, the transverse bending stresses are found using the bending moments of 34.2 and 22.9 lb-in., as for Zircaloy. The longitudinal stresses are listed on page 90. The following is the fatigue analysis tabulation for the top flange of the steel portion of the section shown in Fig. F21 when this section is used as the simple beam of Fig. F23:

|                | Stresses at Top of Flange (psi) |            |            | Stresses at Bottom of Flange (psi) |            |            |
|----------------|---------------------------------|------------|------------|------------------------------------|------------|------------|
|                | $\sigma_p$                      | $\sigma_l$ | $\sigma_t$ | $\sigma_p$                         | $\sigma_l$ | $\sigma_t$ |
| 30° ↘ Roll     | 0                               | -10,350    | -4200      | 0                                  | -6,800     | +4600      |
| 30° ↗ Roll     | 0                               | 0          | -2700      | 0                                  | 0          | +3100      |
|                | $S_{pl}$                        | $S_{lt}$   | $S_{tp}$   | $S_{pl}$                           | $S_{lt}$   | $S_{tp}$   |
| 30° ↘ Roll     | 10,350                          | -6,150     | -4200      | 6800                               | -11,400    | 4600       |
| 30° ↗ Roll     | 0                               | 2,700      | -2700      | 0                                  | -3,100     | 3100       |
| $S_{rxy}$      | 10,350                          | 8,850      | 1500       | 6800                               | 8,300      | 1500       |
| $S_{alt}$      | 5,175                           | 4,425      | 750        | 3400                               | 4,150      | 750        |
| $S'_{mean xy}$ | 5,175                           | 1,725      | 3450       | 3400                               | 7,250      | 3850       |

The primary stress intensity is 11,400 psi. This exceeds the 11,000 psi and the 9000 psi allowed for AISI types 304 and 304L stainless steel, respectively, at 600°F by the Navy Code.<sup>2</sup> A stronger stainless steel, AISI type 347, having an allowable primary stress intensity of 14,000 psi at 600°F was therefore specified.<sup>3</sup> The significant point for the fatigue analysis is  $S_{mean} = 7250$  psi and  $S_{alt} = 4150$  psi, which is satisfactory since it would fall in the "safe" zone of a figure constructed for steel similar to that constructed for Zircaloy in Fig. H3a. The cross section shown in Fig. F21 is therefore satisfactory here.

<sup>2</sup>"Tentative Structural Design Basis for Reactor Pressure Vessels and Directly Associated Components," p. 26, PB151987, 1 December 1958 Revision, Department of Commerce, Office of Technical Services.

<sup>3</sup>Ibid., p. 27.

Connecting Member for AF, Bottom Frame, Column 2 Model

With a thickness of 0.22 in. at mid-span, the fuel-element container wall is adequate at mid-span without support. In order, however, for the stresses at the corner to be considered secondary (see p. 81), support is needed at the mid-span that is either rigid enough to restrict the mid-span deflection or strong enough to carry additional load in the event of yielding at the corner of the fuel-element container. For this purpose, the use of the same connecting member as for the preceding case is assumed.

Referring to page 69, it may be seen that because of pressure alone  $D\delta_2 = 182 \text{ lb-in.}^3$ . With  $D = 3000 \text{ lb-in.}^2$  (see p. 80),  $\delta_2 = 0.0606 \text{ in.}$  On page 64,  $\delta_1$  is given as  $0.00137/t = 0.0098 \text{ in.}$  On page 108, the foundation modulus,  $k$ , for this beam is found to be  $490 \text{ lb/in.}\cdot\text{in.}$  With  $E = 29,000,000 \text{ psi}$  and  $I = 0.32 \text{ in.}^4$ ,

$$\lambda = \left( \frac{k}{4EI} \right)^{1/4} = 0.0605 \text{ in.}^{-1} ,$$

and the third component (pp. 77-87) of the total deflection is (pp. 48-57)

$$\begin{aligned} \delta_C &= \frac{P\lambda}{2k} \\ &= \frac{(154)(0.0605)}{980} = 0.0095 \text{ in.} \end{aligned}$$

Hence, the total deflection of

$$\delta_{K_B} = 0.0606 + 0.0098 + 0.0095 = 0.08 \text{ in.}$$

By reviewing the calculations on page 83, it may be seen that limiting the deflection of  $K_B$  to 0.08 in. will reduce the end bending moments to approximately 50 lb-in., and the design appears to be adequate. A check such as that on pages 89-91 would again show that the connecting member is adequate here.

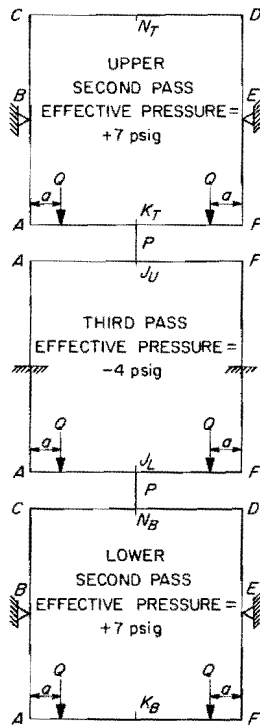
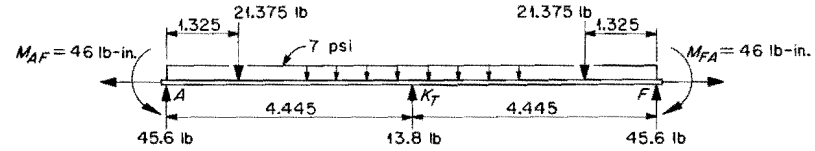


Fig. F4. Column 2 Fuel-Element Container Assembly Model.

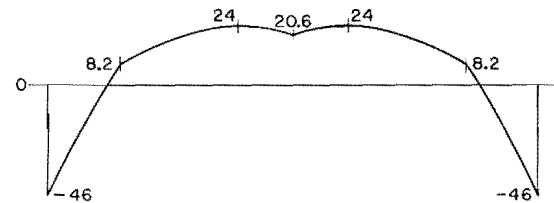


Fig. F2. Model Beam and Bending-Moment Diagram for the Bottom of the Upper Second Pass Fuel-Element Container in Column 2, at Mid-Height of the Core, for Core II Type Fuel Elements.

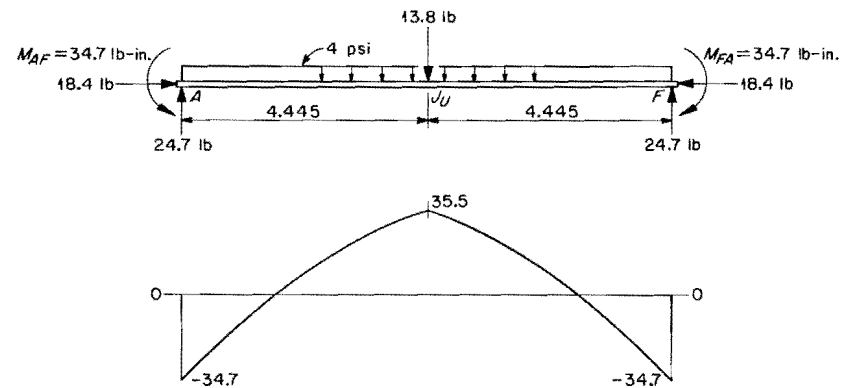


Fig. F3. Model Beam and Bending-Moment Diagram for the Top of the Third Pass Fuel-Element Container in Column 2, at Mid-Height of the Core, for Core II Type Fuel Elements.

UNCLASSIFIED  
ORNL-LR-DWG 77601

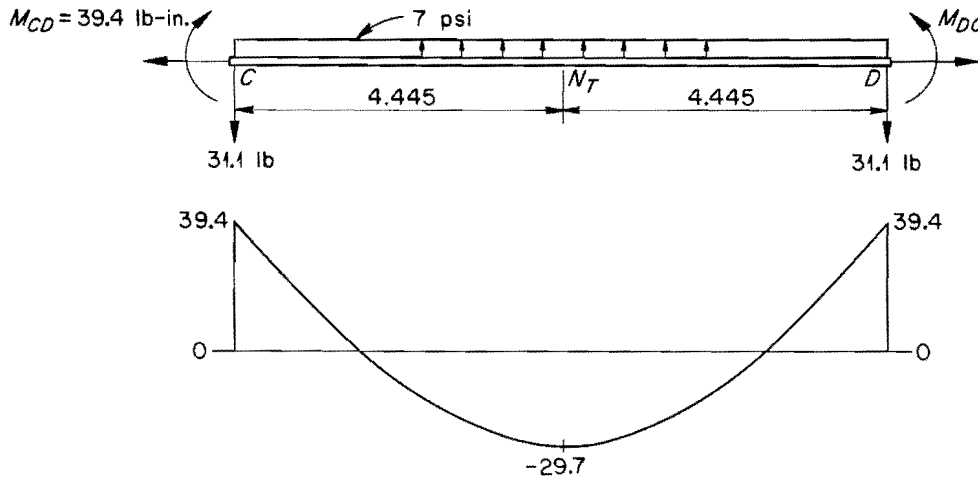


Fig. F4. Model Beam and Bending-Moment Diagram for the Top of the Upper Second Pass Fuel-Element Container in Column 2, at Mid-Height of the Core, for Core II Type Fuel Elements.

UNCLASSIFIED  
ORNL-LR-DWG 77602

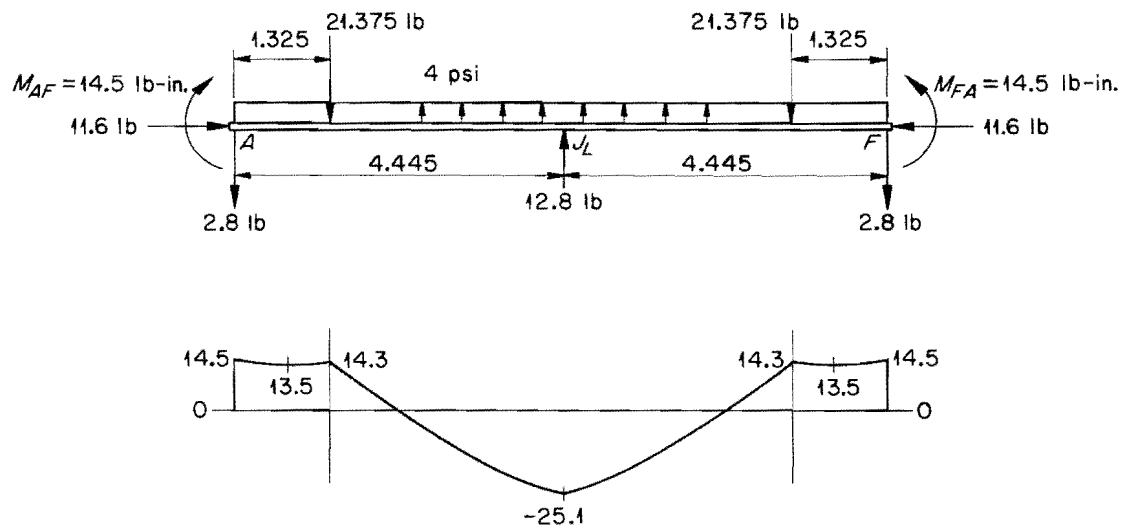


Fig. F5. Model Beam and Bending-Moment Diagram for the Bottom of the Third Pass Fuel-Element Container in Column 2, at Mid-Height of the Core, for Core II Type Fuel Elements.

UNCLASSIFIED  
ORNL-LR-DWG 77603

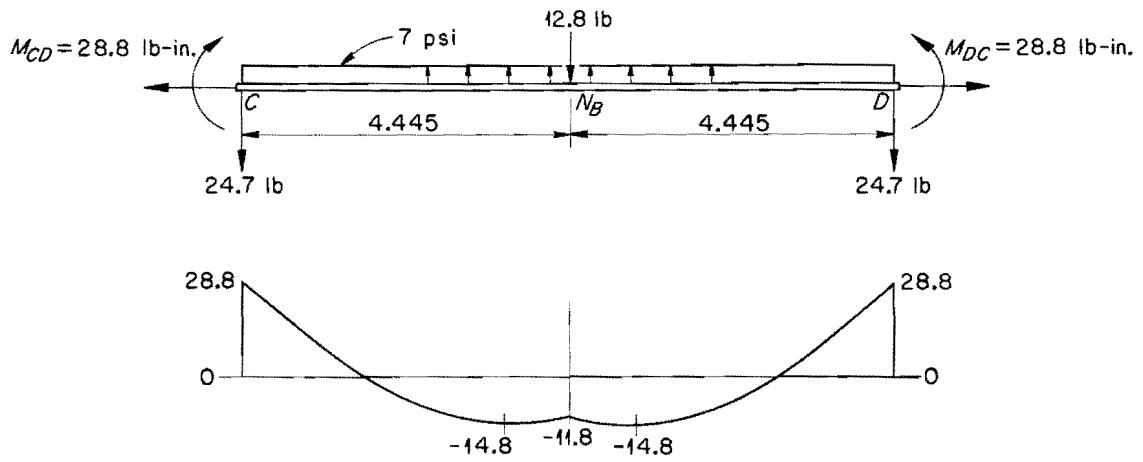


Fig. F6. Model Beam and Bending-Moment Diagram for the Top of the Lower Second Pass Fuel-Element Container in Column 2, at Mid-Height of the Core, for Core II Type Fuel Elements.

UNCLASSIFIED  
ORNL-LR-DWG 77604

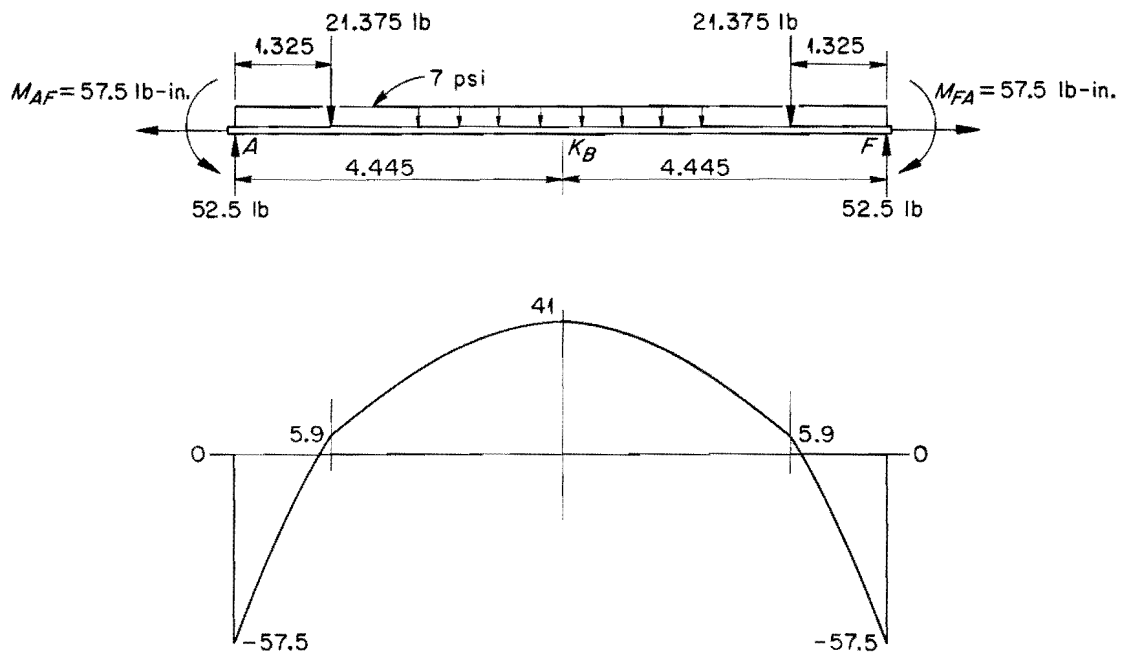


Fig. F7. Model Beam and Bending-Moment Diagram for the Bottom of the Lower Second Pass Fuel-Element Container in Column 2, at Mid-Height of the Core, for Core II Type Fuel Elements.

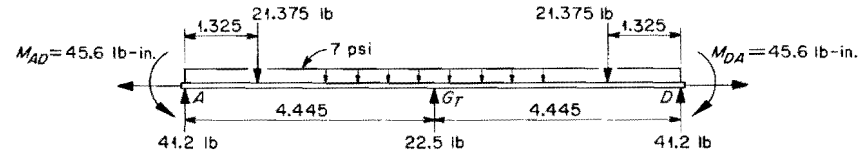


Fig. F9. Model Beam and Bending-Moment Diagram for the Bottom of the Top Fuel-Element Container in Column 1, at Mid-Height of the Core, for Core II Type Fuel Elements.

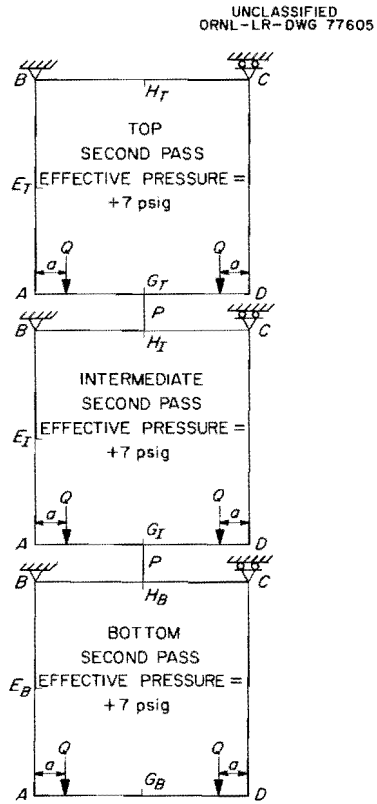


Fig. F8. Column 1 Fuel-Element Container Assembly Model.

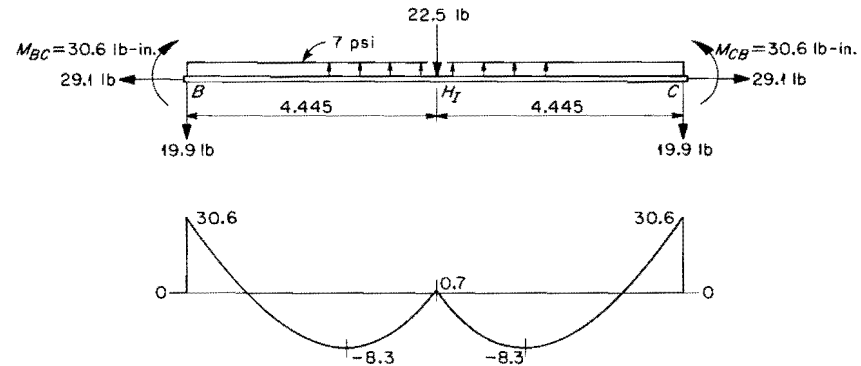


Fig. F10. Model Beam and Bending-Moment Diagram for the Top of the Intermediate Fuel-Element Container in Column 1, at Mid-Height of the Core, for Core II Type Fuel Elements.

UNCLASSIFIED  
ORNL-LR-DWG 77608

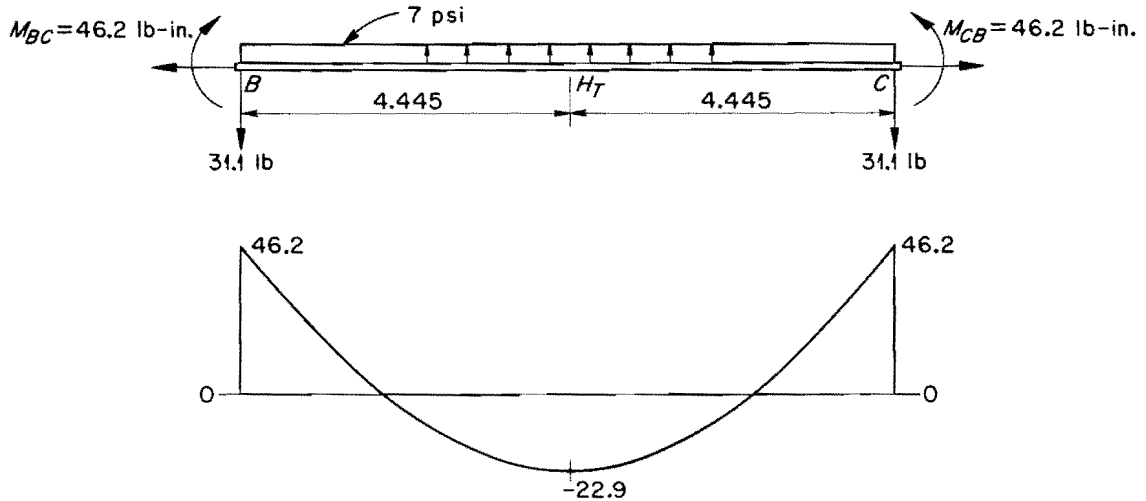


Fig. F11. Model Beam and Bending-Moment Diagram for the Top of the Top Fuel-Element Container in Column 1, at Mid-Height of the Core, for Core II Type Fuel Elements.

UNCLASSIFIED  
ORNL-LR-DWG 77609

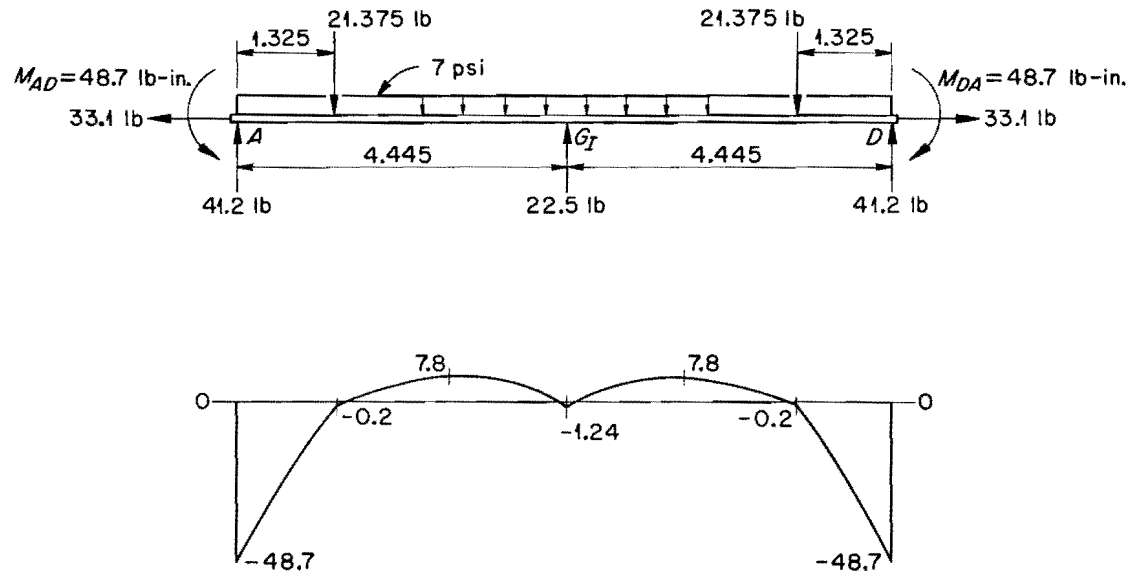


Fig. F12. Model Beam and Bending-Moment Diagram for the Bottom of the Intermediate Fuel-Element Container in Column 1, at Mid-Height of the Core, for Core II Type Fuel Elements.

UNCLASSIFIED  
ORNL-LR-DWG 77610

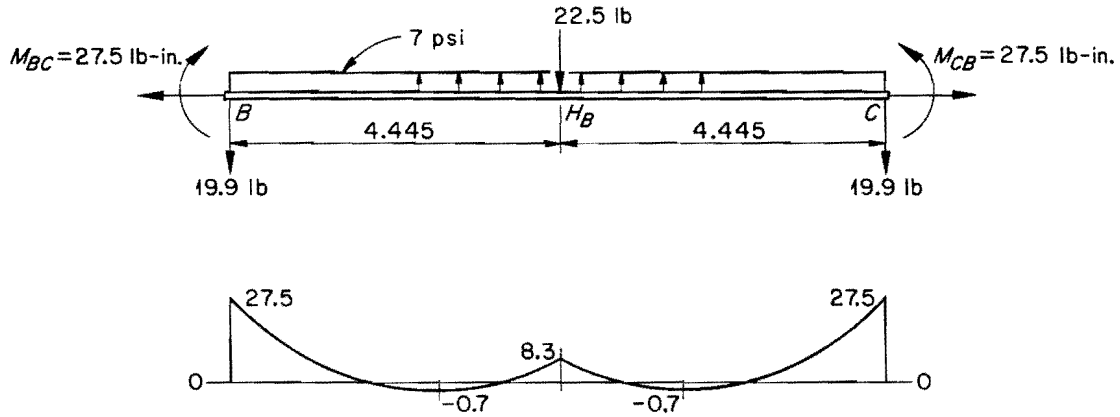


Fig. F13. Model Beam and Bending-Moment Diagram for the Top of the Bottom Fuel-Element Container in Column 1, at Mid-Height of the Core, for Core II Type Fuel Elements.

UNCLASSIFIED  
ORNL-LR-DWG 77611

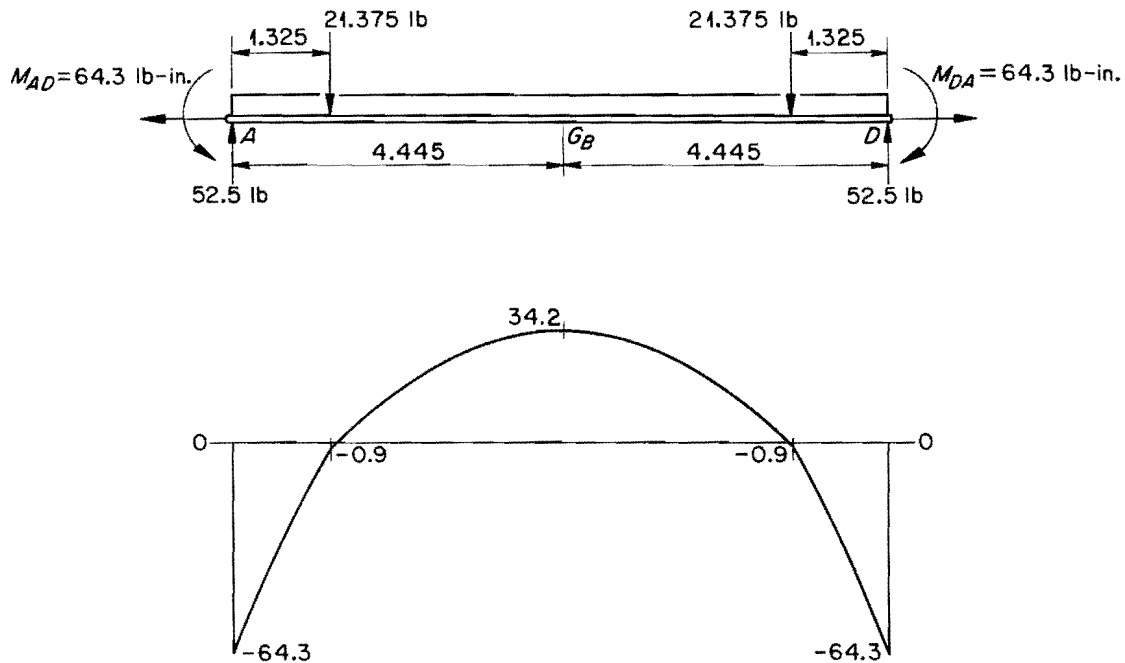
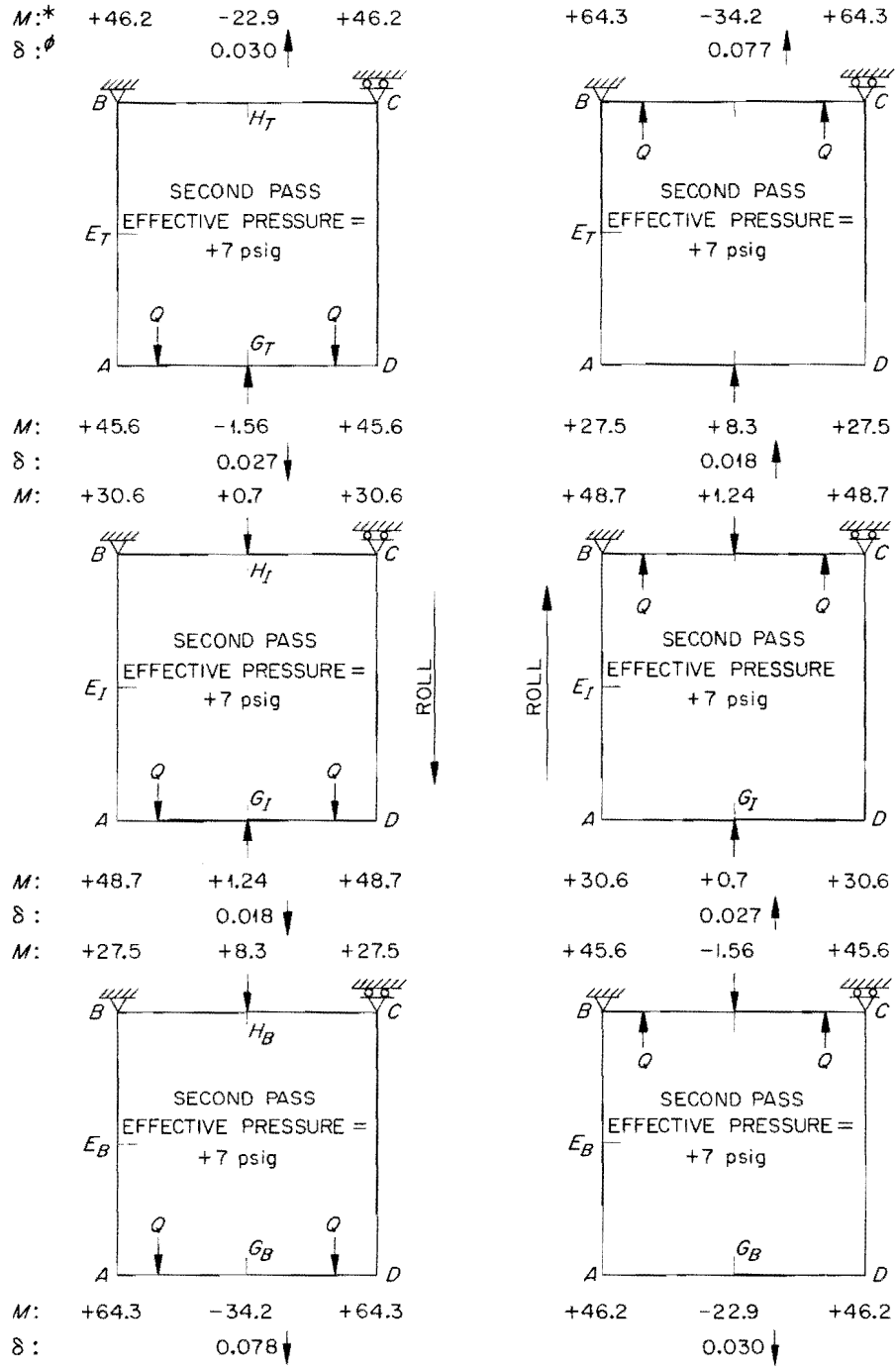


Fig. F14. Model Beam and Bending-Moment Diagram for the Bottom of the Bottom Fuel-Element Container in Column 1, at Mid-Height of the Core, for Core II Type Fuel Elements.

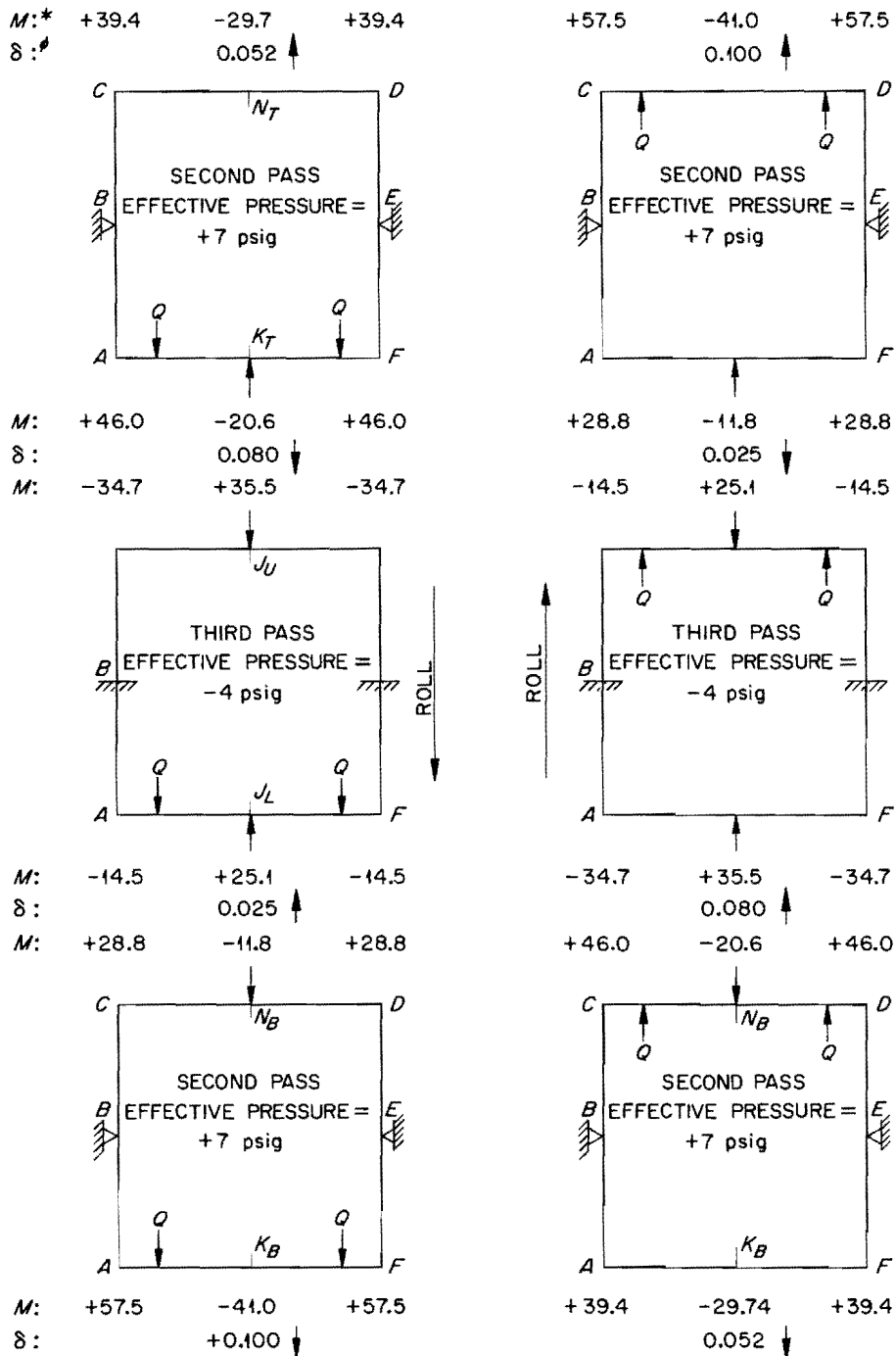
UNCLASSIFIED  
ORNL-LR-DWG 77612



\* POSITIVE MOMENT INDICATES TENSION ON THE INNER SURFACE. UNITS ARE lb-in.  
 $\emptyset$  DEFLECTIONS ARE IN INCHES FOR A PLATE THICKNESS OF 0.14 in.

Fig. F15. Significant Maximum Bending Moments and Deflections in Column 1, at Core Mid-Height, for Core II Type Fuel Elements and Normal Ship Motions.

UNCLASSIFIED  
ORNL-LR-DWG 77613



\* POSITIVE MOMENT INDICATES TENSION ON THE INNER SURFACE. UNITS ARE lb-in.

φ DEFLECTIONS ARE IN INCHES FOR A PLATE THICKNESS OF 0.14 in.

Fig. F16. Significant Maximum Bending Moments and Deflections in Column 2, at Core Mid-Height, for Core II Type Fuel Elements and Normal Ship Motions.

UNCLASSIFIED  
ORNL-LR-DWG 77614

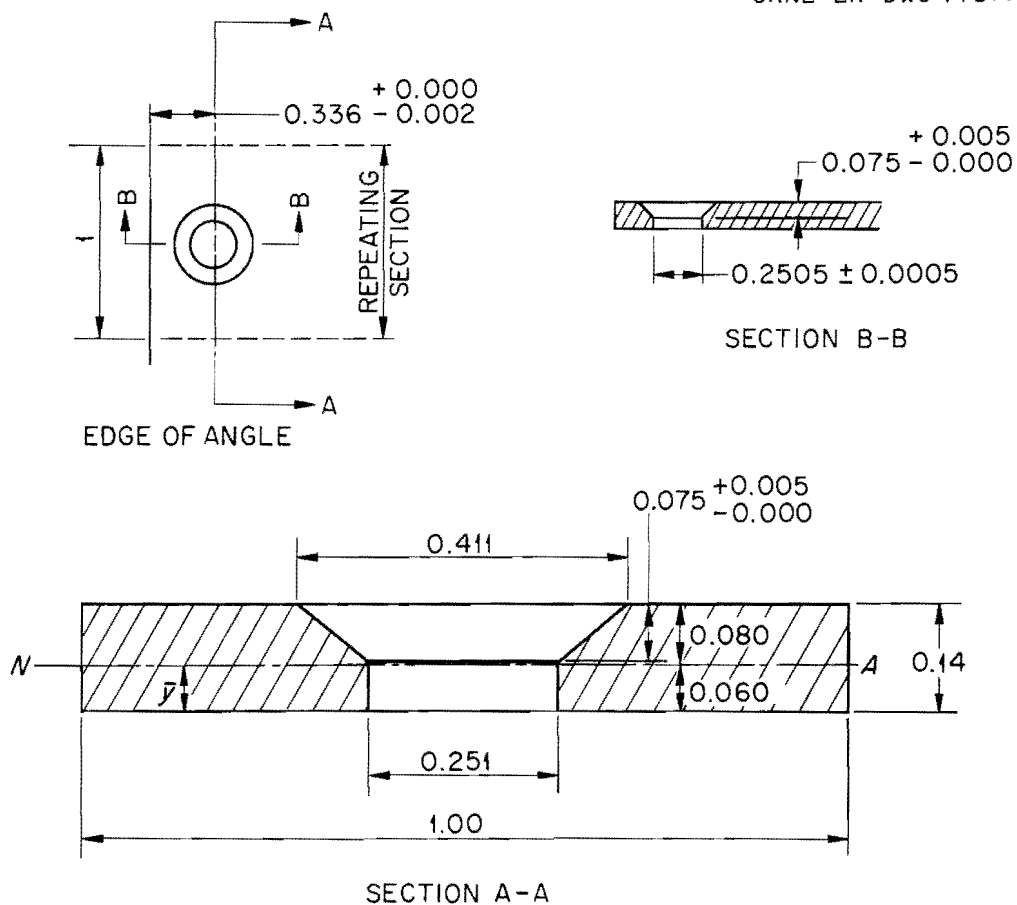


Fig. F17. Repeating Section of Fuel-Element Container Wall at Mid-span with  $t = 0.14$  in.

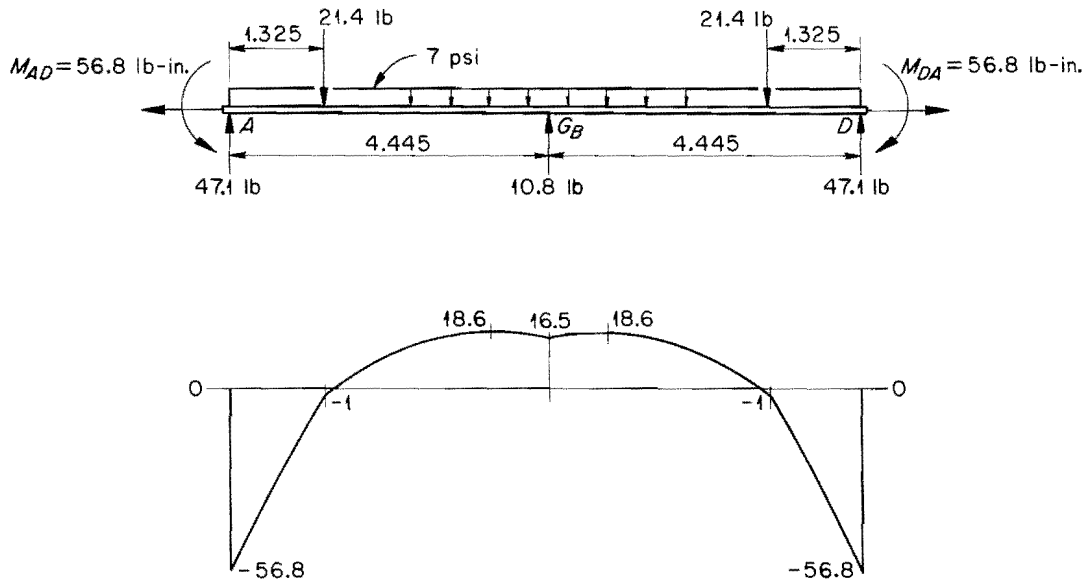


Fig. F18 Model Beam and Bending-Moment Diagram for the Member AD of the Bottom Fuel-Element Container in Column 1, at Mid-Height of the Core, for Core II Type Fuel Elements with the Mid-Span Deflection Limited to 0.05 in.

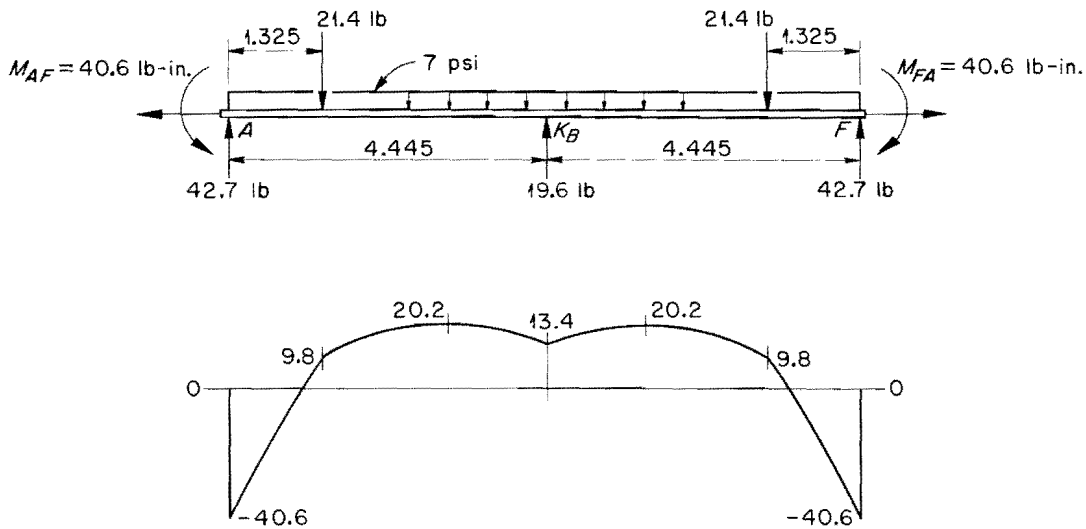
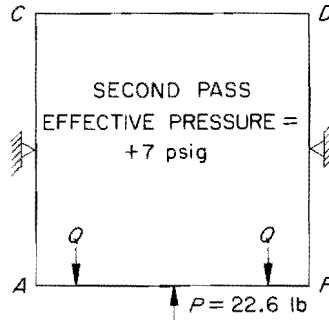
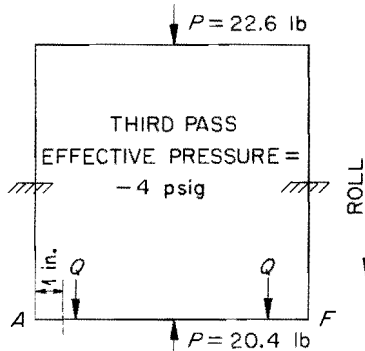


Fig. F19. Model Beam and Bending-Moment Diagram for the Member AF of the Bottom Fuel-Element Container in Column 2, at Mid-Height of the Core, for Core II Type Fuel Elements with the Mid-Span Deflection Limited to 0.06 in.

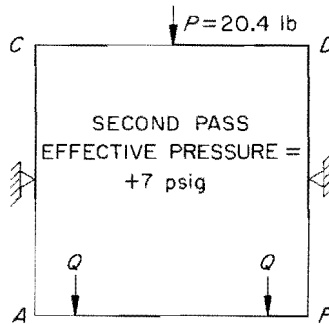
M: \* +39.9      -29.3      +39.9  
 δ: ϕ            0.04 ↑



M: +61.2      -20.6      +61.2  
 δ:            0.10 ↓  
 M: -42.5      +47.2      -42.5



M: +2.3      +24.3      +2.3  
 δ: 0.007 ↓      0.003 ↓  
 M: +22.9      -0.3      +22.9



M: +80.1      -51.8      +80.1  
 δ:            0.15 ↓

\* POSITIVE MOMENT INDICATES TENSION ON THE INNER SURFACE. UNITS ARE lb-in.

ϕ DEFLECTIONS ARE IN INCHES FOR A PLATE THICKNESS OF 0.14 in.

Fig. F20. Significant Maximum Bending Moments and Deflections at Mid-Height of the Core for Core II Type Fuel Elements and Unusual Ship Motions.



Appendix GANALYSES OF THE FUEL-ELEMENT CONTAINER ASSEMBLY AT OR NEAR  
THE TOP OF THE CORE FOR FUEL ELEMENTS OF CORE I TYPE

The critical elevation in the fuel-element containers for core I type fuel elements will be in the upper portion of the core, either near where the fuel-element loads are applied and where  $p_1$  and  $p_2$  are +9.2 and -5.6 psi, respectively, where the deflection is a maximum. Although in the analysis of the fuel-element containers at mid-height for core II type fuel elements the spacer bars were assumed to provide no structural strength, they may make a significant contribution here, for the spacer bars are actually beams on elastic foundations with supports providing some degree of fixity at the ends. A conservative cross section of the spacer bar "beam" which utilized the transverse dimensions of the stainless steel spacer bar was therefore assumed.

Geometrical and Physical Constants of the Spacer Bar "Beam"

The walls of the fuel-element containers are bolted to the spacer bars and therefore serve in somewhat the same capacity as cover plates on structural beams. It is assumed that the spacer bar "beam" is composed of the spacer bar and a cover plate consisting of a portion of the fuel-element container wall. It is assumed further that the AISC specification<sup>1</sup> requiring that the cover plate area not exceed 70% of the total flange area is applicable. The net area of the flange of the spacer bar is  $(1.375 - 0.5)(0.15) = 0.13125$  in.<sup>2</sup>. Therefore, the permissible cover plate area is  $(0.70/0.30)(0.13125) = 0.30625$  in., and the allowable net width of the cover plate is  $0.30625/0.14 = 2.19$  in. It is noted that this width also complies with the AISC specification<sup>2</sup> limiting the projection of a plate beyond the rivets to 16 times the plate thickness. In order that the cross section be a conservative one, the net width of

---

<sup>1</sup>Steel Construction, p. 297, 5th Ed., American Institute of Steel Construction, New York, 1950.

<sup>2</sup>Ibid., p. 289.

the cover plates was taken as 2 in. Hence, the assumed cross section of the spacer bar "beam" is as shown in Fig. G1, and the moment of inertia with respect to its neutral axis, N.A., is 0.132425 in.<sup>4</sup>. Subsequent modifications made the cross section more conservative.

It was realized that the fuel-element container walls will not be subjected to uniform compression along one edge in a direction parallel to a perpendicular edge; however, it was considered advisable to determine the critical value of the compressive stress for the walls acting as rectangular plates if they are to serve as "cover plates" for the spacer bar "beam."

For a rectangular plate simply supported on all four sides, the critical value of the compressive stress is given by the equation<sup>3</sup>

$$\sigma_{cr} = \Omega \sigma_e ,$$

in which  $\Omega$  is a constant depending on the length-to-width ratio and

$$\sigma_e = \frac{\pi^2 E t^2}{12 b^2 (1 - \mu^2)} ,$$

where  $t$  is the thickness of the plate and  $b$  is its width. If it is assumed that the sides of the containers consist of two plates, each of which is 4.5 in. wide and 80 in. long, it is found that

$$\begin{aligned} \sigma_e &= \frac{(9.87)(11,000,000)(0.0196)}{12(20.25)(0.84)} \\ &= 10,400 \text{ psi} . \end{aligned}$$

A good approximation<sup>3</sup> for  $\Omega$  is 4, since the length-to-width ratio

---

<sup>3</sup>S. Timoshenko, Strength of Materials, p. 195, Part II, 3rd Ed., D. Van Nostrand, New York, 1956.

exceeds 3. Therefore,

$$\sigma_{cr} = 4(10,400) = 41,600 \text{ psi .}$$

For a rectangular plate simply supported along three sides and free along the fourth side, which is parallel to the direction of compression, the equation

$$\sigma_{cr} = \psi \frac{\pi^2 D}{b^2 t}$$

gives the critical value of the compressive stress,<sup>4</sup> where

$$\psi = 0.456 + (b/a)^2,$$

b = width of plate,

a = length of plate (parallel to compressive stress),

t = thickness of plate,

$$D = \frac{Et^3}{12(1 - \mu^2)},$$

$\mu$  = Poisson's ratio.

If it is assumed again that the sides of the containers consist of two plates, each of which is 4.5 in. wide and 80 in. long,

$$\psi = 0.456 + \left(\frac{4.5}{80}\right)^2 = 0.459$$

and

$$\begin{aligned} \sigma_{cr} &= \frac{(0.459)(9.87)(11,000,000)(0.002744)}{(20.25)(0.14)(12)(0.84)} \\ &= 47,900 \text{ psi .} \end{aligned}$$

---

<sup>4</sup>S. P. Timoshenko and J. M. Gere, Theory of Elastic Stability, p. 362, 2nd Ed., McGraw-Hill, New York, 1961.

The membrane stress of 17,000 psi allowed for Zircaloy is well below either of these buckling stresses, and any load condition satisfying the 17,000-psi limitation will not cause buckling in the container walls. Utilization of a portion of the container walls as cover plates is therefore acceptable.

The modulus  $k$  of the elastic foundation is defined here as the force per unit length required to cause a deflection of 1 in. For the upper container adjacent to the upper spacer bar,

$$D\delta_{K_T} = \frac{67PL^3}{7680},$$

from Eq. D(13). With

$$D = 1,091,270t^3 = 3000 \text{ lb-in.}^2$$

for  $t = 0.14$  in. (see p. 64),

$$P = - \frac{(7680)(D)(1)}{67(703)} = -490 = 490 \text{ lb } \downarrow .$$

For the lower container adjacent to the upper spacer bar,

$$D\delta_{J_U} = \frac{PL^3}{120},$$

from Eq. D(20), and

$$P = \frac{(120)(D)(1)}{703} = 512 \text{ lb } \downarrow .$$

The modulus  $k$  of the elastic foundation of the spacer bar "beam" is therefore  $\sim 1000$  psi.

It was necessary to determine the load resulting from the pressures in pounds per lineal inch of spacer bar since throughout most of

the length of the bar there is no fuel-element load. This was done by multiplying the spacer bar deflection from pressure by the k factor just determined.

At the bottom of the core the effective pressures in the second- and third-pass containers are +4.5 and -2 psi, respectively. Utilizing equations D(13) and D(20), it is found that

$$D\delta_{K_T} = \frac{-67PL^3}{7680} + \frac{4.5L^4}{240}$$

and

$$D\delta_{J_U} = \frac{PL^3}{120} - \frac{(-2)L^4}{240},$$

where the terms involving the fuel element loads  $Q$  have been omitted. With  $D = 3000 \text{ lb-in.}^2$ , simultaneous solution of these equations yields  $\delta = 0.028 \text{ in.}$  Multiplying this value by the k factor of 1000 psi gives a load per lineal inch of  $\sim 28 \text{ lb.}$  This is the value of  $q$  (see Figs. E1, E2, or E3), which is the intensity of the uniformly distributed load on the beam.

At the top of the core the effective pressures in the second- and third-pass containers are +9.2 and -5.6 psi, respectively. Proceeding as for the bottom of the core gives a load of  $\sim 64 \text{ lb}$  per lineal inch, and  $64 - 28 = 36 \text{ lb}$  per lineal inch is the value of  $q_0$  (see Figs. E1, E2, or E3), which is the maximum intensity of the triangularly distributed load on the beam.

The values 28 and 64 lb may also be approximated by considering the spacer bar to carry half of the load applied by pressure to the container walls. At the bottom and at the top of the core it is found that  $(1/2)(4.5 + 2)8.891 = 28.89$  and  $(1/2)(9.2 + 5.6)8.891 = 65.79 \text{ lb}$  per lineal inch of spacer bar; these values are reasonably close checks on 28 and 64 psi.

The value of  $P$  (see Figs. E1, E2, or E3), the concentrated load applied by the fuel bundle, was approximated by a method suggested by the previous paragraph and as indicated in Fig. G2. By considering each half of the container wall to be a simply supported beam, it is found that

$$P = 154 \text{ lb.}$$

#### Moments and Deflections in the Spacer Bar "Beams"

As was stated in the first paragraph of this appendix, the spacer bar "beams" are partially fixed at the ends, but the degree of fixity is unknown. The "beams" were therefore analyzed for two boundary conditions; they were considered to be simply supported, as shown in Fig. E2, for one condition and completely fixed, as shown in Fig. E3, for the other.

The values of  $P$ ,  $q$ , and  $q_0$ , as shown in Figs. E2 and E3, and the values of  $k$  and  $I$  were determined earlier in this appendix. The distance  $e$  from the point of support to the fuel-element load was assigned values of 3 and 5 in., after it was observed that this distance was different for the core I and core II type fuel elements. The deflections and bending moments at 1-in. increments along the beam were then determined by an IBM-7090 computation.\* The maximum moments and deflections are listed in Table G1 for 18 different cases involving three values of the net "cover plate" width  $b$ . The different values of  $b$  were used to check the effect of the "cover plate" width on the moments and deflections. It is noted that the effect is much more evident in the maximum bending moment than in the maximum deflection.

#### Transverse Sections of the Intermediate Fuel-Element Container Walls

All frames of column 1 are subjected to the same internal pressure at any particular elevation in the core and therefore tend to support

---

\*The author is indebted to D. Griffin, Math Panel, Oak Ridge National Laboratory, for writing the program.

Table G1. Moments and Deflections in the Assumed Spacer Bar "Beam"

| End Condition | e (in.)  | b (in.) | I (in. <sup>4</sup> ) | $\lambda$ (in. <sup>-1</sup> ) | P (lb)   | M <sub>max</sub> (lb-in.) | $\delta_{max}$ (in.) |         |
|---------------|----------|---------|-----------------------|--------------------------------|----------|---------------------------|----------------------|---------|
| Hinged        | 3        | 0       | 0.024323              | 0.174837                       | 154      | 558.90                    | 0.06637              |         |
|               |          | 2       | 0.132425              | 0.114458                       | 154      | 971.05                    | 0.06133              |         |
|               |          | 4       | 0.240527              | 0.098593                       | 154      | 1234.3                    | 0.05968              |         |
|               | 5        | 0       | 0.024323              | 0.174837                       | 154      | 599.69                    | 0.06974              |         |
|               |          | 2       | 0.132425              | 0.114458                       | 154      | 1136.1                    | 0.06264              |         |
|               |          | 4       | 0.240527              | 0.098593                       | 154      | 1388.6                    | 0.06060              |         |
|               | $\infty$ | 0       | 0.024323              | 0.174837                       | 0        | 334.99                    | 0.06255              |         |
|               |          | 2       | 0.132425              | 0.114458                       | 0        | 787.43                    | 0.05973              |         |
|               |          | 4       | 0.240527              | 0.098593                       | 0        | 1061.6                    | 0.05845              |         |
|               | Fixed    | 3       | 0                     | 0.024323                       | 0.174837 | 154                       | -1265.8              | 0.05968 |
|               |          |         | 2                     | 0.132425                       | 0.114458 | 154                       | -2614.0              | 0.05570 |
|               |          |         | 4                     | 0.240527                       | 0.098593 | 154                       | -3395.4              | 0.05401 |
| 5             |          | 0       | 0.024323              | 0.174837                       | 154      | -1286.6                   | 0.06095              |         |
|               |          | 2       | 0.132425              | 0.114458                       | 154      | -2703.8                   | 0.05603              |         |
|               |          | 4       | 0.240527              | 0.098593                       | 154      | -3508.2                   | 0.05423              |         |
| $\infty$      |          | 0       | 0.024323              | 0.174837                       | 0        | -1004.7                   | 0.05921              |         |
|               |          | 2       | 0.132425              | 0.114458                       | 0        | -2292.7                   | 0.05554              |         |
|               |          | 4       | 0.240527              | 0.098593                       | 0        | -3056.7                   | 0.05390              |         |

each other at mid-span through the spacer bar. An increase in the effective pressure as the top is approached will increase (positively) the bending moments at A for both clockwise and counterclockwise roll so that the bending moment differentials should change little, if any. A similar statement applies at G<sub>I</sub>. Furthermore, as the top of the core is approached, the spacer bar "beams" support, to a certain extent, the walls of the fuel-element containers so that the column 1 model becomes somewhat like the column 2 model. Hence, this part of the investigation was limited to the region between the top second-pass and the adjacent third-pass containers in column 2.

#### Transverse Section at the Point of Maximum Deflection

Referring again to Table G1, it may be observed that the maximum deflection for b = 2 in. is 0.06264 in. A check of the machine output showed this deflection to occur at 16 in. from the hinge providing

simple support. At this location the remote fuel-element loads at the bottom of the core were assumed to have no direct effect on the model frames, and the pressure in the second-pass container is +8.2 psi. By using Eq. D(13),

$$\downarrow EI\delta_K = -\frac{67PL^3}{7680} + \frac{9}{320} QaL^2 + \frac{31}{320} Qa^2L - \frac{Qa^3}{6} + \frac{pL^4}{240} + \frac{RL^3}{2560},$$

and the above data, it is possible to calculate the magnitude of the force P exerted on the second-pass container by the spacer bar "beam." Substitution of  $\delta = 0.06264$  in.,  $EI = D = 3000$  lb-in.<sup>2</sup> (see p. 80), and of  $p = +8.2$  psi yields  $P = 4.25$  lb, since R is assumed to be zero. Use of Eq. D(8),

$$M_{AF} = -\frac{31PL}{320} - \frac{RL}{320} + \frac{31Qa(L-a)}{40L} + \frac{17pL^2}{240},$$

gives  $M_{AF} = 42.2$  lb-in. The values were used to construct the bending-moment diagram for the bottom of the second-pass container shown in Fig. G3a.

Inspection of the IBM-7090 output indicated that roll reversal and the attendant reversal of the fuel-element loads change the deflection at 16 in. from the assumed simple support at the top of the core to 0.05624 in. The corresponding values of P and  $M_{AF}$  are 7.2 lb and 39.7 lb-in., respectively. With these values the bending-moment diagram of Fig. G3b was constructed.

In the third-pass container at the point of 0.06264-in. deflection, the pressure is -4.9 psi. From Eq. D(20), with  $Q = 0$ , the equation

$$EI\delta_J = \frac{PL^3}{120} - \frac{pL^4}{240}$$

is obtained; substitution of  $EI = D = 3000$  lb-in.<sup>2</sup>,  $\delta = 0.06264$  in., and  $p = -4.9$  psi yields  $P = 10.3$  lb. From Eq. D(18), with  $Q = 0$ ,

$$M_{AF} = \frac{PL}{10} - \frac{17}{240} pL^2 .$$

With  $p = -4.9$  psi and  $P = 10.3$  lb, solution of this equation gives  $M_{AF} = 36.5$  lb-in. The above values were used to construct the bending-moment diagram for the top of the third-pass container shown in Fig. G4a.

As pointed out on page 112, roll reversal causes the deflection at this section to change to 0.05624 in. Corresponding values of  $P$  and  $M_{AF}$  are 6 lb and 32.7 lb-in., respectively. With these values the bending-moment diagram of Fig. G4b was constructed.

It is noted that the stress conditions at this section of maximum deflection, 16 in. from the simple support, are less severe than those shown to be satisfactory on pages 78-79 and 81-82. The bending-moment diagrams indicate that the maximum deflection occurs at mid-span, where the deflection is 0.06264 in. Hence, this section in the intermediate fuel-element containers is satisfactory.

#### Transverse Sections Near the Top Point of Application of the Fuel-Element Loads

The adequacy of the interior fuel-element containers near the top point of application of the fuel-element loads was established by investigating five different conservative load and position conditions. Because of the proximity of the support, the fuel-element loads were distributed over a length of  $2e$ ,  $e$  inches on each side of  $P$  (see Figs. E1, E2, or E3).

At Top End of Spacer Bar "Beam,"  $e = 3$  in. At the top end of the spacer bar "beam," a transverse section of the fuel-element container is subjected to the same loads irrespective of the end conditions assumed for the "beam," and the deflection is zero. The most severe condition for this transverse section is that for  $e = 3$  in. The fuel element loads are  $Q = 2(21.375) = 42.75$  lb (see p. 63), and the effective pressures in the second- and third-pass containers are +9.2 and -5.6 psi, respectively.

For the bottom of the second-pass fuel-element container, the above data and Eq. D(13) were used to obtain  $P = 67.4$  lb, and then, from

Eq. D(8),  $M_{AF} = 30.8$  lb-in. These data were used to obtain the bending-moment diagram for clockwise roll shown in Fig. G5a for the bottom of the second-pass fuel-element container. For counterclockwise roll, the necessary data were obtained in a similar way. The bending-moment diagram is shown in Fig. G5b.

For the top of the third-pass fuel-element container, Eqs. D(20) and D(18) were solved, after substituting the above values for pressures, deflection, and  $Q$ , to obtain

$$P = -24.9 \text{ lb}$$

and

$$M_{AF} = +9.15 \text{ lb-in.}$$

The use of these data permitted the construction of the bending-moment diagram for the top of the third-pass container shown in Fig. G6a for clockwise roll. The diagram shown in Fig. G6b for counterclockwise roll was similarly obtained.

Examination of Figs. G5 and G6 shows that the end conditions are satisfactory, since they are less severe than those shown to be satisfactory on pages 76-78, 81-82, and 83-84. The mid-span condition in Fig. G5 is slightly more severe, because of the stress range, than that shown on pages 78-79 to be satisfactory. The analysis on pages 85-86 for  $t = 0.22$  in. indicates, however, that the mid-span region of the second-pass container as well as of the third-pass container is satisfactory. The maximum deflections in the beams of Figs. G5 and G6 do not occur at mid-span. The deflection of the beam shown in Fig. G6 is obviously less than that of the beam shown in Fig. G5. The maximum deflection for the beam of Fig. G5a was calculated by area moment methods and found to be 0.0105 in. at a point approximately 1.9 in. from either end of the span. Hence, it is concluded that this section is adequate.

Section at 10 in. from Simply Supported End of Spacer Bar "Beam,"  
 $e = 5$  in. For  $e = 5$  in., the deflection at 10 in. from the simple support for  $30^\circ$  clockwise roll is 0.0566 in., based on the IBM-7090 output.

For 30° counterclockwise roll it is 0.0456 in. At this same elevation the effective pressures in the second- and third-pass containers are, respectively, +8.6 and -5.2 psi. The Q loads (see p. 63) are 12/10 of 21.375 or 25.65 lb. Use of Eq. D(13) and D(8) yields  $P = 25.9$  lb and  $M_{AF} = 48.3$  lb-in., respectively. These values of  $P$  and  $M_{AF}$  were used to construct the bending-moment diagram of Fig. G7a. The diagram of Fig. G7b was similarly obtained. Equations D(20) and D(18) yield, respectively,  $P = 5.95$  lb and 34.4 lb-in., and the bending-moment diagram shown in Fig. G8a for the top of the third-pass container was constructed through use of this data. The diagram shown in Fig. G8b for 30° counterclockwise roll was similarly obtained.

For this location and load condition, that is, 10 in. from the simple support with  $e = 5$  in., the stress conditions are less severe than those shown on pages 76-78 and 78-79 to be acceptable. As can be determined by referring to the moment diagrams in Figs. G7 and G8, the maximum deflection occurs at the spacer bar. This maximum deflection is 0.0566 in., which is permissible. The design is therefore adequate for this section.

Section at 10 in. from Fixed End of Spacer Bar "Beam,"  $e = 5$  in.  
For  $e = 5$  in., the deflection at 10 in. from the fixed support for 30° clockwise roll is 0.0360 in., based on the IBM-7090 output. For 30° counterclockwise roll it is 0.0312 in. As for the preceding case, the Q loads and the effective pressures in the second- and third-pass containers are 25.65 lb, +8.6 psi, and -5.2 psi, respectively.

Equations D(13) and D(8) were used to obtain, respectively,  $P = 36$  lb and  $M_{AF} = 39.6$  lb-in., and with this data the diagram of Fig. G9a was constructed. The diagram of G9b was similarly obtained.

Equations D(20) and D(18) were used to obtain, respectively,  $P = -4.6$  lb = 4.6 lb  $\uparrow$  and  $M_{AF} = 25$  lb-in. The diagram of Fig. G10a was constructed through use of this data, and the diagram of Fig. G10b was obtained in a similar way.

Section at 6 in. from Simply Supported End of Spacer Bar "Beam,"  $e = 3$  in.  
For  $e = 3$  in., the deflection at 6 in. from the simple support for 30° clockwise roll is 0.040 in., based on the IBM-7090 output.

For 30° counterclockwise roll it is 0.0327 in. For this elevation and loading the effective pressures and Q loadings are +8.9 psi, -5.3 psi, and 42.75 lb, respectively. Only the end results are shown in Figs. G11 and G12.

Section at 6 in. from Fixed End of Spacer Bar "Beam," e = 3 in.

For e = 3 in., the deflection at 6 in. from the fixed support for 30° clockwise roll is 0.0182 in., based on the IBM-7090 output. For 30° counterclockwise roll it is 0.0162 in. As for the preceding case, the Q loads and the effective pressures in the second- and third-pass containers are 42.75 lb, +8.9 psi, and -5.3 psi, respectively. Only the end results are shown in Figs. G13 and G14.

Comments. Comparison of the mid-span moments of Figs. G9 through G14 with the transverse moments used in the analysis on pages 85-86 and of moments at other points with the end moments used in the analysis on pages 76-78 indicates that these last three cases are satisfactory stress-wise. Checking Fig. G13a against Fig. G5a and the lower part of page 114, it may be seen that the deflection is not a critical item. It is concluded that these last three cases are satisfactory.

Spacer Bar "Beam" at Top of Core

By referring to Table G1, it is observed that the maximum bending moment occurs in the beam with the fixed end in all cases, as was expected. Using the flexure formula,  $\sigma = Mc/I$ , with  $M = 2703$  lb-in. and  $c = 0.5075$  in., it is found that the maximum flexure stresses in the beam are 7400, 10,360, and 19,440 psi for values of b, the net "cover plate" width, of 4, 2, and 0 in., respectively.

For a roll such as that indicated on the left in Fig. F16, P (as shown in Fig. G15) is positive, and the longitudinal stresses  $\sigma_{L1}$  through  $\sigma_{L6}$ , as indicated in Fig. G15 for a fixed end beam, are +10,360, +7500, +4440, -4440, -7500, and -10,360 psi, respectively, if M is taken as 2703 lb-in. For the same condition, the transverse bending moment (in a plane perpendicular to the axis of the spacer bar) in the second-pass container wall at the bolt centerline is obtained from

Fig. G5a and is  $-22.1 \text{ lb-in./in.}$  Because of this moment the stresses  $\sigma_{T_1}$  and  $\sigma_{T_2}$  are 10,200 and  $-9400 \text{ psi}$ , respectively, if the reinforcing effect of the spacer bar flange is neglected.

For a roll such as that indicated on the right in Fig. F16, P is negative, that is, it acts upward, and the stresses  $\sigma_{L_1}$  through  $\sigma_{L_6}$  are, respectively,  $+7220$ ,  $+5220$ ,  $+3090$ ,  $-3090$ ,  $-5220$ , and  $-7220 \text{ psi}$ ; the stresses  $\sigma_{T_1}$  and  $\sigma_{T_2}$  are  $+3600$  and  $-3320 \text{ psi}$ , respectively.

The fatigue analysis was based on a fuel-element container wall thickness of  $0.14 \text{ in.}$  and on the assumption that the appropriate foregoing stresses could be developed at points on the surfaces of the second-pass container wall. The following is the fatigue analysis of the spacer bar region of the second-pass container wall near the top of the core with the spacer bar "beam" fixed at that end and a wall thickness of  $0.14 \text{ in.}$ :

|                     |      | Container Interior Wall<br>Stresses (psi) |               |            | Container Exterior Wall<br>Stresses (psi) |               |            |
|---------------------|------|---|---------------|------------|---|---------------|------------|
|                     |      | $\sigma_p$                                | $\sigma_\ell$ | $\sigma_t$ | $\sigma_p$                                | $\sigma_\ell$ | $\sigma_t$ |
| $30^\circ \searrow$ | Roll | 0   | 10,360        | 10,200     | 0   | 7,500         | -9400      |
| $30^\circ \nearrow$ | Roll | 0   | 7,220         | 3,600      | 0   | 5,220         | -3320      |
|                     |      | $S_{p\ell}$                               | $S_{\ell t}$  | $S_{tp}$   | $S_{p\ell}$                               | $S_{\ell t}$  | $S_{tp}$   |
| $30^\circ \searrow$ | Roll | -10,360                                   | 160           | 10,200     | -7500                                     | 16,900        | -9400      |
| $30^\circ \nearrow$ | Roll | -7,220                                    | 3,620         | 3,600      | -5220                                     | 8,540         | -3320      |
| $S_r$               |      | 3,140                                     | 3,460         | 6,600      | 2280                                      | 8,360         | 6080       |
| $S_{alt}$           |      | 1,570                                     | 1,730         | 3,300      | 1140                                      | 4,180         | 3040       |
| $S'_{mean}$         |      | 8,790                                     | 1,890         | 6,900      | 6360                                      | 12,720        | 6360       |

Since  $S'_{mean} + S_{alt} < 48,500 \text{ psi} = S_b = S_y$  of cold-worked Zircaloy,  $S'_{mean} = S_{mean}$ . Through the use of Fig. H3a, it is found that the set of values  $S_{mean} = 12,800 \text{ psi}$  and  $S_{alt} = 4200$  is equivalent to an allowable alternating stress intensity,  $S_a$ , of  $5500 \text{ psi}$ . This exceeds the endurance limit of  $4800 \text{ psi}$  obtained by using a factor of safety of 2.4, as explained on page 136.

Subsequent to the foregoing analysis it was decided to increase the thickness of the fuel-element container walls at mid-span to 0.22 in. (see p. 85). With this increased thickness, the transverse stresses  $\sigma_{T_1}$  and  $\sigma_{T_2}$  are, respectively, 4310 and -3570 psi for 30° clockwise roll and +1550 and -960 psi for 30° counterclockwise roll, if account is taken of a stress of +260 psi as a result of the axial load in the member. Use of the previous values for  $\sigma_p$  and  $\sigma_\ell$ , which is conservative, permitted the following fatigue analysis of the spacer bar region of the second-pass container wall near the top of the core with the spacer bar "beam" fixed at that end and  $t = 0.22$  in.:

|             |      | Container Interior Wall<br>Stresses (psi) |               |            | Container Exterior Wall<br>Stresses (psi) |               |            |
|-------------|------|---|---------------|------------|---|---------------|------------|
|             |      | $\sigma_p$                                | $\sigma_\ell$ | $\sigma_t$ | $\sigma_p$                                | $\sigma_\ell$ | $\sigma_t$ |
| 30° ↘       | Roll | 0   | 10,360        | 4310       | 0   | 7,500         | -3570      |
| 30° ↗       | Roll | 0   | 7,220         | 1550       | 0   | 5,220         | -960       |
|             |      | $S_{p\ell}$                               | $S_{\ell t}$  | $S_{tp}$   | $S_{p\ell}$                               | $S_{\ell t}$  | $S_{tp}$   |
| 30° ↘       | Roll | -10,360                                   | 6,050         | 4310       | -7500                                     | 11,070        | -3570      |
| 30° ↗       | Roll | -7,220                                    | 5,670         | 1550       | -5220                                     | 6,180         | -960       |
| $S_r$       |      | 3,140                                     | 380           | 2760       | 2280                                      | 4,890         | 2610       |
| $S_{alt}$   |      | 1,570                                     | 190           | 1380       | 1140                                      | 2,445         | 1305       |
| $S'_{mean}$ |      | 8,790                                     | 5,860         | 2930       | 6360                                      | 8,625         | 2265       |

Since  $S'_{mean} + S_{alt} < 48,500$  psi and therefore  $S'_{mean} = S_{mean}$ , the significant set of values for  $S_{mean}$  and  $S_{alt}$  are 8700 and 2500 psi, respectively. This point lies in the "safe" zone of Fig. H3a, and the wall design is adequate.

Sound construction requires that the thicknesses of the flanges and of the web of the spacer bars be approximately 0.25 in. Such a flange thickness would leave only 0.075 in. between the backs of the flanges, since the fuel-element container walls at the points of attachment to the spacer bars are now 0.22 in. thick. Bars of rectangular cross section, 0.575 in. by 1.325 in., are therefore being specified.

Use of the mid-span moments of -33 and -14 lb-in. was also checked. It was found that the significant point (10,300 psi, 2500 psi) was also satisfactory.

The transverse moment at the edge of the spacer bar is found to be ~12 lb-in./in. from Fig. G5a. If this moment is assumed to be developed by tension in the bolt, the tension is  $12/0.3515 = 34$  lb and the tensile stress in the bolt is  $34/(\pi/64) = 693$  psi. The shearing stress and bearing stress in the bolt head will be less, and the bolt is adequate here and elsewhere in the containers.

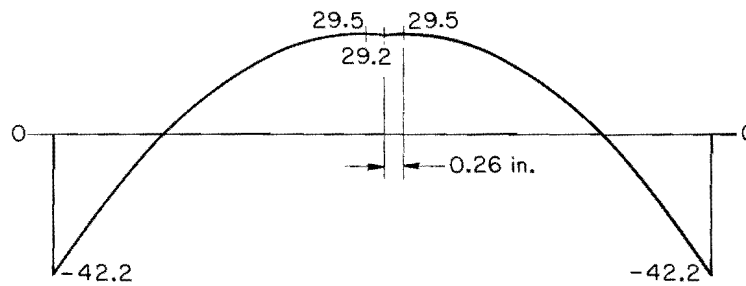
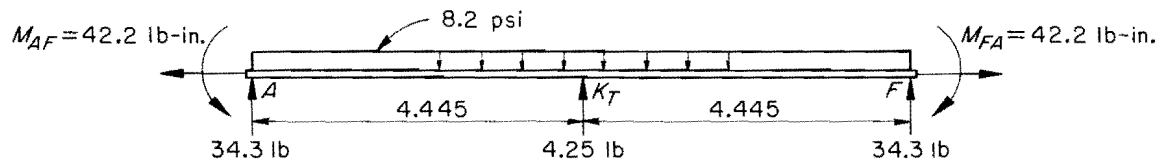
Figure G6 shows that the transverse moments and hence the transverse stresses are much less for the third-pass container wall than for the second-pass container wall. The longitudinal stresses are the same as for the corresponding locations in the second-pass container wall. These facts dictate that the  $S_a$  values must be less in this area than the respective values in the area of the second-pass container wall. Fatigue analyses were not done because it was evident that the design was adequate for the spacer bar-spacer bar flange-third-pass container wall area.

#### Transverse Sections of Peripheral Container Walls

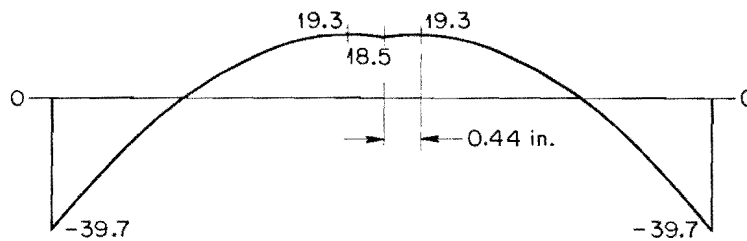
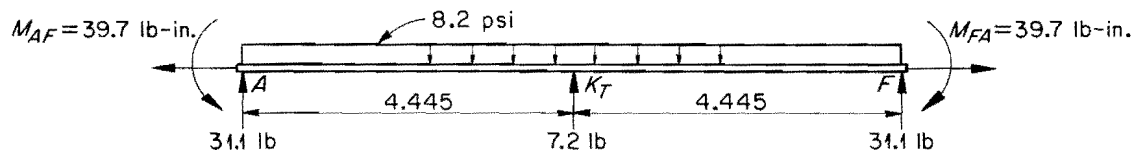
The transverse sections of the peripheral container walls were analyzed for core II type fuel elements on pages 79-92, but pages 87-92 seem most pertinent here. If it is assumed that the loads other than the 7-psi pressure load, which the fuel container can safely carry, are carried by the same connecting member, the beam loaded as shown in Fig. G16 is obtained.

For the beam shown above,  $R_1$  and  $R_2$  are 321 and 187 lb, respectively. The maximum bending moment occurs 25.7 in. to the right of  $R_1$  and is 2250 lb-in. This is less than half the maximum bending moment of 4580 lb-in. in the beam of Fig. F24, for which the connecting member of Fig. F22 was shown to be adequate. The connecting member is therefore adequate for fuel elements of either core I or core II type.





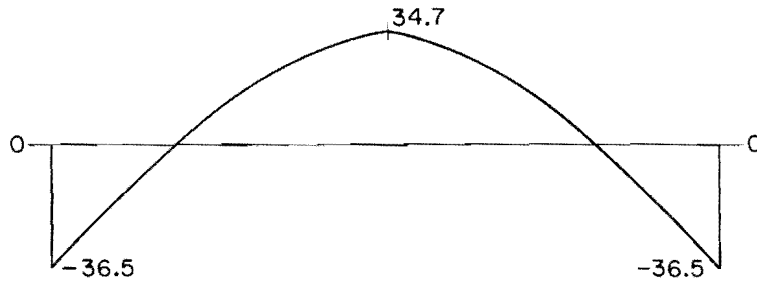
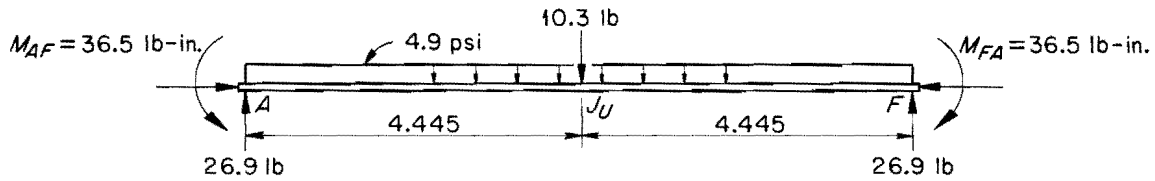
(a) 30° CLOCKWISE ROLL



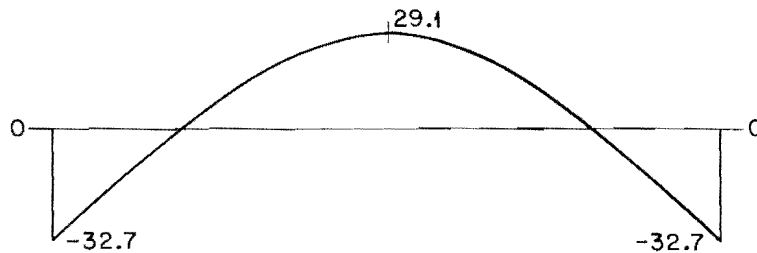
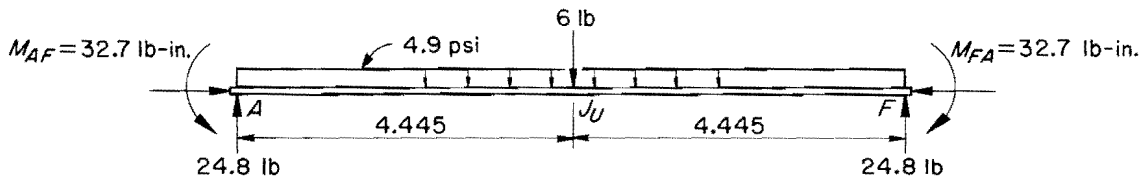
(b) 30° COUNTERCLOCKWISE ROLL

Fig. G3. Model Beams and Bending-Moment Diagrams for the Bottom of the Upper Second Pass Fuel-Element Container in Column 2, 16 in. from the Assumed Simple Support at the Top of the Core, for Core I Type Fuel Elements.

UNCLASSIFIED  
ORNL-LR-DWG 77624



(a) 30° CLOCKWISE ROLL



(b) 30° COUNTERCLOCKWISE ROLL

Fig. G4. Model Beams and Bending-Moment Diagrams for the Top of the Third Pass Fuel-Element Container in Column 2, 16 in. from the Assumed Simple Support at the Top of the Core, for Core I Type Fuel Elements.

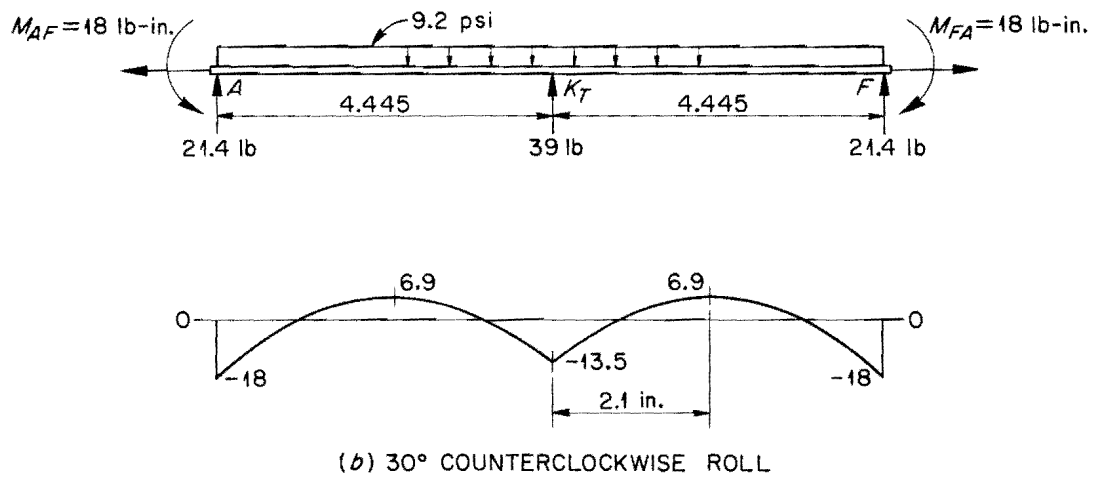
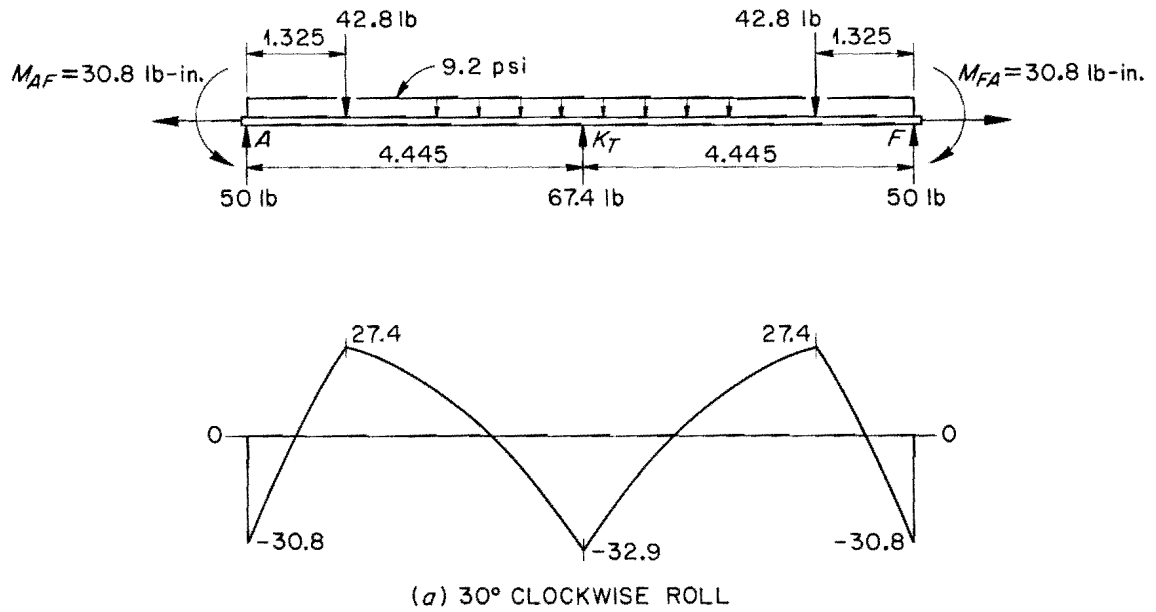


Fig. G5. Model Beams and Bending-Moment Diagrams for the Bottom of the Upper Second Pass Fuel-Element Container in Column 2, at the Top of the Core, for Core I Type Fuel Elements, with  $e=3$  in.

UNCLASSIFIED  
ORNL-LR-DWG 77626

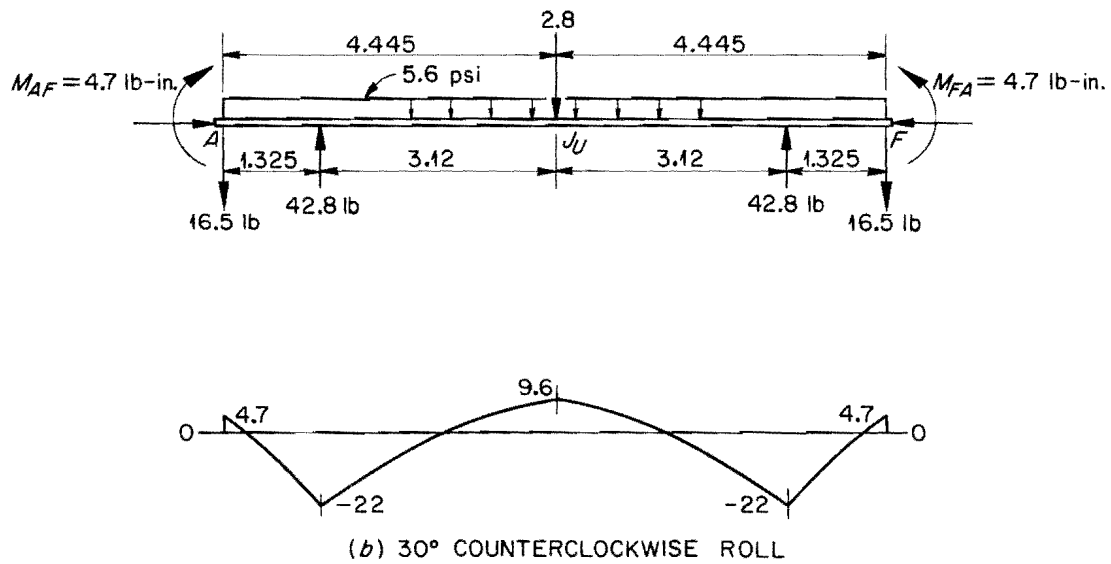
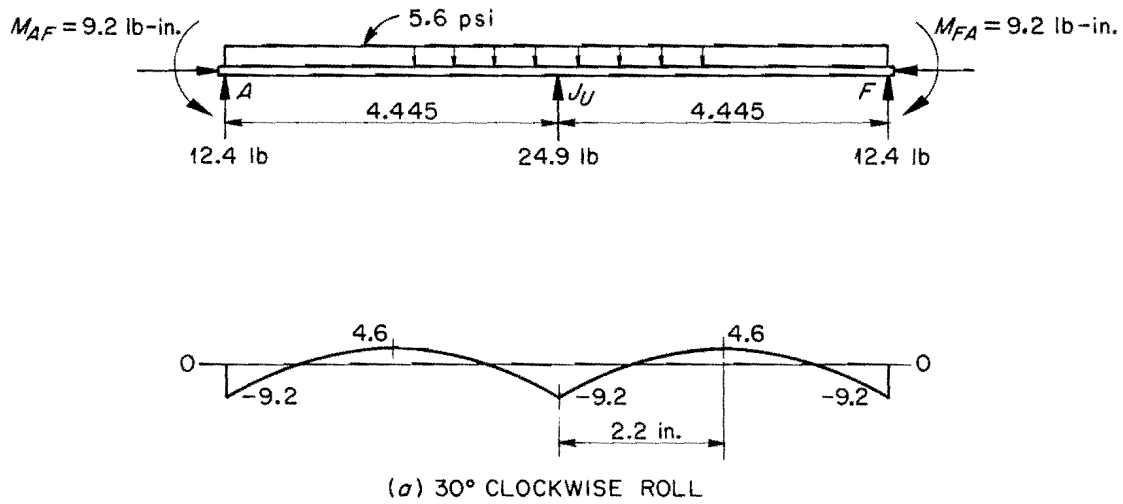
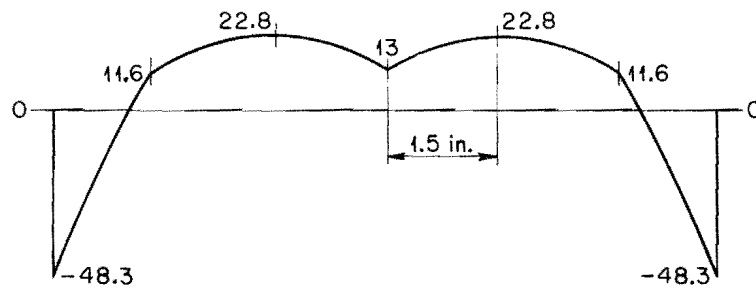
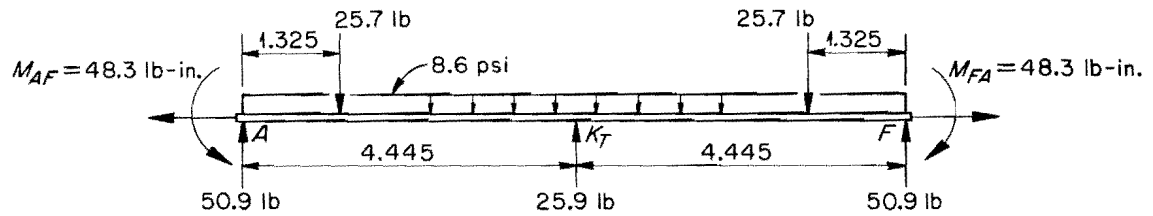
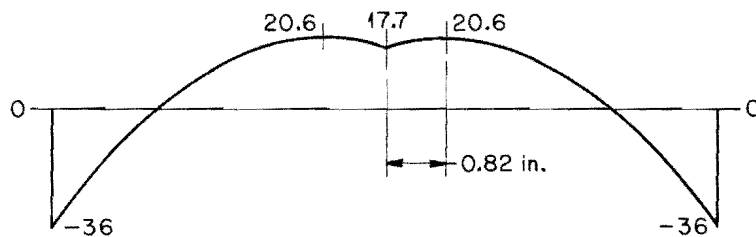
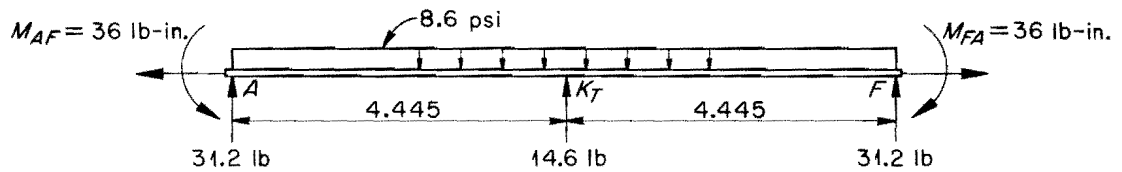


Fig. G6. Model Beams and Bending-Moment Diagrams for the Top of the Third Pass Fuel-Element Container in Column 2, at the Top of the Core, for Core I Type Fuel Elements, with  $e = 3$  in.



(a) 30° CLOCKWISE ROLL



(b) 30° COUNTERCLOCKWISE ROLL

Fig. G7. Model Beams and Bending-Moment Diagrams for the Bottom of the Upper Second Pass Fuel-Element Container in Column 2, 10 in. from the Assumed Simple Support at the Top of the Core, for Core I Type Fuel Elements, with  $e = 5$  in.

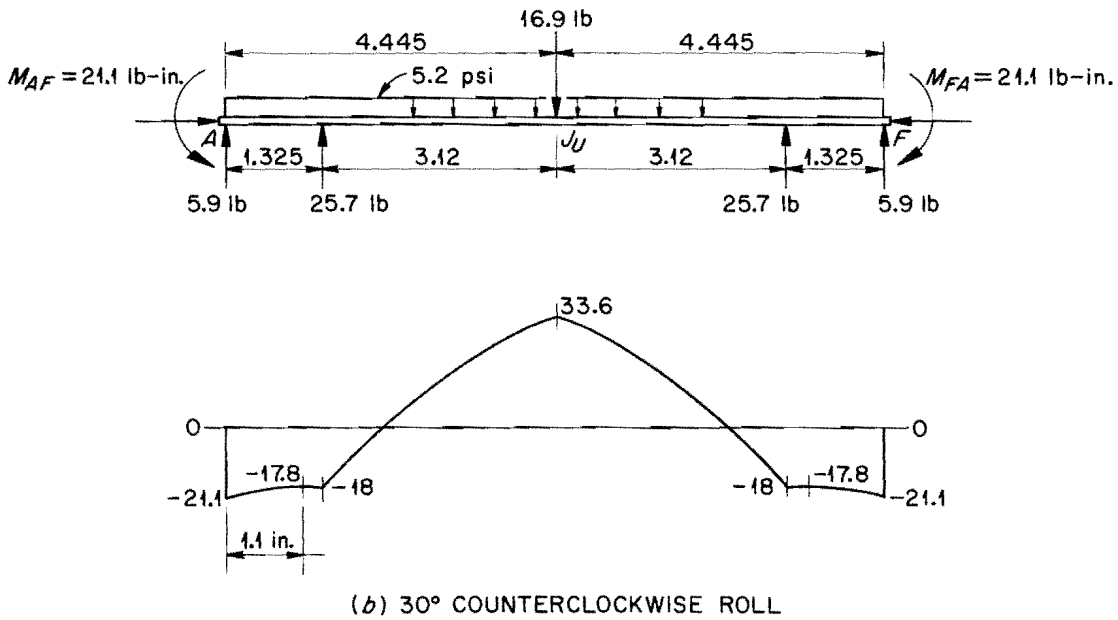
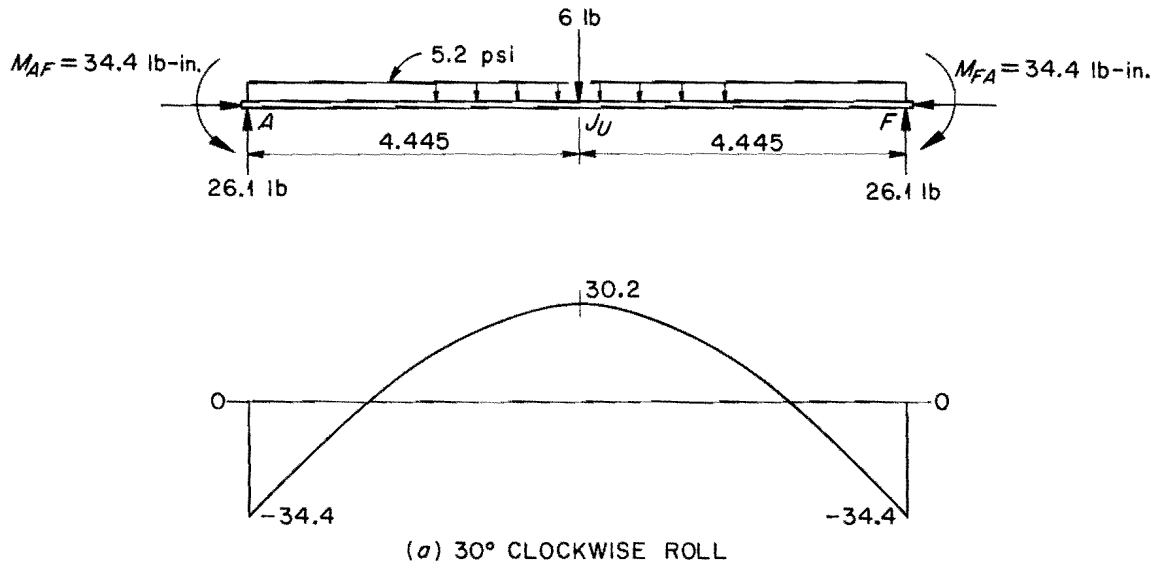
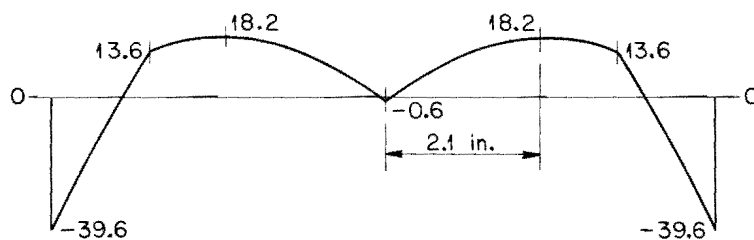
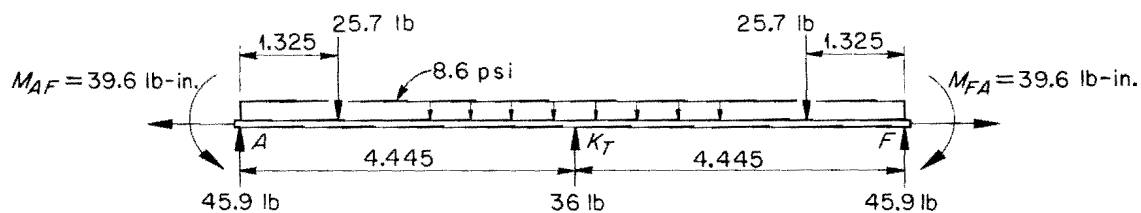
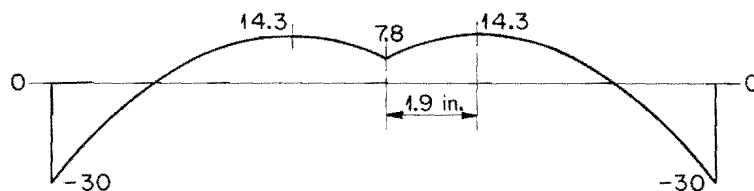
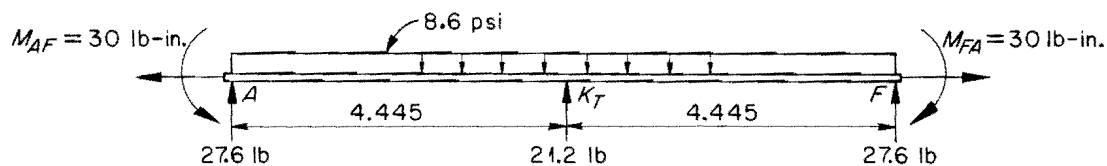


Fig. G8. Model Beams and Bending-Moment Diagrams for the Top of the Third Pass Fuel-Element Container in Column 2, 10 in. from the Assumed Simple Support at the Top of the Core, for Core I Type Fuel Elements, with  $e = 5$  in.



(a) 30° CLOCKWISE ROLL



(b) 30° COUNTERCLOCKWISE ROLL

Fig. G9. Model Beams and Bending-Moment Diagrams for the Bottom of the Upper Second Pass Fuel-Element Container in Column 2, 10 in. from the Assumed Fixed End at the Top of the Core, for Core I Type Fuel Elements, with  $e = 5$  in.

UNCLASSIFIED  
ORNL-LR-DWG 77630

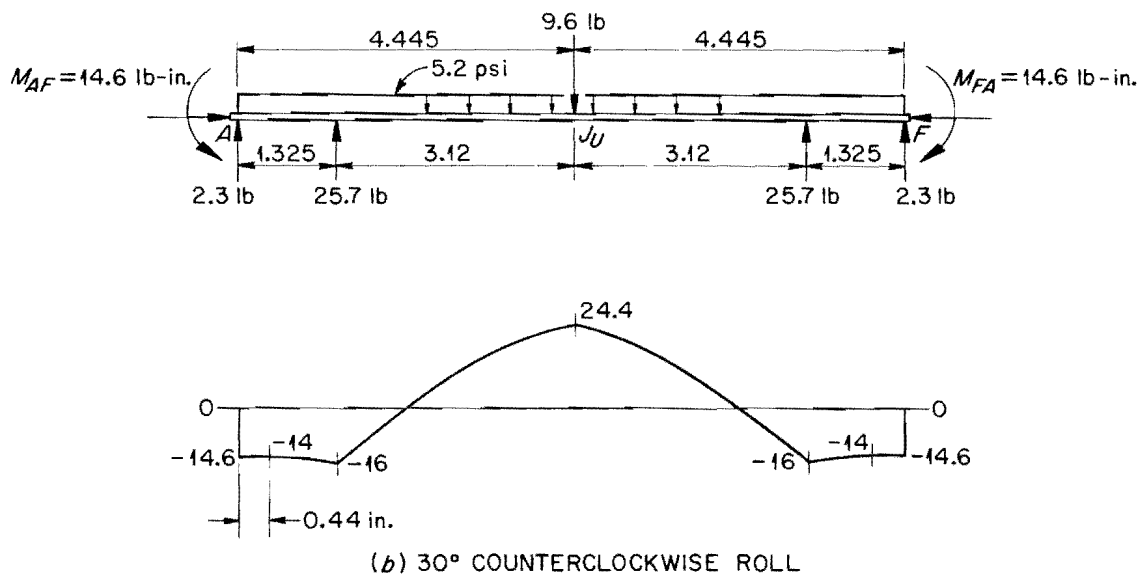
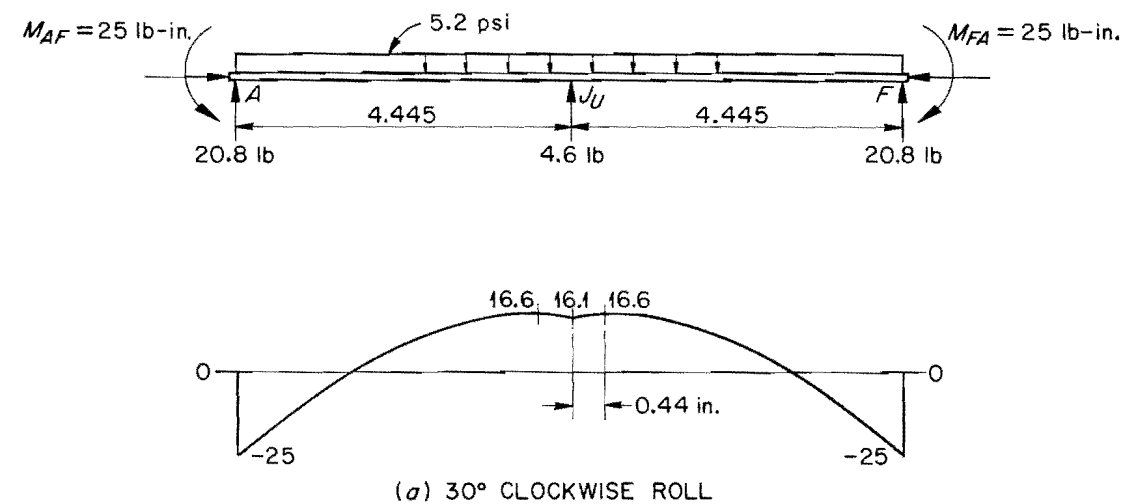
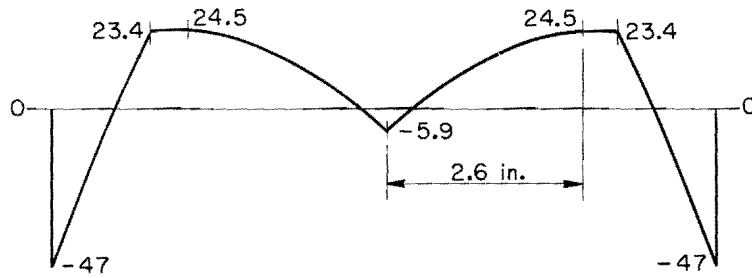
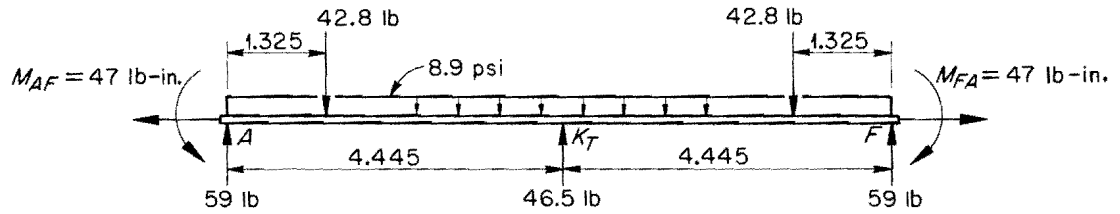
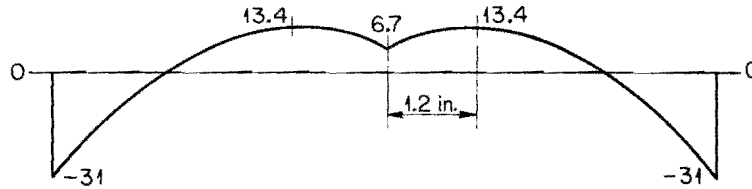
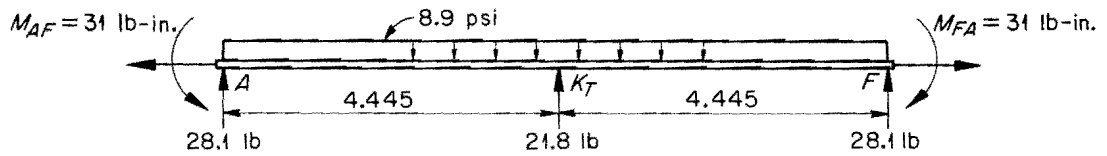


Fig. G10. Model Beams and Bending-Moment Diagrams for the Top of the Third Pass Fuel-Element Container in Column 2, 10 in. from the Assumed Fixed End at the Top of the Core, for Core I Type Fuel Elements, with  $e = 5$  in.



(a) 30° CLOCKWISE ROLL



(b) 30° COUNTERCLOCKWISE ROLL

Fig. G11. Model Beams and Bending-Moment Diagrams for the Bottom of the Upper Second Pass Fuel-Element Container in Column 2, 6 in. from the Assumed Simple Support at the Top of the Core, for Core I Type Fuel Elements, with  $e=3$  in.

UNCLASSIFIED  
ORNL-LR-DWG 77632

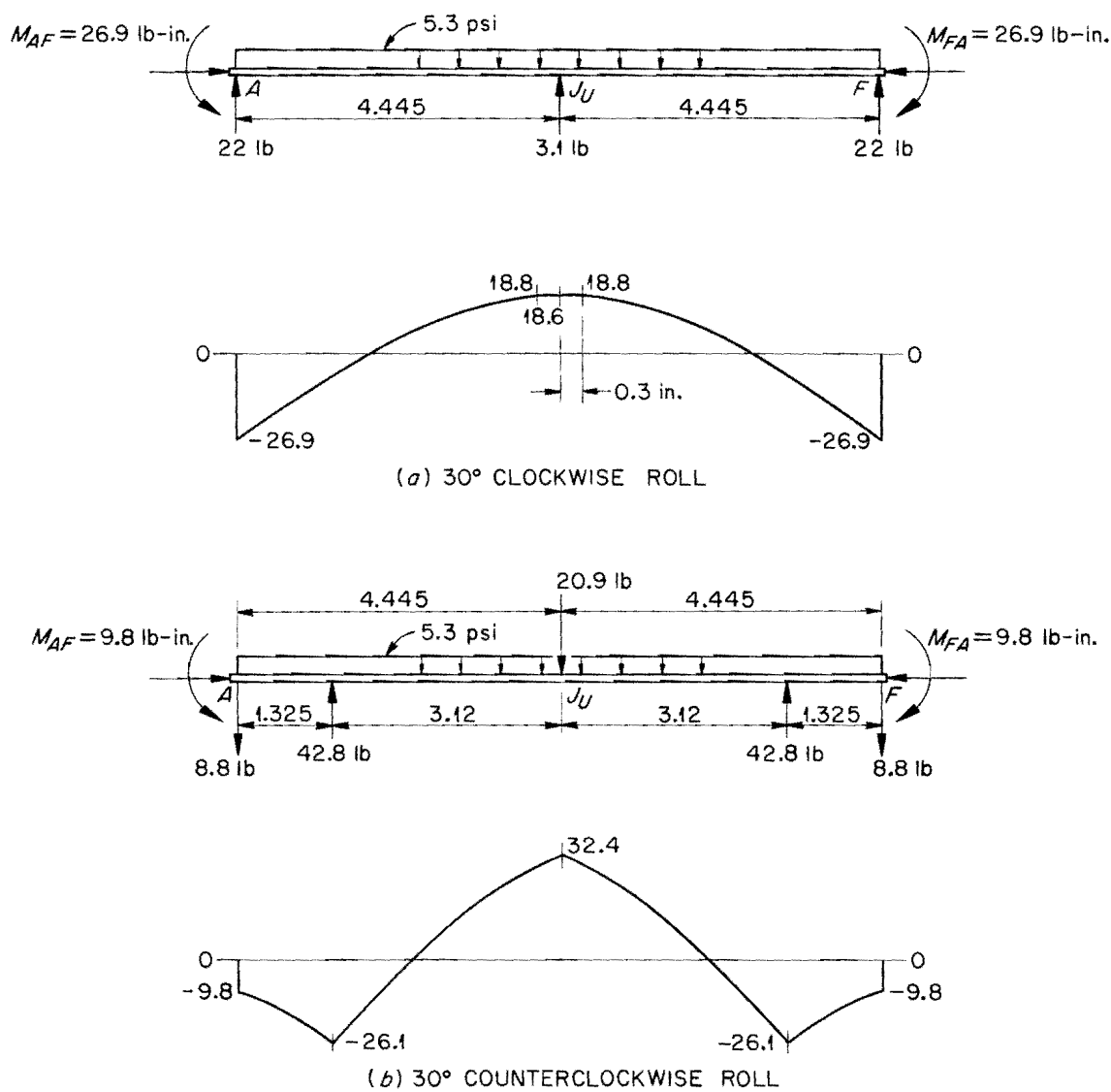
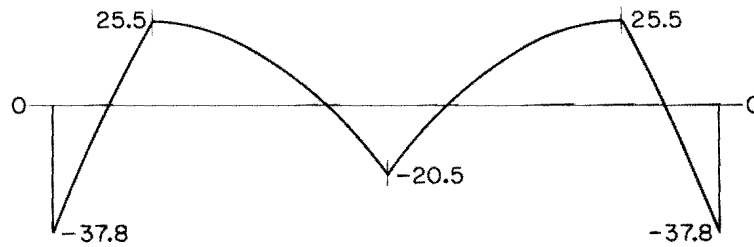
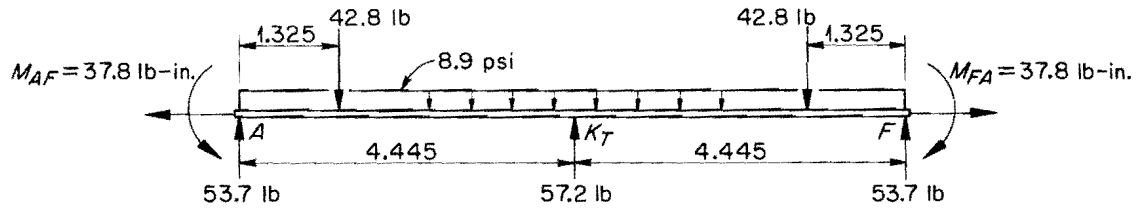
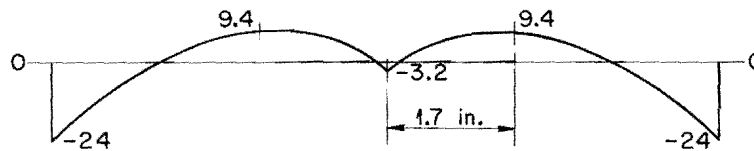
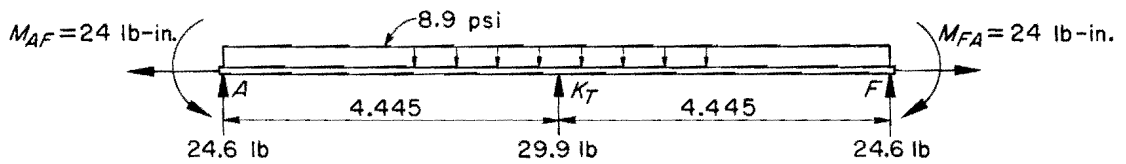


Fig. G12. Model Beams and Bending-Moment Diagrams for the Top of the Third Pass Fuel-Element Container in Column 2, 6 in. from the Assumed Simple Support at the Top of the Core, for Core I Type Fuel Elements, with  $e = 3$  in.



(a) 30° CLOCKWISE ROLL



(b) 30° COUNTERCLOCKWISE ROLL

Fig. G13. Model Beams and Bending-Moment Diagrams for the Bottom of the Upper Second Pass Fuel-Element Container in Column 2, 6 in. from the Assumed Fixed End at the Top of the Core, for Core I Type Fuel Elements, with  $e = 3$  in.

UNCLASSIFIED  
ORNL-LR-DWG 77634

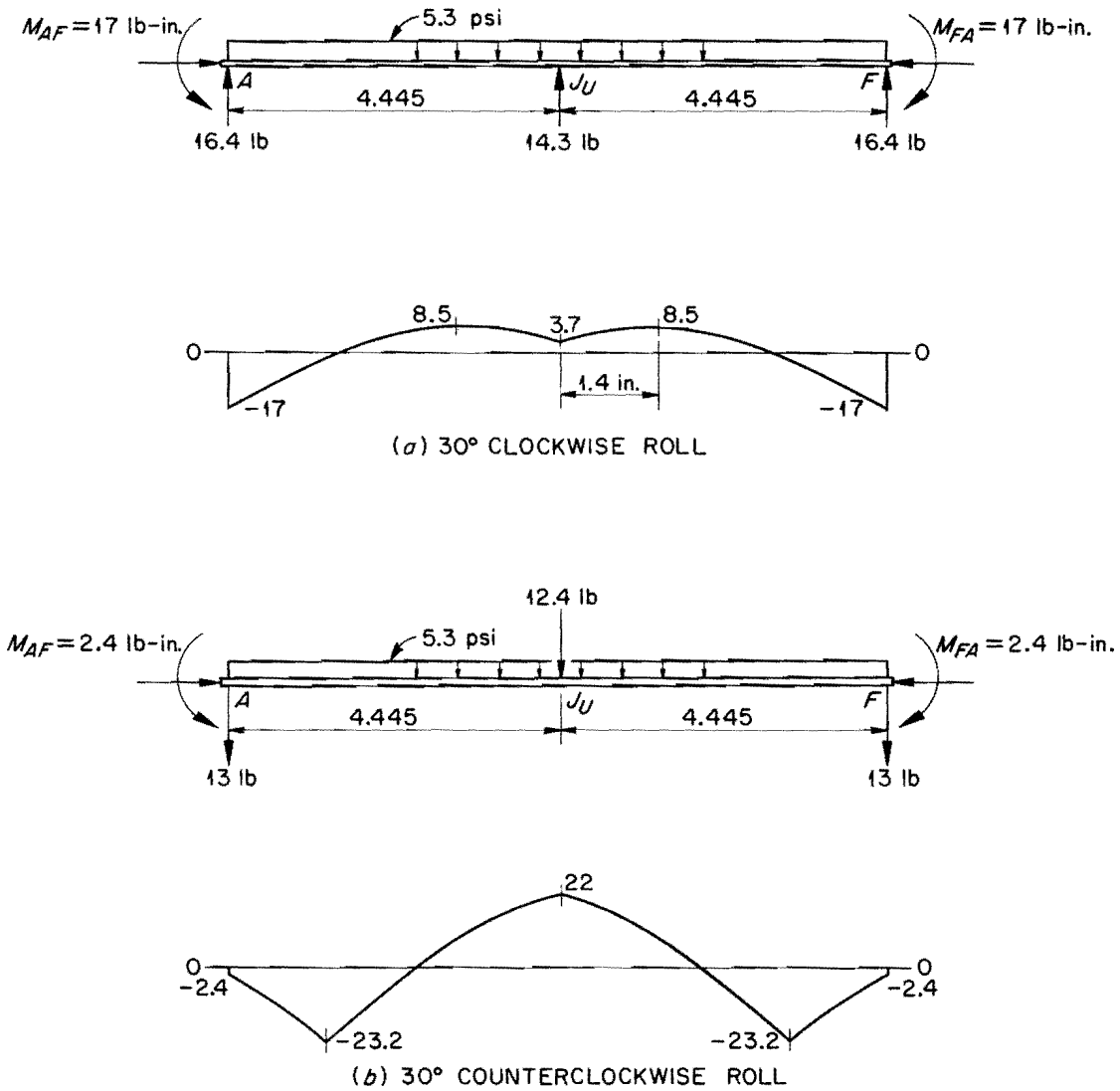
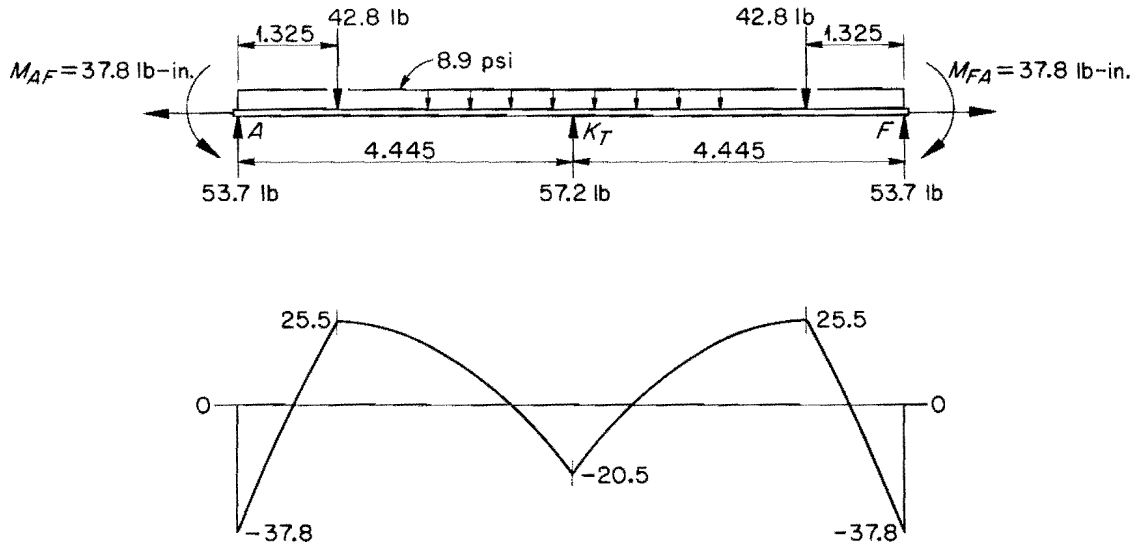
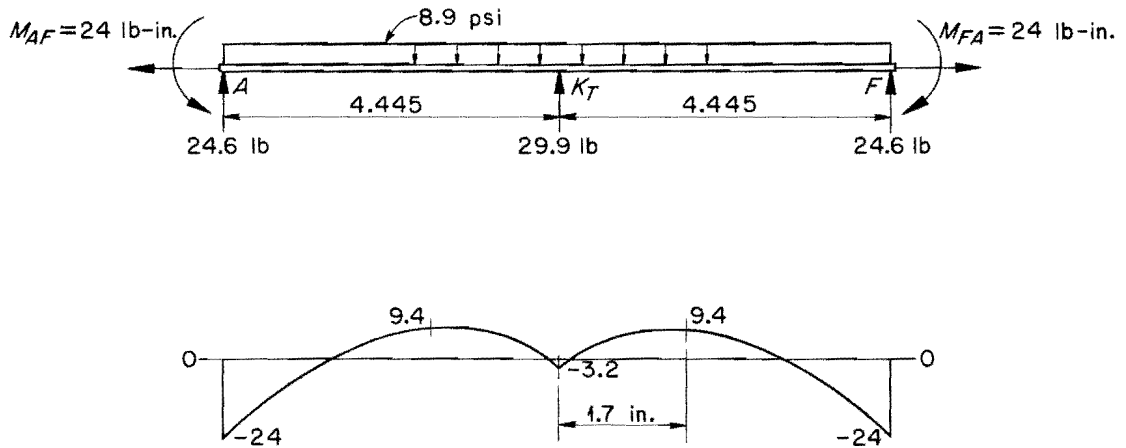


Fig. G14. Model Beams and Bending-Moment Diagrams for the Top of the Third Pass Fuel-Element Container in Column 2, 6 in. from the Assumed Fixed End at the Top of the Core, for Core I Type Fuel Elements, with  $e = 3$  in.



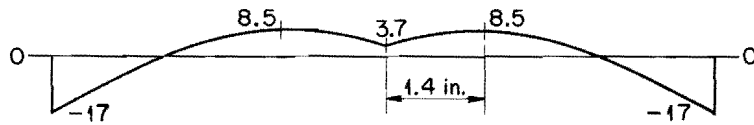
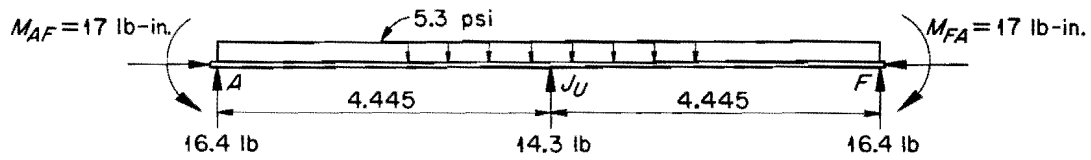
(a) 30° CLOCKWISE ROLL



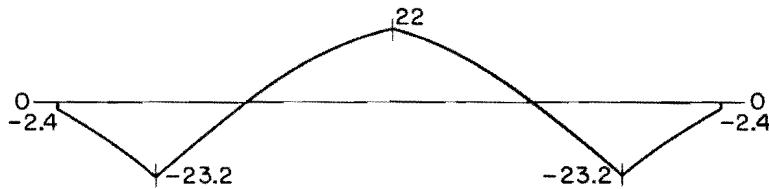
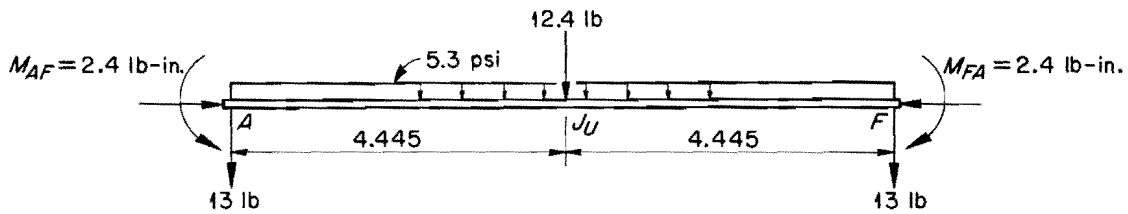
(b) 30° COUNTERCLOCKWISE ROLL

Fig. G13. Model Beams and Bending-Moment Diagrams for the Bottom of the Upper Second Pass Fuel-Element Container in Column 2, 6 in. from the Assumed Fixed End at the Top of the Core, for Core I Type Fuel Elements, with  $e = 3$  in.

UNCLASSIFIED  
ORNL-LR-DWG 77634



(a) 30° CLOCKWISE ROLL



(b) 30° COUNTERCLOCKWISE ROLL

Fig. G14. Model Beams and Bending-Moment Diagrams for the Top of the Third Pass Fuel-Element Container in Column 2, 6 in. from the Assumed Fixed End at the Top of the Core, for Core I Type Fuel Elements, with  $e = 3$  in.

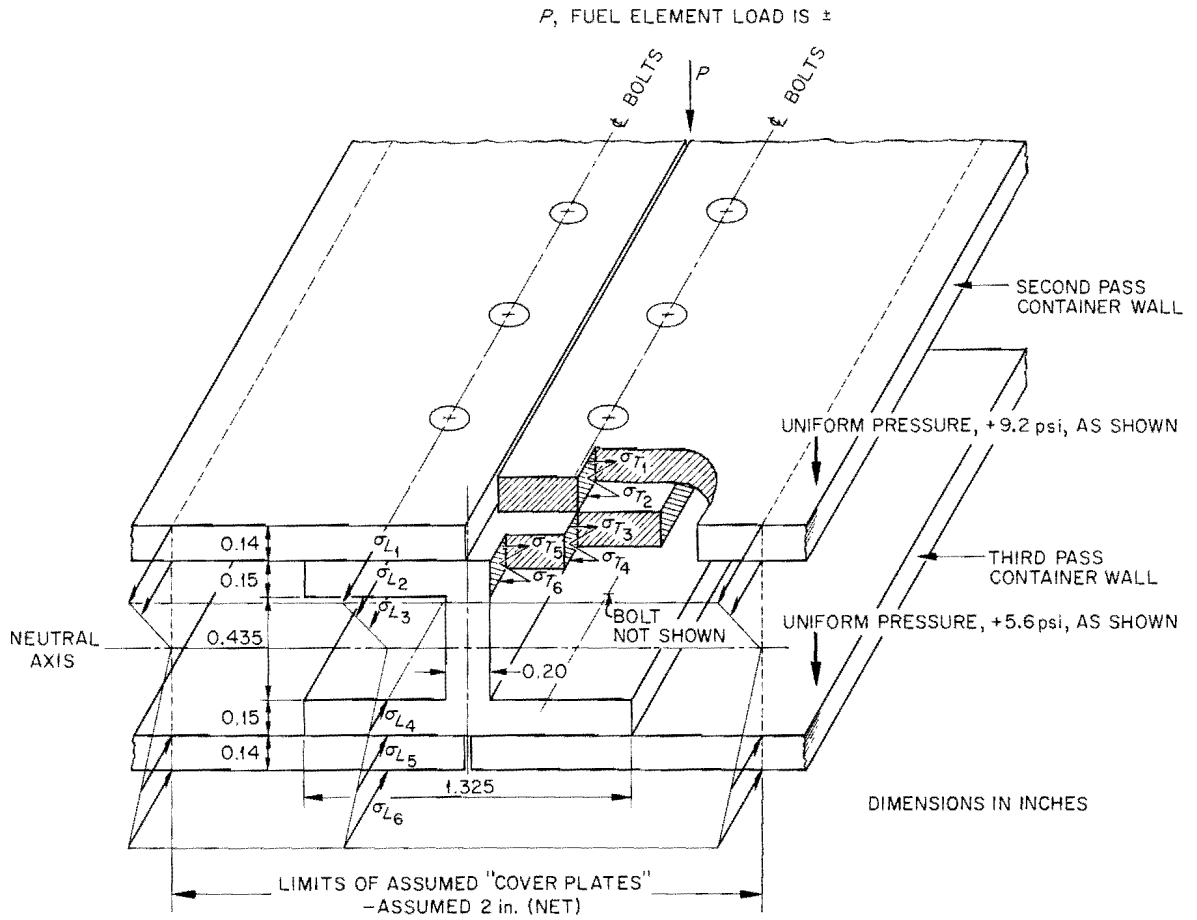


Fig. G15. Fixed End of Spacer Bar "Beam" First Assumed.



Fig. G16. The Connecting Member as a Simple Beam for Core 1 Type Fuel Elements.

Appendix H

## STRESS AND FATIGUE STRENGTH DATA\*

The structural integrity of the proposed Zircaloy-2 fuel-element containers was evaluated in accordance with the preliminary design basis developed by the Navy.<sup>1</sup> In using the Navy Code for a problem of this type, two separate types of stresses must be recognized and considered; these are primary and secondary. The primary stresses are direct or shear stresses developed by the imposed loading which are necessary to satisfy only the simple laws of equilibrium of external and internal forces and moments. Simple membrane pressure stresses in a thin shell are an example of primary stresses. The stresses developed in a cantilever beam by a load applied at the end of the beam are a second example of primary stresses. Secondary stresses are direct or shear stresses developed by the constraint of adjacent parts or by self-constraint of the structure. These differ from primary stresses in that they may be relaxed by yielding of the material. Stress concentrations are neglected in both primary and secondary stresses.

When the analysis of stresses in a member reveals a biaxial or triaxial stress condition, it is necessary to make some assumption regarding the failure criterion to be used. The Navy Code uses the maximum shear theory of failure. The stresses upon which limitations are established are defined as the "equivalent intensity of combined stresses" and are numerically equal to twice the maximum shear stress. The primary membrane stress intensities are not to exceed 62.5% of the yield strength in tension or 33.3% of the ultimate strength in tension, whichever is less. The primary-plus-secondary stress intensities are not to exceed 90% of the yield strength in tension, or 60% of the ultimate strength in tension, whichever is less. In addition to the above allowable stress limits, the Navy Code specifies that the primary-plus-

---

\*The author is indebted to J. M. Corum for the writing of this appendix.

<sup>1</sup>"Tentative Structural Design Basis for Reactor Pressure Vessels and Directly Associated Components," PB 151987, 1 December 1958 Revision, Department of Commerce, Office of Technical Services.

secondary stresses, together with stress concentrations and thermal stresses, shall be evaluated in accordance with a modified Goodman fatigue diagram. A discussion of the allowable stress limits for the Zircaloy-2 fuel containers and a description of the applicable modified Goodman diagram are given below.

The Zircaloy-2 material for the fuel containers was taken to be approximately 15% cold-worked, and the operating temperature for the fuel containers was taken as 600°F. The tensile properties for the material were taken from a report by Whitmarsh.<sup>2</sup> The ultimate tensile strength and the yield strength (0.2% offset) in tension for annealed Zircaloy-2 at 600°F are given below:

|              | Ultimate Strength<br>(psi) | Yield Strength<br>(psi) |
|--------------|----------------------------|-------------------------|
| Transverse   | 27,000                     | 20,000                  |
| Longitudinal | 30,500                     | 17,000                  |

For 15% cold-worked material, the ultimate strength is increased by a factor of approximately 1.96 over the ultimate strength for annealed material, and the yield strength is increased by a factor of approximately 2.85 over the yield strength for annealed material. By applying these factors to the minimum values of ultimate and yield strength given in the above table for annealed material, the representative ultimate and yield strength values used herein were obtained:

|                   |            |
|-------------------|------------|
| Ultimate strength | 52,900 psi |
| Yield strength    | 48,500 psi |

Based on these values, the allowable primary membrane stress intensity, which is designated by  $S_m$ , is 17,600 psi. The allowable primary-plus-secondary stress intensity, which is designated by  $S_p$ , is 31,700 psi.

A plot of the allowable amplitude of alternating stress intensity,  $S_a$ , versus number of cycles for annealed Zircaloy-2 at 600°F is shown in Fig. H1. The curve is based on Navy Code requirements and was

---

<sup>2</sup>C. L. Whitmarsh, "Review of Zircaloy-2 and Zircaloy-4 Properties Relevant to N.S. SAVANNAH Reactor Design," USAEC Report ORNL-3281, Oak Ridge National Laboratory, July 9, 1962.

derived from mechanical strain-cycling data and rotating-beam stress-fatigue data.<sup>2</sup> The strain-cycling data were converted to stress amplitude versus cycles to failure by multiplying the total strain range by  $E/2$ , where  $E$  is the modulus of elasticity ( $11.0 \times 10^6$  psi at  $600^\circ\text{F}$ ). As specified in the Navy Code, the curve representing the allowable amplitude of alternating stress intensity versus the number of cycles has a factor of safety of at least 20 based on cycles to failure, or a factor of safety of at least 2 based on strain range (see B.1.4.1, page 126, ref.1). The design fatigue strength curve for 15% cold-worked material would be slightly higher than the curve for annealed material. Since no fatigue data were available, however, for cold-worked material, the curve in Fig. H1 was used.

The modified Goodman diagram may be constructed from the tensile data and the data in Fig. H1, but stress concentration factors must be considered at some points in the construction. For pure bending of a finite-width plate with a transverse hole, where the hole diameter-to-plate thickness ratio is 1.8 and the hole diameter-to-plate width ratio is 0.3, a stress concentration factor of 1.63 based on the net section is obtained.<sup>3</sup> The concentration of stress from a load applied through a pin fitting in a hole in a flat plate was studied by Frocht and Hill,<sup>4</sup> and their results were shown by Murphy.<sup>5</sup> For a hole diameter-to-plate width ratio of 0.3, the stress concentration factor in the perforated plate loaded by a pin through the hole is approximately 1.5 times the stress concentration factor in the same plate subjected to tension. The stress concentration factor in a perforated plate subjected to bending by a load applied by a pin in the hole was thus taken to be  $1.5 \times 1.63$  or 2.4.

---

<sup>3</sup>R. E. Peterson, Stress Concentration Design Factors, p. 102, John Wiley and Sons, New York, 1953.

<sup>4</sup>M. M. Frocht and H. N. Hill, "Stress Concentration Factors Around a Central Circular Hole in a Plate Loaded Through a Pin in the Hole," J. Appl. Mech., pp. A5-A9, March 1940.

<sup>5</sup>G. Murphy, Advanced Mechanics of Materials, p. 98, McGraw-Hill, New York, 1946.

Manson<sup>6</sup> presents experimental evidence to substantiate the theory that, regardless of the theoretical stress concentration factors, all fatigue strength curves converge to a common point and that the full theoretical stress concentration factor should be applied only to the endurance limit. The curve in Fig. H1 was replaced by two straight lines and redrawn in Fig. H2. The endurance limit for a piece with a stress concentration factor of 2.4 is  $11,500/2.4$  or 4800 psi. The corresponding design fatigue strength curve was obtained by drawing a straight line from the point of convergence, which was arbitrarily taken at ten cycles, to the reduced endurance limit at the abscissa of the knee of the curve from Fig. H1. The lower curve in Fig. H2 is thus the design fatigue strength curve for points subject to stress concentration factors.

Modified Goodman fatigue diagrams for no stress concentration factor and for a stress concentration factor of 2.4 are shown in Fig. H3. The curves were constructed in accordance with the Navy Code by first drawing a line between the allowable amplitude of alternating stress,  $S_a$ , plotted on the ordinate and the ultimate strength plotted on the abscissa. The  $S_a$  values correspond to the endurance limit. Next, the limit of elastic behavior, which is the larger of the endurance limit or the yield strength, was located on the abscissa, and a 45-deg line was drawn to intersect the previous line. All points to the left of and below the solid lines in Fig. H3 will safely withstand an infinite number of cycles.

---

<sup>6</sup>S. S. Manson, "Part 22 - Cumulative Fatigue Damage," Machine Design, 160-166 (August 1960).

UNCLASSIFIED  
ORNL-LR-DWG 77637

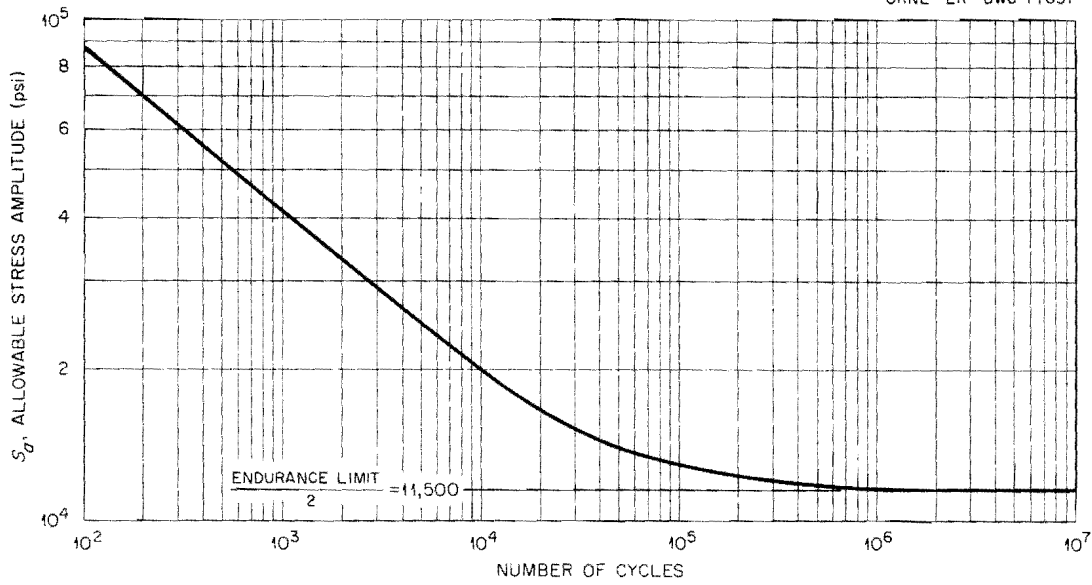


Fig. H1. Design Fatigue Strength Curve for Annealed Zircaloy-2 at 600 °F Based on Navy Code Requirements.

UNCLASSIFIED  
ORNL-LR-DWG 77638

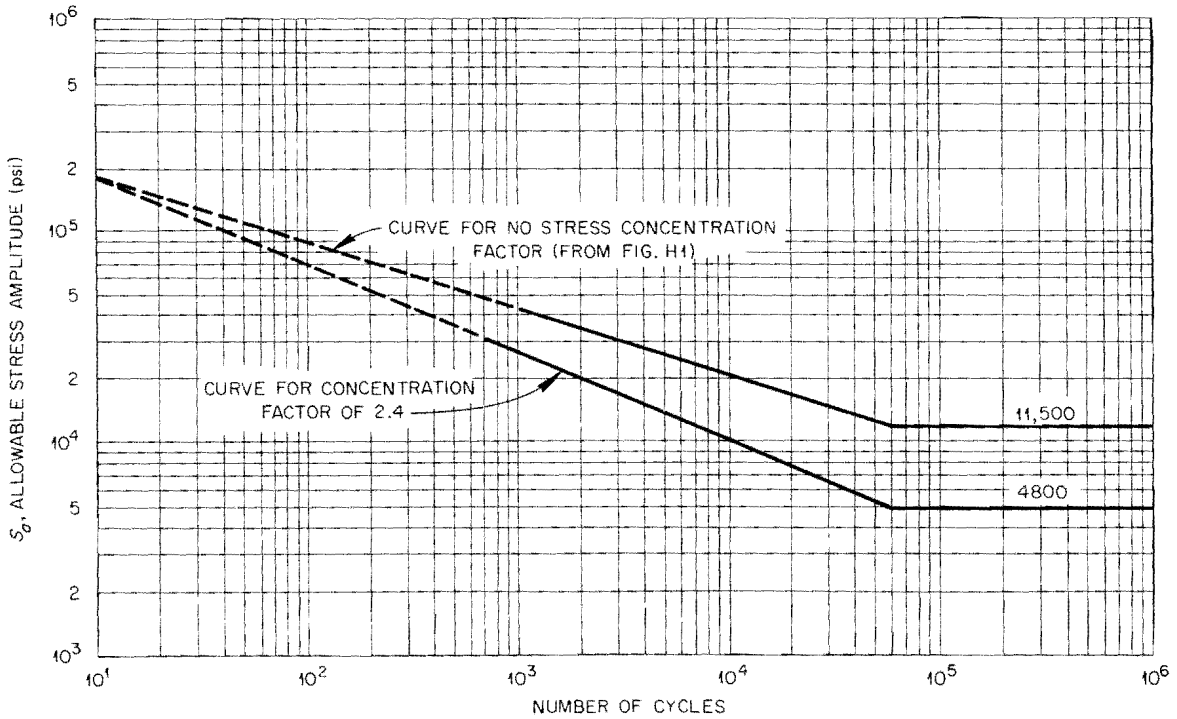


Fig. H2. Design Fatigue Strength Curves.

UNCLASSIFIED  
ORNL-LR-DWG 77639

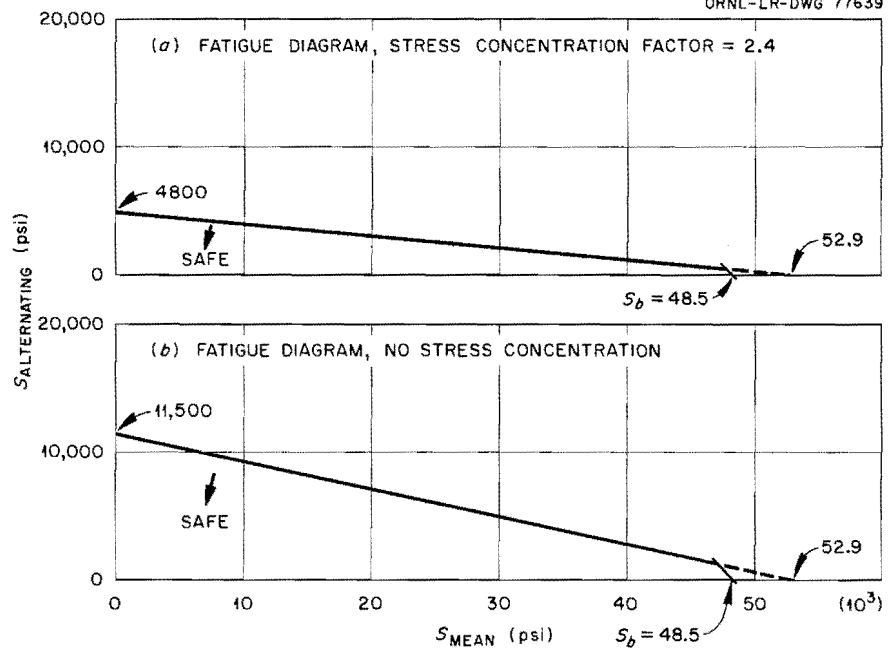


Fig. H3. Modified Goodman Fatigue Diagrams.

.

.

.

.

.

.

.

.

Internal Distribution

- |        |                   |        |                                 |
|--------|-------------------|--------|---------------------------------|
| 1.     | T. D. Anderson    | 33.    | A. M. Perry                     |
| 2.     | S. E. Beall       | 34.    | C. A. Preskitt                  |
| 3.     | M. Bender         | 35.    | G. C. Robinson                  |
| 4.     | A. L. Boch        | 36.    | M. W. Rosenthal                 |
| 5.     | R. B. Briggs      | 37.    | G. Samuels                      |
| 6.     | W. H. Carter      | 38.    | H. W. Savage                    |
| 7.     | B. W. Colston     | 39.    | A. W. Savolainen                |
| 8.     | R. D. Cheverton   | 40.    | L. D. Schaffer                  |
| 9.     | J. M. Corum       | 41-50. | L. R. Shobe                     |
| 10.    | D. A. Douglas     | 51.    | M. J. Skinner                   |
| 11.    | J. Foster         | 52.    | J. E. Smith                     |
| 12.    | A. P. Fraas       | 53.    | I. Spiewak                      |
| 13.    | D. R. Gilfillan   | 54.    | F. J. Stanek                    |
| 14-17. | B. L. Greenstreet | 55.    | J. A. Swartout                  |
| 18.    | E. E. Gross       | 56.    | J. R. Tallackson                |
| 19.    | V. O. Haynes      | 57.    | W. C. Thurber                   |
| 20.    | S. I. Kaplan      | 58.    | D. B. Trauger                   |
| 21.    | P. R. Kasten      | 59.    | J. R. Weir                      |
| 22.    | O. H. Klepper     | 60.    | J. H. Westsik                   |
| 23.    | M. E. LaVerne     | 61.    | C. L. Whitmarsh                 |
| 24.    | R. N. Lyon        | 62.    | M. L. Winton                    |
| 25.    | H. G. MacPherson  | 63.    | F. J. Witt                      |
| 26.    | H. C. McCurdy     | 64.    | G. T. Yahr                      |
| 27.    | W. D. Manly       | 65.    | F. C. Zapp                      |
| 28.    | R. L. Maxwell     | 66-67. | Central Research Library        |
| 29.    | J. T. Meador      | 68-70. | Y-12 Document Reference Section |
| 30.    | J. C. Merkle      | 71-75. | Laboratory Records Department   |
| 31.    | A. J. Miller      | 76.    | Laboratory Records, R.C.        |
| 32.    | S. E. Moore       |        |                                 |

External Distribution

77. W. E. Crowe, Los Alamos Scientific Laboratory
- 78-80. A. T. Granger, University of Tennessee
81. R. O. Mehann, States Marine Lines, Inc.
- 82-85. J. E. Robb, Division of Reactor Development (Maritime Reactors), AEC, Washington
- 86-89. R. T. Schomer, The Babcock & Wilcox Company, Atomic Energy Division, Lynchburg, Va.
90. H. Lawrence Snider, Lockheed, Marietta, Ga.
91. W. C. Stamm, Ebasco Services, Inc., New York, N.Y.
- 92-106. Division of Technical Information Extension (DTIE)
107. Research and Development Division, ORO
- 108-109. Reactor Division, ORO





